Summer 9-1-2014

Neutron Star Models in Alternative Theories of Gravity

Dimitrios Manolidis
Washington University in St. Louis

WASHINGTON UNIVERSITY IN ST. LOUIS

Department of Physics

Dissertation Examination Committee:
Clifford M. Will, Chair
Mark G. Alford
Ramanath Cowsik
Francesc Ferrer
Renato Feres
Henric Krawczynski

Neutron Star Models in Alternative Theories of Gravity

by

Dimitrios Manolidis

A dissertation presented to the
Graduate School of Arts and Sciences
of Washington University in
partial fulfillment of the
requirements for the degree
of Doctor of Philosophy

August 2014

Saint Louis, Missouri

Contents

Bibliography   **87**

Appendices   **92**

A $f(R)$ Potentials   **93**

List of Figures

List of Tables

Notation

Throughout this thesis, geometric units $G = c = 1$ is assumed unless specified otherwise. The metric signature is $(-, +, +, +)$. Greek letters stand for spacetime indexes, while Latin letters stand for spatial indexes only. Einstein summation is assumed throughout the thesis. When referring to Jordan and Einstein frames, tilde variables correspond to the Einstein frame, while un-tilde variables correspond to Jordan frame. We define the following:

Symbol	Description
$\frac{\partial f}{\partial x^\mu} \equiv f_{,\mu}$	Partial derivative
$\nabla_\mu \equiv f_{;\mu}$	Covariant derivative
$\Box \equiv \Box_g \equiv g^{\mu\nu}\nabla_\mu\nabla_\nu$	D' Alembertian
G	Gravitational constant
κ	$\sqrt{8\pi G}$
$g_{\mu\nu}$	Metric tensor
g	Determinant of $g_{\mu\nu}$
$R_{\mu\nu}$	Ricci tensor
R	Ricci scalar or scalar curvature
$T_{\mu\nu}$	Stress-energy tensor
$T \equiv g^{\mu\nu}T_{\mu\nu}$	Trace of stress-energy tensor

Acknowledgements

First and foremost, I would like to thank my advisor, Clifford M. Will for accepting me as his student and for his guidance and support all these years. His great knowledge and experience made it possible for me to be able to complete this thesis. Also, I would like to thank my collaborators Emanuele Berti and Michael Horbatsch. They shared their knowledge with me along with their data and we had long discussions that helped me understand important concepts of my research.

I would like to thank the members of my research group, Saeed Mirshekari, Laleh Sadeghian and Ryan Lang. Our group meetings, the exchange of ideas about our research or just programming languages, their support at conference talks, seminars, etc, all helped tremendously in the completion of this thesis.

Additionally I would like to thank all the professors at Washington University whose courses I took or I was a TA for. I learned a lot from you. I would also like to thank the staff at the Physics Department and especially Sarah Hedley and Julia Hamilton for all their help.

I would like to thank my thesis committee, Mark G. Alford, Ramanath Cowsik, Francesc Ferrer, Renato Feres and Henric Krawczynski for taking the time to participate in my defense and for all their interesting and thought provoking questions.

I would like to thank all my friends and fellow graduate students, Ben Burch, Michael DeSantis, Shawn DeCenzo, John Flavin, Daniel Hunter as well as every graduate student at the Physics Department. The moments we shared together made it easier for me to continue working towards my goal all these years. Finally, I would like to thank my parents and my brother. Anything that I have accomplished in life would have not been possible without my family.

ABSTRACT OF THE DISSERTATION

Neutron Star Models in Alternative Theories of Gravity

by

Dimitrios Manolidis

Doctor of Philosophy in Physics

Washington University in St. Louis, 2014

Professor Clifford M. Will, Chair

We study the structure of neutron stars in a broad class of alternative theories of gravity. In particular, we focus on Scalar-Tensor theories and $f(R)$ theories of gravity. We construct static and slowly rotating numerical star models for a set of equations of state, including a polytropic model and more realistic equations of state motivated by nuclear physics. Observable quantities such as masses, radii, etc are calculated for a set of parameters of the theories.

Specifically for Scalar-Tensor theories, we also calculate the sensitivities of the mass and moment of inertia of the models to variations in the asymptotic value of the scalar field at infinity. These quantities enter post-Newtonian equations of motion and gravitational waveforms of two body systems that are used for gravitational-wave parameter estimation, in order to test these theories against observations.

The construction of numerical models of neutron stars in $f(R)$ theories of gravity has been difficult in the past. Using a new formalism by Jaime, Patino and Salgado we were able to construct models with high interior pressure, namely $p_c > \rho_c/3$, both for constant density models and models with a polytropic equation of state. Thus, we have shown that

earlier objections to $f(R)$ theories on the basis of the inability to construct viable neutron star models are unfounded.

Chapter 1

Introduction

1.1 Gravity and General Relativity

Sir Isaac Newton was the first to propose a mathematical description of the laws of gravity, in 1687. Newton's theory remained as the widely accepted theory of gravity until the beginning of the 20th century. In 1915, Albert Einstein introduced his theory of General Relativity. It was a revolutionary theory that changed the way physicists think about gravity. Today, General Relativity is considered a well established theory that is studied as a standard textbook subject [47], [31], [58].

Unlike Newtonian gravity, where gravity is described as a force from a distance, in General Relativity gravity arises from curvature in geometry. It is the curvature that affects the the motion of particles in spacetime. On the other hand, massive bodies and energy sources cause the spacetime to curve. To study the curvature we employ a mathematical description of the squared length of an infinitesimal displacement in an arbitrary direction. This squared length, or "line element", is given by

$$ds^2 = g_{\mu\nu}dx^\mu dx^\nu \tag{1.1}$$

where x^μ are the coordinates describing the spacetime and $g_{\mu\nu}$ is the metric tensor. The

metric tensor is one of the fundamental quantities in General Relativity. Given the metric tensor the geometry of the spacetime can be fully described. If the geometry of the spacetime is known, the motion of test particles can be predicted.

The equations that we use to derive the elements of the metric tensor are called Einstein field equations and they are given by

$$G_{\mu\nu} = 8\pi T_{\mu\nu}. \tag{1.2}$$

The right hand side of the equation is called the stress-energy tensor and it describes the mass-energy part of the equation. It is a measurement of the flux of the 4-momentum through a surface in a direction of one of the spacetime coordinates. More specifically the component T^{00} is the energy density. The component T^{0i} is the flux of energy across a surface of constant x^i. The component T^{i0} is the i component of the momentum density. Finally, T^{ij} is the flux of i-th component of momentum across a surface whose normal is in the j direction. The stress energy tensor is symmetric like the metric tensor. The elements of the stress-energy tensor depend on the system under study. As an example, the stress energy tensor of a perfect fluid is given by

$$T^{\mu\nu} = (\rho + p)u^\mu u^\nu + pg^{\mu\nu}. \tag{1.3}$$

We will use this stress energy tensor repeatedly in this thesis.

The left hand side of the equation is called the Einstein tensor $G_{\mu\nu}$ and it describes the geometric part of the equation. It is a function of the metric tensor. More specifically, the Einstein tensor depends on the Riemann tensor, which is a measurement of the curvature of the spacetime. The Riemann tensor is given by

$$R^\alpha{}_{\beta\mu\nu} = \Gamma^\alpha{}_{\beta\nu,\mu} - \Gamma^\alpha{}_{\beta\mu,\nu} + \Gamma^\alpha{}_{\mu\gamma}\Gamma^\gamma{}_{\beta\nu} - \Gamma^\alpha{}_{\nu\gamma}\Gamma^\gamma{}_{\beta\mu} \tag{1.4}$$

where $\Gamma^{\alpha}_{\beta\gamma}$ are the Christoffel symbols, given by

$$\Gamma^{\alpha}{}_{\beta\gamma} = \frac{1}{2}g^{\alpha\mu}(g_{\mu\beta,\gamma} + g_{\mu\gamma,\beta} - g_{\beta\gamma,\mu}).$$ (1.5)

The contracted Riemann tensor is called Ricci tensor

$$R_{\mu\nu} = R^{\gamma}{}_{\mu\gamma\nu}$$ (1.6)

and the contracted Ricci tensor is called the Ricci scalar, or scalar curvature

$$R = R^{\gamma}{}_{\gamma}.$$ (1.7)

Finally the Einstein tensor is given by

$$G_{\mu\nu} = R_{\mu\nu} - \frac{1}{2}g_{\mu\nu}R$$ (1.8)

The local conservation of energy and momentum implies that stress-energy tensor satisfies the equation

$$T^{\mu\nu}{}_{;\nu} = T^{\mu\nu}{}_{,\nu} + \Gamma^{\mu}{}_{\nu\gamma}T^{\gamma\nu} + \Gamma^{\nu}{}_{\nu\gamma}T^{\gamma\mu} = 0,$$ (1.9)

where a semicolon denotes a covariant derivative. One the other hand, using the Bianchi identity

$$R_{\mu\nu\alpha\beta;\gamma} + R_{\mu\nu\beta\gamma;\alpha} + R_{\mu\nu\gamma\alpha;\beta} = 0,$$ (1.10)

we can show that

$$G^{\mu\nu}{}_{;\nu} = 0,$$ (1.11)

which is compatible with the local conservation of energy.

1.2 Alternative theories of gravity

Even though General Relativity has passed all the local experimental tests, the strong field regime still remains mostly unexplored. In addition, a unification of General Relativity with the other three interactions has not been possible. In order to address these issues, physicists search for alternatives to General Relativity. Numerous theories have been presented to this date. Some of these theories were shown to be non-viable since their predictions did not agree with the new and more accurate experimental results. There exist, however, several viable theories today that pass the experimental tests, yet their predictions differ from those of General Relativity in the strong field regime. In this thesis we will focus on two types of alternative theories of gravity. Scalar Tensor theories and $f(R)$ theories of gravity.

1.2.1 Scalar Tensor theories

One of the most well studied attempts to modify General Relativity is the class of Scalar Tensor theories of gravity. The existence of the scalar field was initially motivated from Kaluza-Klein theories and later from superstring and super-gravity theories, which all give rise to scalar fields coupled to matter. The first scalar tensor theory was introduced by Fierz[27], Jordan[35], Brans and Dicke[9], so we will refer to it as FJBD theory. The theory introduces a dynamical scalar filed ϕ in addition to the metric $g_{\mu\nu}$, which is the central part of General Relativity. The action of the FJBD theory reads as follows

$$S = \frac{1}{2\kappa^2} \int d^4x \sqrt{-g} \left(\phi R + \frac{\omega}{\phi} g^{\mu\nu} \phi_{,\mu} \phi_{,\nu} \right) + S_M \tag{1.12}$$

where S_M is the matter part of the action. The matter action contains the variables of non-gravitational fields, and the metric, but does not contain the scalar field. The theory contains one arbitrary parameter ω which value is to be constrained by local gravity experiments. The theory reduces to General Relativity in the limit $\omega \to \infty$. Later on, Bergmann[7],

Wagoner[69] and Nordvedt[52] generalized the theory, where the free parameter ω becomes a free function $\omega(\phi)$ of the scalar field ϕ, and the scalar field can have an arbitrary potential. Thus, the action of the generalized theory is

$$S = \frac{1}{2\kappa^2} \int d^4x \sqrt{-g} \left[\phi R + \frac{\omega(\phi)}{\phi} g^{\mu\nu} \phi_{,\mu} \phi_{,\nu} + 2\phi\lambda(\phi) \right] + S_M \tag{1.13}$$

where $\lambda(\phi)$ is another free function which plays a role similar to that of the cosmological constant in General Relativity. Since the function $\omega(\phi)$ is arbitrary, the action describes a class of Scalar Tensor theories. In order to choose a specific theory to work with, we need to choose a specific function for $\omega(\phi)$.

The field equations of the theory can be obtained by varying the action with respect to the tensor field $g_{\mu\nu}$ and the scalar field ϕ [70]

$$R_{\mu\nu} - \frac{1}{2} g_{\mu\nu} R - \lambda(\phi) g_{\mu\nu} = \frac{\kappa^2}{\phi} T_{\mu\nu} + \frac{\omega}{\phi^2} (\phi_{,\mu} \phi_{,\nu} - \frac{1}{2} g_{\mu\nu} \phi_{,\lambda} \phi^{,\lambda}) + \frac{1}{\phi} (\phi_{;\mu\nu} - g_{\mu\nu} \Box \phi) \tag{1.14}$$

$$\Box\phi + \frac{1}{2} \phi_{,\lambda} \phi^{,\lambda} \frac{d}{d\phi} \ln \left(\frac{\omega(\phi)}{\phi} \right) + \frac{1}{2} \frac{\phi}{\omega(\phi)} \left[R + 2 \frac{d}{d\phi} (\phi\lambda(\phi)) \right] = 0. \tag{1.15}$$

The equation for the scalar field ϕ can be rewritten as

$$\Box\phi + \frac{2\phi^2 d\lambda/d\phi - 2\phi\lambda(\phi)}{3 + 2\omega(\phi)} = \frac{1}{3 + 2\omega(\phi)} \left(\kappa^2 T - \frac{d\omega}{d\phi} \phi_{,\lambda} \phi^{,\lambda} \right) \tag{1.16}$$

,where $T_{\mu\nu} \equiv 2(-g)^{-1/2} \delta S_M / \delta g^{\mu\nu}$ is the stress energy tensor and $T = T_\mu^\mu$. The asymptotic value of the scalar field ϕ_0, in the weak field limit, is related to the gravitational constant G. In geometrized units,

$$G \equiv \left[\frac{4 + 2\omega(\phi_0)}{3 + 2\omega(\phi_0)} \right] \phi_0^{-1} = 1. \tag{1.17}$$

Like every other theory of gravity, Scalar Tensor theories need to be experimentally tested to determine their viability. In order to test the theory a very powerful tool is used, called

the Parametrized Post-Newtonian (PPN) Formalism [70]. This is done by firstly assuming that the matter in the solar system can be modeled as a perfect fluid. Then we express the metric as a series of potentials whose source is the various matter variables. We replace the coefficients of the terms in the metric by arbitrary parameters. By choosing specific values for the parameters of this metric we obtain the Post-Newtonian metric of a particular theory of gravity. The most general case of this metric, under certain assumptions for the Post-Newtonian functionals contains ten parameters γ, β, ξ, α_1, α_2, α_3, ζ_1, ζ_2, ζ_3 and ζ_4. The metric reads

$$
\begin{aligned}
g_{00} =\ & -1 + 2U - 2\beta U^2 - 2\xi \Phi_W + (2\gamma + 2 + \alpha_3 + \zeta_1 - 2\xi)\Phi_1 \\
& + 2(3\gamma - 2\beta + 1 + \zeta_2 + \xi)\Phi_2 + (1 + \zeta_3)\Phi_3 \\
& + 2(3\gamma + 3\zeta_4 - 2\xi)\Phi_4 - (\zeta_1 - 2\xi)\mathcal{A} \\
g_{0i} =\ & \frac{1}{2}(4\gamma + 3 + \alpha_1 - \alpha_2 + \zeta_1 - 2\xi)V_i - \frac{1}{2}(1 + \alpha_2 - \zeta_1 + 2\xi)W_i \\
g_{jk} =\ & (1 + 2\gamma U)\delta_{jk}
\end{aligned}
\tag{1.18}
$$

General Relativity corresponds to the case $\gamma = \beta = 1$ and $\xi = \alpha_1 = \alpha_2 = \alpha_3 = \zeta_1 = \zeta_2 = \zeta_3 = 0$. The PPN parameters of Scalar Tensor theories are

$$
\begin{aligned}
\gamma &= \frac{1+\omega}{2+\omega} \\
\beta &= 1 + \omega'(3 + 2\omega)^{-2}(4 + 2\omega)^{-1} \\
\xi &= \alpha_1 = \alpha_2 = \alpha_3 = \zeta_1 = \zeta_2 = \zeta_3 = 0
\end{aligned}
\tag{1.19}
$$

where $\omega = \omega(\phi_0)$ and $\omega' = \frac{d\omega}{d\phi}(\phi_0)$, where ϕ_0 is the value of the scalar field far from the solar system.

The PPN Formalism can be used now to test the theory against the experimental findings of solar system experiments. The most important of these experiments are

- **The deflection of light around the Sun.** The deflection angle of a light ray passing near the Sun is given by [71]

$$\delta\theta = \frac{1}{2}(1+\gamma)\frac{4M_\odot}{d}\frac{1+\cos\phi}{2}, \tag{1.20}$$

where $M_\odot$ is the mass of the Sun, d is the distance at which the ray passes the Sun and ϕ is the angle between the Earth-Sun line and the incoming direction of the photon. Using very-long-baseline radio interferometry the best result for this technique yields a value for gamma [39]

$$\gamma - 1 = (-1.6 \pm 1.5) \times 10^{-4}. \tag{1.21}$$

- **The Shapiro time delay.** Radar signals that travel past the Sun and return back to Earth experience a time delay, as first pointed out by Irwin Shapiro. The time delay is given by the formula [71]

$$\delta t = \frac{1}{2}(1+\gamma)\left(240 - \ln\frac{d^2}{r}\right) \ \mu s, \tag{1.22}$$

where d is the distance of closest approach of the ray in solar radii, and r is the distance of the object receiving the signal from the Sun, in astronomical units. The most stringiest bound on the value of gamma comes from the Doppler tracking of the Cassini spacecraft in 2003 [8] which yields the result

$$\gamma - 1 = (2.1 \pm 2.3) \times 10^{-5}. \tag{1.23}$$

- **The perihelion shift of Mercury.** The advance of the perihelion of Mercury has been measured to be 43 arcseconds per century. The theoretical value taking into account both relativistic PPN contributions and the solar quadrupole moment is given

by [71]

$$\dot{\tilde{\omega}} = 42.''98 \left(\frac{1}{3}(2 + 2\gamma - \beta) + 3 \times 10^4 \frac{J_2}{10^{-7}} \right), \tag{1.24}$$

where $J_2 = (2.2 \pm 0.1) \times 10^{-7}$ [45], [3] is the quadrupole moment. Comparing the theoretical value to the experimental one we get

$$| \, 2\gamma - \beta - 1 \, | < 3 \times 10^{-4}, \tag{1.25}$$

which combined with the Cassini result gives a bound on β [26], [68]

$$\beta - 1 = (-4.1 \pm 7.8) \times 10^{-5}. \tag{1.26}$$

The bound on the PPN parameter γ can be translated to a bound on the parameter ω of the FJBD theory according to the equation (1.19)

$$\omega > 400000. \tag{1.27}$$

The action of scalar tensor theory can be re-written in such a way that it looks similar to that of General Relativity. This non-metric representation is called the "Einstein frame" while the regular metric representation is called the "Jordan frame". The metric is conformally transformed to a new metric variable that is coupled to the scalar field [24],[16]

$$g_{\mu\nu} \rightarrow \tilde{g}_{\mu\nu} = \Omega^2(\phi)g_{\mu\nu} \tag{1.28}$$

Because of this, $\tilde{g}_{\mu\nu}$ is no longer the physically measured metric; nevertheless it is a useful variable for representing this class of theories. The scalar curvature transforms as

$$R = \Omega^2 \tilde{R} + 6\frac{\Box \Omega}{\Omega} \tag{1.29}$$

8

The determinant of $g_{\mu\nu}$ transforms as

$$\sqrt{-\tilde{g}} = \Omega^4 \sqrt{-g} \tag{1.30}$$

We now use the transformation

$$d\varphi = \frac{1}{2} \sqrt{2\omega(\phi) + 3} \, \frac{d\phi}{\phi} \tag{1.31}$$

$$\Omega^2(\phi) = \phi \tag{1.32}$$

Substituting the previous equations into the action (1.13) for $\lambda(\phi) = 0$ we get

$$S = \frac{1}{2\kappa^2} \int d^4x \sqrt{-\tilde{g}} \left[\tilde{R} - 2\tilde{g}^{\mu\nu} \varphi_{,\mu} \varphi_{,\nu} \right] \tag{1.33}$$

where φ is the new scalar field. This is the action in the Einstein frame. Following the notation of Damour and Esposito-Farese [17] we define some useful parameters

$$A(\varphi) = \Omega^{-1} \tag{1.34}$$

$$\tilde{\alpha}(\varphi) \equiv \frac{d\ln A(\varphi)}{d\varphi} = \frac{1}{\sqrt{3 + 2\omega(\phi)}} \tag{1.35}$$

$$\tilde{\beta}(\varphi) = \frac{d\tilde{\alpha}(\varphi)}{d\varphi} \tag{1.36}$$

The field equations in the Einstein frame, derived from the action (1.33) are

$$\tilde{R}_{\mu\nu} = 2\tilde{g}^{\mu\nu} \partial_\mu \varphi \partial_\nu \varphi + \kappa^2 \left(\tilde{T}_{\mu\nu} - \frac{1}{2} \tilde{T} \tilde{g}_{\mu\nu} \right) \tag{1.37}$$

$$\Box_{\tilde{g}} \varphi = -\frac{\kappa^2}{2} \tilde{\alpha}(\varphi) \tilde{T} \tag{1.38}$$

where $\tilde{T}_{\mu\nu} \equiv 2(\tilde{g})^{-1/2} \delta S_M / \delta \tilde{g}^{\mu\nu}$ is the stress energy tensor and $\tilde{T} = \tilde{T}_\mu{}^\mu$. We can now define the PPN parameters in the Einstein frame

$$\gamma - 1 = -\frac{2\tilde{\alpha}_0^2}{1 + \tilde{\alpha}_0^2} \tag{1.39}$$

$$\beta - 1 = \frac{1}{2}\tilde{\beta}_0 \frac{\tilde{\alpha}_0^2}{(1 + \tilde{\alpha}_0^2)^2} \tag{1.40}$$

where $\tilde{\alpha}_0 = \tilde{\alpha}(\varphi_0)$ and $\tilde{\beta}_0 = \tilde{\beta}(\varphi_0)$ are the asymptotic values of the parameters $\tilde{\alpha}$ and $\tilde{\beta}$ far from the source. As we will see later on, the Einstein frame is routinely used in numerical simulations since the field equations have a simpler form preferred for numerical analysis.

1.2.2 $f(R)$ theories of gravity

The second type of alternative theories of gravity that we study in this thesis is $f(R)$ theories of gravity. Such theories have existed since the 1960's. But during the last two decades these theories have grown in interest in an attempt to explain the accelerated expansion of the universe. Nowadays $f(R)$ theories are well established, and are considered a potential dynamical alternative to Dark Energy [20],[60]. Depending on the choice of $f(R)$, such theories can retain many of the successful features of General Relativity at solar-system and astrophysical scales, while introducing dramatically different features at cosmological scales.

The Einstein-Hilbert action

$$S = \frac{1}{2\kappa^2} \int d^4x \sqrt{-g}\, R + \int d^4x\, \mathcal{L}_M(g_{\mu\nu}, \psi_M), \tag{1.41}$$

is modified to

$$S = \frac{1}{2\kappa^2} \int d^4x \sqrt{-g} f(R) + \int d^4x\, \mathcal{L}_M(g_{\mu\nu}, \psi_M), \tag{1.42}$$

where $\kappa^2 = 8\pi G$ and $S_M = \int d^4x \mathcal{L}_M(g_{\mu\nu}, \psi_M)$ is the matter part of the action, which depends

on the metric $g_{\mu\nu}$ and the matter fields ψ_M.

We can obtain the field equations by varying the action with respect to the metric $g_{\mu\nu}$ as follows

$$f_R(R)R_{\mu\nu} - \frac{1}{2}f(R)g_{\mu\nu} - \nabla_\mu\nabla_\nu f_R(R) + g_{\mu\nu}\Box f_R(R) = \kappa^2 T_{\mu\nu}, \tag{1.43}$$

where $f_R(R) = f'(R)$ is the first derivative of f with respect to R and

$$T_{\mu\nu} = -\frac{2}{\sqrt{-g}}\frac{\delta\mathcal{L}_M}{\delta g^{\mu\nu}}. \tag{1.44}$$

It has been shown that the left hand side of equation (1.43) is divergence free, which implies

$$T^{\mu\nu}{}_{;\nu} = 0. \tag{1.45}$$

We can easily see that substituting $f(R) = R$, $f_R(R) = 1$ recovers the well known field equations of General Relativity. The trace of equation (1.43) is

$$f_R R + 3\Box f_R - 2f(R) = \kappa^2 T \tag{1.46}$$

When the stress energy tensor $T = 0$, the Ricci scalar R is no longer necessarily zero.

If there exists a point where the Ricci scalar is constant and $T_{\mu\nu} = 0$, equation (1.43) becomes

$$f_R R - 2f(R) = 0 \tag{1.47}$$

The root of equation (1.47) is $R = C$ and the maximally symmetric solution is de Sitter. If $C = 0$ the maximally symmetric solution is the Minkowski spacetime.

We can also rewrite the field equations in the Einstein equations form

$$G_{\mu\nu} = R_{\mu\nu} - \frac{1}{2}g_{\mu\nu}R = \frac{\kappa^2}{f_R}(T_{\mu\nu} + T^{eff}_{\mu\nu}), \tag{1.48}$$

where

$$T_{\mu\nu}^{eff} = \frac{1}{8\pi G} \left(\frac{f(R) - Rf_R}{2} + \nabla_\mu \nabla_\nu f_R - g_{\mu\nu}\Box f_R \right). \tag{1.49}$$

The simplest model that was first introduced was $f(R) = R + \alpha R^2$ [62] but it does not strongly affect large scale cosmological behavior. Once the acceleration of the expansion of the universe was well established, additional models were proposed in order to explain the said acceleration. One of the first choices to attempt to account for cosmological acceleration was [10],[11],[12],[51]

$$f(R) = R - \mu^4/R, \tag{1.50}$$

but it was then shown that the model suffered from instabilities [22]. One can show that the field equation with first order corrections for the curvature contains a term with a very large coefficient. The characteristic time of the instability is $\sim 10^{-26}$ sec, so the instability grows very fast and reaches high values. This motivated the derivation of the conditions required for a viable $f(R)$ theory.

A viable $f(R)$ theory must satisfy both cosmological observations and local gravity constraints. Amendola et al. [2] derived the conditions for a cosmologically viable $f(R)$ theory. The sequence of the cosmological eras dominated by radiation, then by matter, and finally by acceleration, must be preserved in such a theory. Starting with a spatially flat Friedmann-Lematre-Robertson-Walker spacetime, we consider the metric

$$ds^2 = -dt^2 + a(t)d\mathbf{x}^2 \tag{1.51}$$

The Ricci scalar becomes

$$R = 6(2H^2 + \dot{H}), \tag{1.52}$$

where $H = \dot{a}/a$ is the Hubble parameter. The stress energy tensor is that of a perfect fluid

$T^\mu_\nu = (-\rho_M, p_M, p_M, p_M)$. Considering non-relativistic equation for matter and radiation

$$\dot{\rho}_m + 3H\rho_m = 0 \tag{1.53}$$

$$\dot{\rho}_r + 4H\rho_r = 0 \tag{1.54}$$

the field equations (1.43) become

$$3f_R H^2 = (f_R R - f(R))/2 - 3H\dot{f}_R + \kappa^2(\rho_m + \rho_r) \tag{1.55}$$

$$-2f_R\dot{H} = \ddot{f}_R - H\dot{f}_R + \kappa^2(\rho_m + 4/3\rho_r) \tag{1.56}$$

We define the following variables

$$x_1 = \frac{\dot{f}_R}{Hf_R}, \; x_2 = \frac{-f}{6H^2 f_R}, \; x_3 = \frac{R}{6H^2}, \; x_4 = \frac{\kappa\rho_r}{3H^2 f_R} \tag{1.57}$$

plus the density parameters

$$\Omega_m = \frac{\kappa\rho_m}{3H^2 f_R} = 1 - x_1 - x_2 - x_3 - x_4, \; \Omega_r = x_4, \; \Omega_{DE} = x_1 + x_2 + x_3 \tag{1.58}$$

We derive the following system of equations

$$\frac{dx_1}{dN} = -1 - x_3 - 3x_2 + x_1^2 - x_1 x_3 + x_4 \tag{1.59}$$

$$\frac{dx_2}{dN} = \frac{x_1 x_3}{m} - x_2(2x_3 - 4 - x_1) \tag{1.60}$$

$$\frac{dx_3}{dN} = -\frac{x_1 x_3}{m} - 2x_3(x_3 - 2) \tag{1.61}$$

$$\frac{dx_4}{dN} = -2x_3 x_4 + x_1 x_4 \tag{1.62}$$

where $N = \ln a$ is the number of e-foldings and

$$m = \frac{d \ln f_R}{d \ln R} = \frac{R f_{RR}}{f_R} \tag{1.63}$$

$$r = \frac{d \ln f(R)}{d \ln R} = \frac{R f_R}{f(R)} \tag{1.64}$$

Finally, the effective equation of state of the system is

$$w_{eff} = -1 - 2\dot{H}/(3H^2) \tag{1.65}$$

An analysis of the above dynamical system reveals that the critical points (ignoring radiation, $x_4 = 0$), namely the points where the derivatives $\frac{dx_i}{dN}$ all become zero, are

$$
\begin{aligned}
P1: \quad & (x_1, x_2, x_3) = (0, -1, 2), \quad \Omega_m = 0, \quad w_{eff} = -1 \\[2mm]
P2: \quad & (x_1, x_2, x_3) = (-1, 0, 0), \quad \Omega_m = 2, \quad w_{eff} = 1/3 \\[2mm]
P3: \quad & (x_1, x_2, x_3) = (1, 0, 0), \quad \Omega_m = 0, \quad w_{eff} = 1/3 \\[2mm]
P4: \quad & (x_1, x_2, x_3) = (-4, 5, 0), \quad \Omega_m = 0, \quad w_{eff} = 1/3 \\[2mm]
P5: \quad & (x_1, x_2, x_3) = (\frac{3m}{1+m}, -\frac{1+4m}{2(1+m)^2}, \frac{1+4m}{2(1+m)}), \\[2mm]
& \Omega_m = 1 - \frac{m(7+10m)}{2(1+m)^2}, \quad w_{eff} = -\frac{m}{1+m} \\[2mm]
P6: \quad & (x_1, x_2, x_3) = (\frac{2(1-m)}{1+2m}, \frac{1-4m}{m(1+2m)}, -\frac{(1-4m)(1+m)}{m(1+2m)}), \\[2mm]
& \Omega_m = 0, \quad w_{eff} = \frac{2-5m-6m^2}{3m(1+2m)} \tag{1.66}
\end{aligned}
$$

The point P_5 can be identified as the matter-dominated epoch, for m close to zero. Points P_1 or P_6 can either be identified as the later accelerated epoch. The stability of the above fixed points is analyzed by considering only time-dependent linear perturbations around them. The trajectories that start from the saddle matter point P_5 and then approach the stable

14

points P_1 or P_6 can be considered viable. The stability analysis reveals that m needs to satisfy the condition

$$0 < m \leq 1 \tag{1.67}$$

Finally, we end up with two classes of models that are cosmologically viable.

Class A: Models that connect P_5 $(r \simeq 1, m \simeq +0)$ to P_1 $(r = 2, 0 < m \leq 1)$

Class B: Models that connect P_5 $(r \simeq 1, m \simeq +0)$ to P_6 $(m = r1, (\sqrt{3}1)/2 < m < 1)$.

According to the above analysis the models $f(R) = R + \alpha R^n$ and $f(R) = R - \mu^4/R$ are non-viable.

The models should also satisfy local gravity constraints. This is done by considering spherically symmetrical linear perturbations in a flat background metric [50],[53],[25],[60]

$$ds^2 = -[1 + 2\Psi(r)]dt^2 + a(t)[1 + 2\Phi(r)]dr^2 + r^2 d\Omega^2 \tag{1.68}$$

We write the Ricci scalar as

$$R(t,r) = R_0(t) + R_1(r) \tag{1.69}$$

where R_0 is the background curvature and R_1 is the perturbation to this background. We assume that the matter source has mass density $\rho(r)$ and negligible pressure. The trace equation (1.46) now becomes

$$\nabla^2 R_1 - m_f^2 R_1 = -\frac{\kappa\rho}{3f_{RR}(R_0)} \tag{1.70}$$

where

$$m_f^2 = \frac{f_R(R_0) - f_{RR}(R_0)}{3f_{RR}(R_0)}. \tag{1.71}$$

Since $0 < m(R_0) < 1$ as it was shown earlier (1.67), this means that $m_f^2 > 0$. Assuming the

the field is light, $m_f r \ll 1$, yields the solution

$$R_1 = \frac{\kappa M_s}{12\pi f_{RR}(R_0)r} \qquad , m_f r \ll 1 \tag{1.72}$$

where M_s is the total mass of the source. Using this assumption, we can solve the linearized field equations for the PPN potentials $\Psi(r)$ and $\Phi(r)$,

$$\Psi(r) \simeq -\frac{\kappa M_s}{6\pi f_R(R_0)r} \tag{1.73}$$

$$\Phi(r) \simeq \frac{\kappa M_s}{12\pi f_R(R_0)r}. \tag{1.74}$$

According to this solution we can calculate the Post-Newtonian parameter γ

$$\gamma = -\frac{\Phi(r)}{\Psi(r)} \simeq \frac{1}{2} \tag{1.75}$$

This violates the strict experimental bound on the parameter $|\gamma - 1| < 2.3 \times 10^{-5}$ which comes from the Cassini solar experiment. This would mean the non-viability of $f(R)$ theories. Fortunately, usually the condition $m_f r \ll 1$ is not satisfied. This is because of the chameleon mechanism [36],[37]. The effective mass of the scalar m_f depends on the density of the surroundings. When the matter density is high, the field also has a high effective mass, while in a low density cosmological environment the field acquires a light mass. In addition to these constraints, a viable model should satisfy [63]

$$f_{RR}(R) > 0, \tag{1.76}$$

which is needed to avoid tachyonic instabilities like the one appearing in model (1.50) and

$$f_R(R) > 0, \tag{1.77}$$

which guarantees the absence of ghost fields.

There exist now several viable models that satisfy both cosmological and local gravity constraints.

- The Hu and Sawicki model [33]

$$f(R) = R - \frac{\mu R_c (R/R_c)^{2n}}{(R/R_c)^{2n} + 1} \tag{1.78}$$

with $n, \mu, R_c > 0$.

- The Starobinsky model [63]

$$f(R) = R - \mu R_c \left[1 - \left(1 + \frac{R^2}{R_c^2} \right)^{-n} \right] \tag{1.79}$$

with $n, \mu, R_c > 0$.

- The Tsujikawa model [66]

$$f(R) = R - \mu R_c \tanh(R/R_c) \tag{1.80}$$

with $\mu, R_c > 0$.

- Recently, Miranda et al. [46] proposed another model

$$f(R) = R - \alpha R_c \ln(1 + R/R_c) \tag{1.81}$$

This is done by noting that the previous models can be seen as special cases of

$$f(R) = R - \mu R_s \left\{ 1 - \left[1 + \left(\frac{R}{R_c} \right)^n \right]^{-1/\mu} \right\} \tag{1.82}$$

then taking the limit $\mu \to \infty$.

All the above models satisfy the conditions (1.76), (1.77) and they show the correct behavior preserving the sequence of the cosmological eras, as it was described earlier on. These are the models that we are going to use later in our analysis in chapter 2.

1.3   Neutron stars

Neutron stars were first proposed by Baade and Zwicky in 1934. The idea was that there exist stars of very high density and small radius. In 1939, Oppenheimer and Volkoff constructed general relativistic models for such objects, assuming that the stars are composed of degenerate free neutrons at high densities. After these ideas were proposed physicists turned their attention to other fields of physics and neutron stars were mostly forgotten. The discovery of pulsars excited new interest for neutron stars. In 1967 a new radio telescope in Cambridge detected a radio source with a very precise period [32]. It was almost immediately proposed by Gold [29] that a highly rotating magnetized neutron star was the source of the radio signal. Soon after, the pulsar located in the Crab Nebula was discovered [57], which confirmed the proposition of Gold and in addition indicated that neutron stars are the remnants of supernovae explosions. In the following years new models were proposed for the structure and the evolution of neutron stars and the theoretical aspects of neutron stars, were extensively studied. Also, new, powerful radio telescopes helped in the continuous discovery of new pulsars and to this date about 2300 pulsars have been discovered.

Today the theoretical framework for neutron stars is well established. Neutron stars are believed to be the remnants of supernovae explosions. Their masses range from one to three solar masses, while the observed range is from about 1 solar mass to just over 2 solar masses, and their radii range roughly from $8\,\mathrm{km}$ to $16\,\mathrm{km}$. The gravitational binding energy of neutron stars is $\frac{M}{R} \sim 0.2$, much larger than that of normal stars. The spin periods of neutron stars can be as low as a few milliseconds and they can have magnetic fields that

reach values of 10^{12} G [43]. Thus, neutron stars are highly rotating relativistic stars and only fully relativistic models should be considered in order to study their properties. The fully relativistic equations that describe a neutron star either in General Relativity or in other metric theories of gravity are a system of non linear differential equations. Analytical solutions to such a system of equations are almost impossible to find, so we need to resort to numerical methods to solve the equations. A large number of numerical models with different numerical techniques have been developed in order to solve the field equations with high accuracy.

The internal structure of a neutron star remains unknown. The density of the matter in the center of a neutron star can exceed values of 10^{15} g cm^{-3}. The domain of such high densities is still unexplored, mostly because it is still not possible to test experimentally. However, various nuclear physics models have been proposed. The most prominent models suggest that the outer crust of a neutron star is composed of a lattice of iron ^{56}Fe. At densities higher than $\sim 10^{7}$ g cm^{-3} the nuclei become more neutron rich because of electron capture. The inner crust which starts at densities $\sim 10^{11}$ g cm^{-3} is mainly composed of free neutrons. These neutrons can be found in a superfluid phase, and some models suggest that certain phases of non-spherical nuclei are present at the bottom of the inner crust, that are called pasta phases [13]. Beyond densities of $\sim 10^{14}$ g cm^{-3} we have the core of the neutron star. It is the goal of nuclear physics to find an equation of state that describes the matter of the neutron star entirely, as we will see later on.

The macroscopic properties of neutron stars are measured by observing pulsar radios sources. As we already mentioned, it is well established that pulsars are highly magnetized rotating neutron stars. There are two different types of pulsars. The regular pulsars with periods $P \sim 0.5$ s that increase with rates $\dot{P} \sim 10^{-15}$ s/s and the millisecond pulsars with periods 1.4 ms $\lesssim P \lesssim 30$ ms that increase with rates $\dot{P} \sim 10^{-19}$ s/s. Models of binary systems show that millisecond pulsars have been spun up to such high speeds by accretion of

matter from an orbiting companion. The lifetime of regular pulsars is, as estimated crudely by $P/\dot{P} \sim 10^7$ yr while the millisecond pulsars have lifetimes close to the age of the Universe $\tau = 13.7$ Gyr. Using samples of a region near our solar system we can estimate the total number of regular and millisecond pulsars in our galaxy. Regular pulsars have a surface density of 156 ± 31 pulsars kpc^{-2} which corresponds to about 160,000 pulsars in our galaxy, while millisecond pulsars have a surface density of 38 ± 16 pulsars kpc^{-2} which corresponds to about 40,000 millisecond pulsars in our galaxy [43].

Of the neutron stars that can be observed, the most important ones are those found in compact binary star systems. Compact binary systems are the best tools to test General Relativity and other theories of gravity. The most interesting compact binaries are the ones containing a neutron star which is a radio pulsar, since the the orbital parameters of the system can be measured from pulsar timing observations. We define the following parameters [55]:

$$M = m_1 + m_2 \tag{1.83}$$

is the total mass of the system and

$$\mu = \frac{m_1 m_2}{M} \tag{1.84}$$

is the reduced mass of the system. Also,

$$\eta = \frac{m_1 m_2}{M^2} \tag{1.85}$$

is the symmetric mass ratio and

$$\mathcal{M} = \eta^{3/2} M = \mu^{3/5} M^{2/3} \tag{1.86}$$

is the chirp mass. The post-Keplerian parameters of the system such as the orbital period's derivative $\dot{P}_b$, the advance of the periaston $\dot{\omega}$, the gravitational redshift γ, the range of the

Shapiro delay r and the angle of inclination i are given in General Reletivity by [43]

$$\dot{\omega} = 3 \left(\frac{P_b}{2\pi}\right)^{-5/3} (T_\odot M)^{2/3} (1 - e^2)^{-1} \tag{1.87}$$

$$\gamma = e \left(\frac{P_b}{2\pi}\right)^{1/3} T_\odot^{2/3} M^{-4/3} m_2 (m_1 + 2m_2) \tag{1.88}$$

$$\dot{P_b} = -\frac{192\pi}{5} \left(\frac{P_b}{2\pi}\right)^{-5/3} T_\odot^{5/3} m_1 m_2 M^{-4/3} \left(1 + \frac{73}{24}e^2 + \frac{37}{96}e^4\right) (1 - e^2)^{-7/2} \tag{1.89}$$

$$\sin i = x \left(\frac{P_b}{2\pi}\right)^{-2/3} T_\odot^{-1/3} M^{2/3} m_2^{-1} \tag{1.90}$$

$$r = T_\odot m_2 \tag{1.91}$$

where e is the eccentricity, $T_\odot = GM_\odot/c^3 = 4.925490947 \ \mu s$ and $x = a \sin i$ is the projected semi-major axis. Measurements of these relativistic effects in a variety of binary pulsar systems have shown excellent agreement with general relativity, including the existence of gravitational radiation, whose emission leads to the decrease of orbital period [72].

We can now compute the gravitational waveforms emitted by a binary system of such compact objects, in various theories of gravity. More specifically, in General Relativity the waveform polarization modes are given by [40], [55]

$$h^+ = -\frac{2\mu M}{Dr}(1 + \cos^2 i) \cos 2\Phi \tag{1.92}$$

$$h^\times = -\frac{4\mu M}{Dr} \cos i \sin 2\Phi \tag{1.93}$$

where D is the distance to the source, r is the orbital separation and Φ is the orbital phase.

On the other hand, in FJBD theory they are given by [14]

$$h^+ = -\left(1 - \frac{1}{2}\xi\right)\frac{2\mu MG}{Dr}(1 + \cos^2 i)\cos 2\Phi \tag{1.94}$$

$$h^\times = -\left(1 - \frac{1}{2}\xi\right)\frac{4\mu MG}{Dr}\cos i \sin 2\Phi \tag{1.95}$$

plus a scalar amplitude (often called a "spin-0" or breathing amplitude), given by

$$h^S = -2\xi\frac{G\mu}{D}\left(\frac{GM}{r}\right)^{1/2}(s_1 - s_2)\sin i \cos \Phi, \tag{1.96}$$

where

$$\xi = \frac{1}{2 + \omega} \tag{1.97}$$

and

$$G = 1 - \xi(s_1 + s_2 - 2s_1s_2). \tag{1.98}$$

The quantities s_1 and s_2 are called the "sensitivities" of the two inspiraling bodies. These quantities measure the sensitivity of the mass of each body to variations in the value of the external scalar field, which controls the gravitational binding energy of each body. This difference in the waveforms should be measurable by the next generation gravitational wave detectors which means that we should be able to constrain the value of the parameter ω of the FJBD theory. The same analysis can be applied to constrain the parameters of other theories of gravity.

The simplest model one can choose to describe a neutron star is that of a static, spherically symmetric star. In General Relativity, the metric of the spacetime of such a star is given by [47]

$$ds^2 = -e^{2\Phi(r)}dt^2 + e^{2\Lambda(r)}dr^2 + r^2d\Omega^2 \tag{1.99}$$

where

$$d\Omega^2 = d\theta^2 + \sin^2\theta d\phi^2. \tag{1.100}$$

The two functions $\Phi(r)$ and $\Lambda(r)$ are to be determined by solving the field equations. The next equation that needs to be defined is the stress-energy tensor of the matter inside the star. We can model the matter of the star as a perfect fluid, to a very good accuracy. The stress energy tensor of a perfect fluid is

$$T^{\mu\nu} = [\rho(r) + p(r)]u^\mu u^\nu + p(r)\, g^{\mu\nu} \tag{1.101}$$

where u^μ is the 4-velocity of the fluid and $\rho(r)$ and $p(r)$ are the density and the pressure of the fluid respectively. The final equation that needs to be provided is the relation between the density $\rho(r)$ and the pressure $p(r)$. This is called the equation of state (EoS). The true equation of state of a neutron star remains unknown. Several nuclear physics motivated models for the equation of state have been proposed as we will see later on this chapter.

We now have all the necessary equations to proceed in our solution. Here it is convenient to rewrite the function $\Lambda(r)$ as

$$e^{2\Lambda} = \left(1 - \frac{2m(r)}{r}\right)^{-1} \tag{1.102}$$

where $m(r)$ is a new function that plays the role of the mass, as will be obvious from our solution. Starting with the $_{tt}$ component of the Einstein equations, we find

$$\frac{dm}{dr} = 4\pi r^2 \rho(r) \tag{1.103}$$

Integrating this from the center of the star to its radius $r = R$ will give us the total mass of

the star. Now, using the $_{rr}$ component of the Einstein equations we find

$$\frac{d\Phi}{dr} = \frac{m + 4\pi r^3 p}{r(r - 2m)} \tag{1.104}$$

Finally, using the energy-momentum conservation equation $T^{\mu\nu}{}_{;\nu} = 0$ we have

$$\frac{dp}{dr} = -(p + \rho)\frac{d\Phi}{dr} \tag{1.105}$$

Substituting equation (1.105) in equation (1.104) we get the final expression

$$\frac{dp}{dr} = -\frac{(\rho + p)(m + 4\pi r^3 p)}{r(r - 2m)}. \tag{1.106}$$

This is the TOV equation, discovered by Tolman [65] and independently by Oppenheimer and Volkoff [54] in 1939 and describes the structure of a static, spherically symmetric star in General Relativity. In order to solve the equation, one needs to provide initial conditions for the quantities $m(r)$, $p(r)$ and $\Phi(r)$ at the center of the star, in addition to an EoS. One then integrates the equation outwards until the pressure vanishes, which denotes the surface of the star. The TOV equation guarantees that the pressure will decrease monotonically as long as $p \geq 0$ and $\rho \geq 0$. In the case of a constant density star the equation has an analytic solution. For a more realistic EoS the equation can only be solved by using numerical methods. This is the basic scheme that we use to construct models of neutron stars in this thesis, but modified for alternative theories of gravity, as we will see in chapter 2.

The previous analysis is done for static stars, but as we already discussed, real neutron stars rotate rapidly. Thus, we need to extend our analysis to include rotation. The metric that describes the spacetime of a rotating star is stationary and axisymmetric. The most

general form for the line element of such a metric is

$$ds^2 = g_{00}dt^2 + 2g_{01}dtd\phi + g_{11}d\phi^2 + g_{22}(dx^2)^2 + g_{23}dx^2dx^3 + g_{33}(dx^3)^2. \qquad (1.107)$$

By exploiting the freedom to choose coordinates, we can rewrite the line element in a more commonly used form

$$ds^2 = -e^{2\nu}dt^2 + e^{2\psi}(d\phi - \omega dt)^2 + e^{2\mu}(dr^2 + r^2d\theta^2) \qquad (1.108)$$

where we usually set

$$e^\psi = r\sin\theta B e^{-\nu}. \qquad (1.109)$$

The functions μ, ν, ω, ψ and B depend only on r and θ. Hartle [30] rewrote the metric in a different form and by only keeping first order terms in the the angular velocity of the star Ω he derived a formalism to numerically treat slowly rotating neutron stars. This slow rotation formalism is able to describe most regular and millisecond pulsars, but fails to describe rapidly rotating stars near the mass-shedding limit. Since then, a lot more complicated numerical schemes have been proposed. For a review of numerical schemes of rapidly rotating relativistic stars see [64].

1.3.1 Equation of state

The true equation of state for the matter inside a neutron star remains unknown. One wishes to determine the EoS of $\sim 10^{57}$ baryons, which corresponds to about one solar mass. The state of the lowest energy of such high numbers of baryons corresponds to multiple $^{56}_{26}$Fe nuclei, since this is the nucleus with the largest (negative) binding energy per unit mass. In addition, relativistic electrons combine with protons to form neutrons by inverse beta decay. As the density increases, the neutron to proton ratio becomes higher until a critical

value is reached, which is called "neutron drip", because the neutrons start escaping from the nucleus and become free. If we keep increasing the density the baryons form a neutron gas, whose quantum degeneracy provides the pressure of the system.

The EoS for densities below the neutron drip density is well understood [59]. One starts with the EoS of an ideal Fermi gas of electrons, which for the limiting cases can be written as

$$P = K\rho_0^\Gamma \tag{1.110}$$

where, for non-relativistic neutrons, $\rho_0 \ll 10^6 \, \mathrm{g \, cm^{-3}}$, $\Gamma = 5/3$,

$$K = \frac{3^{2/3}\pi^{4/3}}{5} \frac{\hbar^2}{m_e m_u^{5/3} \mu_e^{5/3}} = \frac{1.0036 \times 10^{13}}{\mu_e^{5/3}} \, \mathrm{cgs} \tag{1.111}$$

for extremely relativistic neutrons, $\rho_0 \gg 10^6 \, \mathrm{g \, cm^{-3}}$, $\Gamma = 4/3$,

$$K = \frac{3^{1/3}\pi^{2/3}}{5} \frac{\hbar c}{m_u^{4/3} \mu_e^{4/3}} = \frac{1.2435 \times 10^{15}}{\mu_e^{4/3}} \, \mathrm{cgs} \tag{1.112}$$

where m_u is the atomic mass unit and μ_e is the mean molecular weight per electron. As we move into a higher density region, certain corrections need to be applied if a more realistic EoS is to be obtained. The most important corrections are due to electrostatic interactions and inverse beta decay. We can write the total energy density as

$$\varepsilon = n_N M(A, Z) + \varepsilon_e'(n_e) + \varepsilon_n(n_n) \tag{1.113}$$

where, n_N, n_e, n_n are the number densities of nuclei, electrons and neutrons respectively. The function $M(A, Z)$ is the energy of the nucleus and it is given by a semi-empirical formula. The energy of free electrons, ϵ_e and the energy of free neutrons ϵ_n are known functions of the Fermi momentum from Statistical Mechanics. Here, the rest energy of the electrons is included in $M(A, Z)$ so the remainder is denoted by ε_e'. When below the neutron drip, the

free neutron energy can be set to zero. Then, one finds the values of A and Z that minimize the energy of the nucleus and solves for the Fermi momentum. This determines the density $\rho = \varepsilon/c^2$ and the pressure P.

For densities above the neutron drip, the EoS is not well known. At such high densities the nuclei merge in a sea of baryons. Latimer et al [42] summarize the different approaches used to describe the EoS above the neutron drip. The first approach is non-relativistic potential models. Here, the potential of the Hamiltonian is fitted to nucleon-nucleon scattering data. The short-range correlations are treated by a variational method. The second approach involves field-theoretical models. The Lagrangian has both baryon and meson degrees of freedom and starting with a mean field approximation additional effects such as vacuum fluctuations are later taken into account. This approach sacrifices the connection to nucleon-nucleon scattering data. The third approach is the relativistic Dirac-Brueckner-Hartree-Fock approach. Here, the self-energy of a nucleon is assumed to be the sum of two large potentials. The first potential is an attractive scalar potential and the second is a repulsive vector potential. Then, the nucleon-nucleon potential is calculated by the use of the nucleon spinors that are solution of the Dirac equation. The nucleon self-energy is calculated in the Brueckner-Hartree-Fock approximation. As we will see in Chapter 2, for our calculation, we selected equations of state from all 3 approaches.

Chapter 2

Theoretical framework

In this chapter we establish the structure equations for a neutron star in both Scalar Tensor theories and $f(R)$ theories of gravity. This is done by solving the field equations under certain assumptions about the spacetime inside the star. In the case of Scalar Tensor theories, we define the 'sensitivities' of a neutron star, which are to be calculated numerically. We also provide the boundary conditions for our set of equations; these turn out to be rather subtle in the case of $f(R)$ theories. Finally, we discuss the various equations of state for the matter in the neutron stars, which are used when we solve the equations numerically. At the end, all the necessary equations for numerically analysis will be established and we will be ready to proceed with our numerical treatment.

2.1   Scalar tensor theories

We start our study with Scalar Tensor theories of gravity. First, we derive the structure equations for FJBD theory in the Jordan, frame the convention representation of these theories as "metric" theories of gravity. This is done to outline the necessary steps required to derive the structure equations, even though this particular set of equations will not be used for numerical analysis. Then, we show the structure equations in the Einstein frame,

where the representation of the equation is better suited to numerical analysis. This is done for both a static and a slowly rotating metric. The matching of the interior metric of the neutron star, which is calculated numerically, to the exterior metric, which is known in closed form, provides a set of equations for all the physical quantities of the star. Also, a subset of the equations of state discussed at the end of this section is used in our analysis of $f(R)$ theories.

2.1.1 Field equations

We derive now the structure equations for a static spherically symmetric star in the Jordan frame for the FJBD theory. The process is similar to the one described in Chapter 1 for the case of General Relativity. We start with the field equations. The field equations for FJBD theory are a special case of the equations (1.14) and (1.16) with $\omega' = \lambda = 0$ [70].

$$R_{\mu\nu} - \frac{1}{2}g_{\mu\nu}R = \frac{8\pi}{\phi}T_{\mu\nu} + \frac{\omega}{\phi^2}(\phi_{,\mu}\phi_{,\nu} - \frac{1}{2}g_{\mu\nu}\phi_{,\lambda}\phi^{,\lambda}) + \frac{1}{\phi}(\phi_{,\mu;\nu} - g_{\mu\nu}\Box\phi) \qquad (2.1)$$

$$\Box\phi = \phi^{,\mu}_{;\mu} = \frac{1}{\sqrt{-g}}(\sqrt{-g}\phi^{,\mu})_{,\mu} = \frac{8\pi T}{3 + 2\omega} \qquad (2.2)$$

The metric describing the spacetime is a static, spherically symmetric metric

$$ds^2 = -e^{2\Phi(r)}dt^2 + e^{2\Lambda(r)}dt^2 + r^2 d\Omega^2, \qquad e^{2\Lambda} = \left(1 - \frac{2m(r)}{r}\right)^{-1} \qquad (2.3)$$

where $\phi(r)$ and $m(r)$ are the metric functions to be determined, and the coordinate r is interpreted as the proper circumference/2π of a circle of fixed r and t. We model the matter inside the star as a perfect fluid. The stress-energy tensor of the fluid is given by

$$T^{\mu\nu} = (\rho + p)u^\mu u^\nu + pg^{\mu\nu} \qquad (2.4)$$

We now express the field equations under the previous assumptions. The equations take the form

$$\frac{dm}{dr} = 4\pi r^2 \left[\frac{\rho}{\phi} + \frac{\omega \phi_{,r}^2}{16\pi \phi^2} \left(1 - \frac{2m}{r} \right) - \frac{3p - \rho}{\phi(2\omega + 3)} \right] \tag{2.5}$$

$$\frac{d\Phi}{dr} = \frac{1}{r(r - 2m)} \left[m + \frac{4\pi r^3 p}{\phi} - \frac{\phi_{,r}^2 \omega r^3}{4\phi^2} \left(1 - \frac{2m}{r} \right) \right] \tag{2.6}$$

$$\phi_{,rr} + \phi_{,r} \left(\frac{2}{r} + \Phi' - \Lambda' \right) = \frac{8\pi r(3p - \rho)}{(r - 2m)(2\omega + 3)} \tag{2.7}$$

Using the energy-momentum conservation equation $T^{\mu\nu}_{\;;\nu} = 0$ we have

$$\frac{dp}{dr} = -(p + \rho)\frac{d\Phi}{dr} \tag{2.8}$$

We substitute equation (2.7) into equation (2.8) to get

$$\frac{dp}{dr} = -\frac{(p + \rho)}{r(r - 2m)} \left[m + \frac{4\pi r^3 p}{\phi} - \frac{\phi_{,r}^2 \omega r^3}{4\phi^2} \left(1 - \frac{2m}{r} \right) \right] \tag{2.9}$$

Finally, substituting the first two equations (2.5)) and (2.6) into the third one (2.7) we get

$$\phi_{,rr} = \left(\frac{r\omega \phi_{,r}^2}{2\phi^2} - \frac{2 \left(2\pi r^3(\rho - p) - \phi r + m\phi \right)}{(2m - r)r\phi} \right) \phi_{,r} + \frac{4\pi r(3p - \rho)(r\phi_{,r} - 2\phi)}{(2m - r)\phi(2\omega + 3)} \tag{2.10}$$

Equations (2.5), (2.9) and (2.10) are the desired set of equations to be used for numerical analysis. An equation of state will be required as well for the set of equations to be complete. We also define here the total baryon number

$$N = \int_0^R 4\pi n r^2 \left(1 - \frac{2m}{r} \right)^{-1/2} dr \tag{2.11}$$

where $r = R$ is the surface of the star and n the baryon density. It has been found, this set of equations is not ideal for numerical analysis. The set of equations obtained in the Einstein frame is more suitable for numerical analysis.

30

2.1.2 Einstein frame

In this section we formulate the equations in the Einstein frame and also generalize from FJBD theory to the full range of scalar-tensor theories. As we have already seen in chapter 1, the Einstein frame is a non-metric representation of the Scalar Tensor theory, where the action is put in a form that resembles that of General Relativity. The field equations derived from the action (1.33) are given by equations (1.37) and (1.38). Also, the conformal transformation between the Einstein frame and the Jordan frame is described by equations (1.34), (1.35) and (1.36). Again, we use a static and spherically symmetric metric, given by (2.3). Finally the matter is assumed to be a perfect fluid with the stress energy tensor (2.4). Now, expressing the field equations under the above assumptions we obtain the following set of equations [18]

$$M' = \frac{\kappa^2}{2} r^2 A^4(\varphi)\rho + \frac{1}{2}r(r - 2M)\psi^2 \tag{2.12}$$

$$\nu' = \kappa^2 \frac{r^2 A^4(\varphi)p}{r - 2M} + r\psi^2 + \frac{2M}{r(r - 2M)} \tag{2.13}$$

$$\varphi' = \psi \tag{2.14}$$

$$\psi' = \frac{\kappa^2}{2} \frac{r A^4(\varphi)}{r - 2M}[\alpha(\varphi)(\rho - 3p) + r\psi(\rho - p)] - \frac{2(r - M)}{r(r - 2M)}\psi \tag{2.15}$$

$$p' = -(\rho + p)\left[\frac{\kappa^2}{2} \frac{r^2 A^4(\varphi)p}{r - 2M} + \frac{1}{2}r\psi^2 + \frac{M}{r(r - 2M)} + \alpha(\varphi)\psi\right] \tag{2.16}$$

$$\tag{2.17}$$

where primed quantities denote a differentation with respect to r. We have defined the auxiliary field $\psi = \phi'$ in order to recast the equations as a set of first-order differential equations, which lend themselves naturally to numerical integration schemes. We have defined here $M(r) \equiv m(r)$ and $\nu(r) \equiv 2\Phi(r)$ to follow the notation of Damour and Esposito-Farese [18].

31

We also find it useful to define the baryonic mass $\bar{M}(r)$, given by integrating

$$\bar{M}' = 4\pi m_b n A^3(\varphi) \frac{r^2}{\sqrt{1 - 2M/r}} \tag{2.18}$$

from the center of the star to a chosen value of r.

The choice of the coupling function $A(\varphi)$ defines a specific theory. FJBD theory corresponds to the coupling function

$$A(\varphi) = e^{\tilde{\alpha}\varphi} \tag{2.19}$$

with $\tilde{\alpha} = \tilde{\alpha}_0$, a constant, which corresponds to $\omega(\phi) = const$. As we will see later, other choices give more interesting theories, with results that are significantly different from General Relativity.

In order to have a complete set of equations, ready for numerical analysis, we also need to provide the boundary conditions for our system of equations, as well as an equation of state, which relates the pressure and density inside the star. However, first we turn our attention to some quantities called 'sensitivities' of the neutron star, which we wish to calculate numerically.

2.1.3 Sensitivities

In Scalar Tensor theories, the scalar field ϕ produces an external influence on the structure of a compact body. The scalar field is directly related to the value of gravitational constant G, as we saw in (1.17).Thus, the mass of each body can be regarded as a function of $\ln G$. Now, we can expand the field ϕ in a series, around its asymptotic value ϕ_0 in the weak field limit [70]. So the field is given by

$$\phi = \phi_0 + \Delta\phi \tag{2.20}$$

and the mass of a compact body A is given by

$$m_A(\phi) = m_A(\ln G) \tag{2.21}$$

$$= m_{A0} - \left(\frac{\partial m_A}{\partial \ln G}\right)_0 \left[\frac{\Delta\phi}{\phi_0} - \frac{1}{2}\left(\frac{\Delta\phi}{\phi_0}\right)^2\right] \tag{2.22}$$

$$+ \frac{1}{2}\left(\frac{\partial^2 m_A}{\partial \ln G^2}\right)_0 \left(\frac{\Delta\phi}{\phi_0}\right)^2 + O\left(\frac{\Delta\phi}{\phi_0}\right)^3 \tag{2.23}$$

We define the quantities

$$s_A = -\left(\frac{\partial \ln m_A}{\partial \ln G}\right)_0 \tag{2.24}$$

$$s_A' = -\left(\frac{\partial^2 \ln m_A}{\partial \ln G^2}\right)_0 \tag{2.25}$$

$$\tag{2.26}$$

These are called the sensitivities of the compact body A, since they characterize the sensitivity of its mass to changes in G or in ϕ. Then, we can write

$$m_A(\phi) = m_A[1 + s_A(\Delta\phi/\phi_0) - \frac{1}{2}(s_A' - s_A^2 + s_A)(\Delta\phi/\phi_0)^2 + O(\Delta\phi/\phi_0)^3] \tag{2.27}$$

Since the mass of the body depends on the sensitivities s_a, these quantities enter all the post-Newtonian equations of motion for gravitationally self-bound bodies, as well as in the gravitational waveform, and in formulae for gravitational radiation reaction. See for example . In order to do calculations we need to be provided with the value of the sensitivities beforehand. So, we need an independent method of calculating the sensitivities of the compact bodies.

In a first approximation the sensitivity s ~ [gravitational binding energy]/[mass]. That means the value of s for a body like Earth is $s_\oplus \sim 10^{-10}$, for the Sun it is $s_\odot \sim 10^{-6}$ and for

a white dwarf it is $s_{WD} \sim 10^{-3}$. Since these values are several orders of magnitude smaller than unity, they can be ignored in many calculations. On exception is the Earth-Moon system, where the effect of these sensitivities in scalar-tensor theory has led to a strong test of such theories using lunar laser ranging. However, for neutron stars, the sensitivities are of order of unity [44], so an explicit calculation is required. Assuming an EOS for the neutron star of the form $p = p(\rho)$, we can uniquely determine a model by fixing the asymptotic value of G (or ϕ), asymptotically flat conditions on the metric, and the central density ρ_c. We need to compute the sensitivity s holding the baryon number fixed. It can be shown that

$$s = -\left(\frac{\partial \ln m}{\partial \ln G}\right)_N = \left(\frac{\partial \ln m}{\partial \ln G}\right)_{\rho_c} + \left(\frac{\partial \ln m}{\partial \ln N}\right)_G \left(\frac{\partial \ln N}{\partial \ln G}\right)_{\rho_c} \tag{2.28}$$

In this thesis we will also use the following sensitivities

$$\hat{s}_A = \left(\frac{\partial \ln m}{\partial \ln \phi}\right)_0 \tag{2.29}$$

$$\hat{s}_A' = \left(\frac{\partial \hat{s}_A}{\partial \ln \phi}\right)_0 \tag{2.30}$$

It can be shown that the two different sensitivities are related by

$$\hat{s}_A = s_A \left(1 + \frac{2\omega_0' \phi}{(3 + 2\omega_0)(4 + 2\omega_0)}\right) \tag{2.31}$$

In the case of FJBD theory, $\omega' = 0$, so the two sensitivities are equal, $\hat{s}_A = s_A$.

In the Einstein frame we use equivalent quantities that play the role of sensitivities. Here, we follow the definitions of Damour and Esposito-Farese [17]. We define

$$\alpha_A = \frac{\partial \ln \tilde{m}_A}{\partial \varphi_0} \tag{2.32}$$

$$\beta_A = \frac{\partial \alpha_A}{\partial \varphi_0} \tag{2.33}$$

Here $\tilde{m}_A$ is the mass of the star in the Einstein frame. We need to note that the mass in the Jordan frame and the mass in the Einstein frame are not the same, but they are related by

$$\tilde{m}_A = A(\varphi)m_A \tag{2.34}$$

Using the definitions (1.34), (1.35) and (1.36) we can relate the Jordan frame sensitivities to the Einstein frame sensitivities. We can show that

$$\hat{s}_a = \frac{\tilde{\alpha} - \alpha_A}{2\tilde{\alpha}} \tag{2.35}$$

$$\hat{s}'_a = \frac{1}{4\tilde{\alpha}^2}\left(\beta_A - \frac{\tilde{\beta}}{\tilde{\alpha}}\alpha_A\right) \tag{2.36}$$

Here, following Damour and Esposito-Farese [17] we show a rough estimate of the sensitivity of a neutron star, using data from General Relativity. First, we define the fractional binding energy of a neutron star

$$f \equiv \frac{\bar{m} - m}{m} > 0 \tag{2.37}$$

where $\bar{m}$ is the total baryonic mass. Also, we define

$$c_A = -2\frac{\partial \ln m}{\partial \ln G} = 2s_a \tag{2.38}$$

Keeping the EoS fixed, f depends only on the combination $G^{3/2}\bar{m}$. It then can be shown that

$$c_A = 3\left(\frac{\partial f}{\partial \bar{m}}\right)_A m_A \tag{2.39}$$

The fractional binding energy f, for most analytic equations of state, depends linearly on the total baryonic mass. This leads to a simple relation between c_A and m_A,

$$c_A = km_A \tag{2.40}$$

where the slope k depends on EoS. Damour and Esposito-Farese found that an average value for the slope was $k = 0.21 M_\odot^{-1}$. This gives, for a typical mass of $m_A = 1.4\ M_\odot$, a value $s_A = 0.147$.

2.1.4   Slowly rotating star

We will now derive the structure equations for a slowly rotating neutron star in Scalar Tensor theory. We will only use the Einstein frame equations. Again, here we follow Damour and Esposito-Farese [19]. We have already established the field equations (1.37), (1.38) in a previous section. The metric describing the spacetime, as given by Hartle [30], is the following

$$ds^2 = -e^{\nu(r)}dt^2 + e^{\mu(r)}dr^2 + r^2 d\theta^2 + r^2 \sin^2\theta \left(d\phi + [\omega(r,\theta) - \Omega]dt\right)^2. \qquad (2.41)$$

Here, we only keep first order terms in angular velocity $\Omega = u^\phi/u^t$, so the non-diagonal components of the metric tensor all vanish except $g_{t\phi}$. The stress-energy tensor describing the perfect fluid is

$$T_{\mu\nu} = (\rho + p)u_\mu u_\nu + p g_{\mu\nu} \qquad (2.42)$$

Solving the equations, under these assumptions, we derive the structure equations, which are the same as with the static case, with two additional equations for the quantity ω and

its derivative. The final set of equations is the following

$$M' = \frac{\kappa^2}{2}r^2 A^4(\varphi)\tilde{\rho} + \frac{1}{2}r(r - 2M)\psi^2 \tag{2.43}$$

$$\nu' = \kappa^2 \frac{r^2 A^4(\varphi)\tilde{p}}{r - 2M} + r\psi^2 + \frac{2M}{r(r - 2M)} \tag{2.44}$$

$$\varphi' = \psi \tag{2.45}$$

$$\psi' = \frac{\kappa^2}{2} \frac{r A^4(\varphi)}{r - 2M}[\alpha(\varphi)(\tilde{\rho} - 3\tilde{p}) + r\psi(\tilde{\rho} - \tilde{p})] - \frac{2(r - M)}{r(r - 2M)}\psi \tag{2.46}$$

$$p' = -(\rho + p)\left[\frac{\kappa^2}{2} \frac{r^2 A^4(\varphi)\tilde{p}}{r - 2M} + \frac{1}{2}r\psi^2 + \frac{M}{r(r - 2M)} + \alpha(\varphi)\psi\right] \tag{2.47}$$

$$\omega' = \varpi \tag{2.48}$$

$$\varpi' = \frac{\kappa^2}{2} \frac{r^2}{r - 2M} A^4(\varphi)(\tilde{\rho} + \tilde{p})\left(\varpi + \frac{4\omega}{r}\right)$$

$$+ \left(\psi^2 r - \frac{4}{r}\right)\varpi \tag{2.49}$$

$$\tag{2.50}$$

Because we are working to first order in rotation, the equations for ω and its derivative decouple from the other equations. Again, we need to include the quantity $\bar{M}(r)$, the radial distribution of the baryonic mass, given by (2.18).

2.1.5 Matching conditions

In both cases of static, or slowly rotating metric, the numerical integration can continue after the surface of the star, where the pressure becomes zero. However, the solution for the outer region of the star where $T_{\mu\nu} = 0$, is already known in closed form. We can match the inner solution to the outer solution by using the correct boundary conditions. The metric

for the outer solution is [17],[15]

$$ds^2 = -e^\nu dt^2 + e^{-\nu}[d\xi^2 + e^\lambda(d\theta^2 + \sin^2\theta d\phi^2)] \tag{2.51}$$

$$e^\lambda = \xi^2 - a\xi \tag{2.52}$$

$$e^\nu = \left(1 - \frac{a}{\xi}\right)^{b/a} \tag{2.53}$$

$$\varphi(r) = \varphi_0 + \frac{d}{a}\ln\left(1 - \frac{a}{\xi}\right) \tag{2.54}$$

where a, b and d are integration constants satisfying the relation $a^2 - b^2 = 4d^2$ and d is another constant. These coordinates are related to the Schwarzschild coordinates used earlier by

$$r = \xi\left(1 - \frac{a}{\xi}\right)^{(a-b)/2a} \tag{2.55}$$

$$e^\mu = \left(1 - \frac{a}{\xi}\right)\left(1 + \frac{a+b}{2\xi}\right)^{-2}. \tag{2.56}$$

The parameters a, b and d can be expressed in terms of the total mass m_A and the coupling constant α_A from (2.33).

$$b = 2\frac{G}{c^2}m_A \tag{2.57}$$

$$\frac{b}{a} = (1 + \alpha_A^2)^{1/2} \tag{2.58}$$

$$\frac{d}{b} = \frac{1}{2}\alpha_A \tag{2.59}$$

Now, it has been shown that using the previous equations, all the physical quantities of the star can be expressed in terms of the values of the metric components and their derivatives

at the surface of the star [19]. We define

$$R \equiv r_s \tag{2.60}$$

$$\alpha_A \equiv \frac{2\psi_s}{\nu_s'} \tag{2.61}$$

$$Q_1 \equiv (1 + \alpha_A^2)^{1/2} \tag{2.62}$$

$$Q_2 \equiv \left(1 - \frac{2M_s}{R}\right)^{1/2} \tag{2.63}$$

$$\hat{\nu}_s \equiv -\frac{2}{Q_1} \tanh^{-1}\left(\frac{Q_1}{1 + 2(R\nu_s')^{-1}}\right) \tag{2.64}$$

$$\tag{2.65}$$

We then have

$$\nu_s' = R\psi_s + \frac{2M_s}{R(R - 2M_s)} \tag{2.66}$$

$$\alpha_A = \frac{2\psi_s}{\nu_s'} \tag{2.67}$$

$$\varphi_0 = \varphi_s - \frac{1}{2}\alpha_A\hat{\nu}_s \tag{2.68}$$

$$m_A = \frac{1}{2}\nu_s' R^2 Q_2 e^{\frac{1}{2}\hat{\nu}_s} \tag{2.69}$$

$$\bar{m}_A = \bar{M}_s \tag{2.70}$$

Specifically for the slowly rotating case, we have some additional quantities

$$J_A = \frac{1}{6}\varpi_s' R^4 Q_2 e^{-\frac{1}{2}\hat{\nu}_s} \tag{2.71}$$

$$\Omega = \omega_s - \frac{3J_A}{4m_A^3(3 - \alpha_A^2)}\left\{e^{\hat{\nu}_s} - 1 + \frac{4m_A}{R}e^{\hat{\nu}_s}\right. \tag{2.72}$$

$$\left. \times \left[\frac{2m_A}{R} + e^{\frac{1}{2}\hat{\nu}_s}\cosh\left(\frac{1}{2}Q_1\hat{\nu}_s\right)\right]\right\}$$

$$I_A = \frac{J_A}{\Omega} \tag{2.73}$$

Finally, to be able to solve the equations numerically, we need to provide the initial conditions in the center of the star. The point $r = 0$ is difficult to be treated by the code since $1/r$ terms appear in some expressions. Thus, we set the initial conditions at a point very close to the origin, $r = \Delta r$, which usually is equal to the step size of our numerical integration. We achieve this by Taylor expanding our quantities around $r = 0$. This yields [19]

$$M(\Delta r) = 0 \tag{2.74}$$

$$\nu(\Delta r) = 0 \tag{2.75}$$

$$\varphi(\Delta r) = \varphi_c \tag{2.76}$$

$$p(\Delta r) = p_c \tag{2.77}$$

$$\psi(\Delta r) = \frac{4\pi}{3}\Delta r \, A^4(\varphi_c)\alpha(\varphi_c)(\rho_c - 3p_c) \tag{2.78}$$

$$\bar{M}(\Delta r) = 0 \tag{2.79}$$

Again, for the slowly rotating case we also need

$$\omega(\Delta r) = 1 \tag{2.80}$$

$$\varpi(\Delta r) = \frac{16\pi}{5}\Delta r \, A^4(\varphi_c)\omega(\Delta r)(\rho_c + p_c) \tag{2.81}$$

2.1.6   Equation of state

As we have already discussed, in order to have a complete set of equations for numerical analysis, an EoS needs to be provided. Since the true EoS for the matter inside a neutron star is not known, we will have to use approximation for our EoS. The most common approximate EoS that is used widely in numerical analysis is a polytropic EoS. The EoS is defined by the

equations

$$\rho = m_b n + \frac{K m_b n_0}{\Gamma - 1} \left(\frac{n}{n_0} \right)^{\Gamma} \tag{2.82}$$

$$p = K m_b n_0 \left(\frac{n}{n_0} \right)^{\Gamma} \tag{2.83}$$

These two equations represent a two parameter family of equations of state for different values of K and Γ. The values are chosen by fitting the parameters to more realistic nuclear physics models for the EoS. The constants of the equation of state are given values $m_b = 1.66 \times 10^{-27}$ kg and $n_0 = 0.1$ fm^{-3} throughout this dissertation. This EoS is also used in the case of $f(R)$ theories.

Specifically for the slow rotation case, which is the most realistic, we want to use a realistic EoS as well. The equations of state we use can be found in Lattimer and Prakash [41]. We choose four of the equations of state studied by Lattimer and Prakash, namely AP4 [1], ENG [23], MPA1 [49] and MS1 [48]. Here we use the same notation as Lattimer and Prakash. These equations of state cover all three different methods discussed in section 1.3.1. More specifically, AP4 uses the variational method, MS1 uses the field theoretical method, while MPA1 and ENG use the Brueckner-Hartree-Fock method. The equations of state are in tabulated form. An interpolation algorithm is used to create a continuous function of the data table, which is then used to express the density ρ as a function of the pressure p.

2.2 $f(R)$ theories

In this section we describe different approaches in the derivation of the structure equations of a neutron star in $f(R)$ theories of gravity. Since the construction of neutron star models in $f(R)$ theories has proven to be difficult so far, we want to demonstrate that this is mainly due to the theoretical approach used and not a pathology of the theory itself. We argue that a new approach by Jaime, Patino and Salgado (JPS) [34] is free of some of the difficulties

previous groups had in the construction of neutron star models. At the end we derive the structure equations using the JPS approach, following the same procedure as with Scalar Tensor theories. This study is part of a project with Emanuele Berti, Paolo Pani and Vitor Cardoso.

2.2.1 Field equations

We show here the different approaches that have been used to obtain the field equation used to produce relativistic star models in $f(R)$ theories of gravity. The first approach was used by Kobayashi and Maeda (KM) [38], and later on by Upadhye and Hu (UH) [67]. This approach exploits the fact that $f(R)$ theory can actually be put in a Scalar Tensor theory form. We start with the action

$$S = \frac{1}{2\kappa^2} \int d^4x \sqrt{-g} \left[f(\chi) + f_{,\chi}(\chi)(R - \chi) \right] + \int d^4x \, \mathcal{L}_M(g_{\mu\nu}, \psi_M) \tag{2.84}$$

where f is an arbitrary function of χ, subject to the constraint that $f_{,\chi\chi} \neq 0$, and χ is an auxiliary field. We vary the action with respect to χ. This gives

$$f_{,\chi\chi}(\chi)(R - \chi) = 0 \tag{2.85}$$

Thus, for a non-zero second derivative of $f(\chi)$, it must be that

$$\chi = R \tag{2.86}$$

This shows that the action (2.84) is equivalent to the action (1.42). We define

$$\phi \equiv f_{,\chi}(\chi) \tag{2.87}$$

so the action becomes

$$S = \int d^4x \sqrt{-g} \left[\frac{1}{2\kappa^2}\phi R - U(\phi) \right] + \int d^4x \, \mathcal{L}_M(g_{\mu\nu}, \psi_M), \tag{2.88}$$

where

$$U(\phi) = \frac{\chi(\phi)\phi - f(\chi(\phi))}{2\kappa^2} \tag{2.89}$$

We can easily see that this action is equivalent to 1.13 for $\omega(\phi) = 0$. The field equations derived from the action (2.88) are

$$\phi R_{\mu\nu} - \frac{1}{2}f g_{\mu\nu} - \nabla_\mu \nabla_\nu \phi + g_{\mu\nu}\Box\phi = \kappa^2 T_{\mu\nu}, \tag{2.90}$$

$$\Box\phi = \frac{dV_{\text{KM}}^{eff}(\phi)}{d\phi} = \frac{\kappa}{3}T + \frac{dV_{\text{KM}}(\phi)}{d\phi} \tag{2.91}$$

The derivatives of the potential are

$$V'_{\text{KM}}(\phi) = \frac{1}{3}\left(2f - \phi R\right), \tag{2.92}$$

$$V''_{\text{KM}}(\phi) = \frac{1}{3}\left(\frac{\phi}{\phi'} - R\right), \tag{2.93}$$

where $\phi' = f_{RR}(R)$.

Since the field equations can be put in a Scalar Tensor theory form, we can also conformally transform the equations to the Einstein frame. This is the approach by Babichev and Langlois [5],[6], hereafter BL. They define

$$\varphi \equiv \sqrt{\frac{3}{2\kappa^2}} \log f_R \tag{2.94}$$

$$\tilde{g}_{\mu\nu} = \Omega^{-2} g_{\mu\nu} \tag{2.95}$$

$$\Omega^{-2} \equiv f_R = e^{\sqrt{2\kappa^2/3}\phi} \tag{2.96}$$

so the action becomes

$$S_E = \int d^4x \sqrt{-\tilde{g}} \left[\frac{\tilde{R}}{2\kappa^2} - \frac{1}{2}(\tilde{\nabla}\varphi)^2 - V_{\mathrm{BL}}(\varphi) \right] + S_{\mathrm{mat}} \left[\Omega^2 \tilde{g}_{\mu\nu}, \psi \right] \tag{2.97}$$

where

$$V_{\mathrm{BL}}(\phi) = \frac{Rf_R - f}{2\kappa^2 f_R^2} \tag{2.98}$$

is the scalar potential. Varying the action the obtain the field equations

$$G_{\mu\nu} = \kappa^2 \left\{ \Omega^4 T_{\mu\nu} + \partial_\mu\varphi\partial_\nu\varphi - \frac{g_{\mu\nu}}{2} \left[V_{\mathrm{BL}} + (\partial\phi)^2 \right] \right\} \tag{2.99}$$

$$\Box\varphi = \frac{dV_{\mathrm{BL}}^{\mathrm{eff}}}{d\varphi} \equiv \frac{dV_{\mathrm{BL}}}{d\varphi} - \frac{d\Omega}{d\varphi}\Omega^3 T . \tag{2.100}$$

The derivatives of the potential are

$$V'_{\mathrm{BL}}(\varphi) = \sqrt{\frac{2}{3\kappa^2}} \frac{2f - Rf_R}{2f_R^2} , \tag{2.101}$$

$$V''_{\mathrm{BL}}(\varphi) = \frac{1}{3f_{RR}} \left[1 + \frac{Rf_{RR}}{f_R} - \frac{4ff_{RR}}{f_R^2} \right] . \tag{2.102}$$

Jaime, Patino and Salgado, hereafter JPS, proposed a new approach [34]. In this case the equation (1.43) is rewritten as

$$f_R G_{\mu\nu} - f_{RR}\nabla_\mu\nabla_\nu R - f_{RRR}(\nabla_\mu R)(\nabla_\nu R)$$
$$+ g_{\mu\nu} \left[\frac{1}{2}(Rf_R - f) + f_{RR}\Box R + f_{RRR}(\nabla R)^2 \right] = \kappa^2 T_{\mu\nu} \tag{2.103}$$

where $(\nabla R)^2 = g^{\mu\nu}(\nabla_\mu R)(\nabla_\nu R)$. The trace of (2.103) is

$$\Box R = \frac{1}{3f_{RR}} \left[\kappa^2 T - 3f_{RRR}(\nabla R)^2 + 2f - Rf_R \right] \tag{2.104}$$

44

Combining the two equations we get

$$G_{\mu\nu} = \frac{1}{f_R} \left[f_{RR} \nabla_\mu \nabla_\nu R + f_{RRR} (\nabla_\mu R)(\nabla_\nu R) + \right.$$

$$\left. -\frac{g_{\mu\nu}}{6} \left(R f_R + f + 2\kappa T \right) + \kappa T_{\mu\nu} \right] \tag{2.105}$$

$$\Box R = \frac{d\tilde{V}_{\mathrm{JPS}}^{\mathrm{eff}}}{dR} \equiv \frac{\kappa}{3 f_{RR}} T - \frac{f_{RRR}}{f_{RR}} (\nabla R)^2 + \frac{d\tilde{V}_{\mathrm{JPS}}}{dR} \tag{2.106}$$

where

$$\frac{d\tilde{V}_{\mathrm{JPS}}}{dR} \equiv \frac{2f - R f_R}{3 f_{RR}} \tag{2.107}$$

2.2.2   JPS formulation vs Scalar Tensor formulation

We discuss here the past difficulties encountered in the numerical integration of the field equations of $f(R)$ for neutron stars. We also show how some of these difficulties can be avoided by using the JPS formalism.

At first KM claimed that neutron stars cannot be constructed in $f(R)$ theories because singularities occur in the interior of the neutron star. UH and BL showed that these singularities are a product of numerical instabilities and not a physical property of the theory itself. Using different numerical schemes UH and BL were able to construct numerical models of relativistic star in $f(R)$ theories.

Nevertheless, the problem of numerical instabilities in the interior of the star remains, making the integration of the field equations very difficult. The problem arises because the potentials by KM, UH and BL have finite values at the points in the interior where the Ricci scalar R becomes very large, which means that the solution can access the region of very large R using only finite amount of "potential energy". Let us consider the Starobinsky model (1.79). Inside the neutron star the curvature is much higher than the cosmological value R_c,

$$R \gg R_c. \tag{2.108}$$

We expand the function f in this limit

$$f(R) \sim R - \mu R_c + \mu R_c \left(\frac{R_c}{R}\right)^{2n} \qquad , R \gg R_c \qquad (2.109)$$

It can be shown that the potentials of both the KM and UH formalism and the BL formalism, approach a constant value in this limit

$$V(\phi) \to \text{const } R_c \qquad (2.110)$$

while the derivatives of the potentials diverge. The same argument can be applied to the other $f(R)$ models. The energy density that is required to reach this singularity is on the order of the central density of the star. Although this means that the singularity would be accessible in the interior of the star, the chameleon mechanism, whereby the effective mass of the scalar field (related to the second derivative of the potential) become large in the interior of the star, prevents this from happening, as discussed by UH. Unfortunately, the chameleon mechanism makes the numerical integration even more difficult.

On the other hand, JPS use a different potential, namely

$$V_{JPS}(R) = -\frac{Rf(R)}{3} + \int^R f(x)dx. \qquad (2.111)$$

The derivative of this potential vanishes when the derivative (2.107) vanishes, since $f_{RR} > 0$. This corresponds to a de Sitter solution with $R = R_1 = \text{const}$. This potential, in the high curvature limit, for the Starobinsky model becomes

$$V_{JPS}(R) = R_c^3 \left(\frac{R}{R_c}\right)^{2n+4} \qquad (2.112)$$

which shows that the potential becomes infinite when $R \to \infty$. This guarantees that the singularity cannot be accessed in the interior of the star.

Another issue with mapping $f(R)$ theories to Scalar Tensor theories, is that the scalar field potential might be multi-valued. This is true for example for the Starobinsky model. It is claimed that the numerical calculations will follow the minimum value of the potential and this multi-valueness of the potential does not pose a problem. However, calculations done using a multi-valued potential, especially close enough to a singular point where the potential is discontinuous are less trustworthy and we should try to avoid such potentials if possible. The JPS potential is not multi-valued and does not contain any singular points.

2.2.3   Structure equations in the JPS formulation

We derive now the structure equations describing a neutron star for a static spherically symmetric spacetime. We follow the notation of JPS [34]. The metric is given by

$$ds^2 = -B(r)dt^2 + A(r)dr^2 + r^2 d\Omega^2 \tag{2.113}$$

Here we follow the JPS notation. The field equations then yield

$$R'' = \frac{1}{3f_{RR}} \left[A(\kappa^2 T + 2f - Rf_R) - 3f_{RRR}R'^2 \right] + \left(\frac{A'}{2A} - \frac{B'}{2B} - \frac{2}{r} \right) R' \tag{2.114}$$

$$
\begin{aligned}
A' = \frac{A}{r(2f_R + rR'f_{RR})} &\left\{ 2f_R(1 - A) - 2Ar^2\kappa^2 T^t{}_t \right. \\
&+ \frac{Ar^2}{3}(Rf_R + f + 2\kappa T) + \frac{rR'f_{RR}}{f_R} \left[\frac{Ar^2}{3}(2Rf_R - f + \kappa^2 T) \right. \\
&\left. - \kappa^2 Ar^2(T^t{}_t + T^r{}_r) + 2(1 - A)f_R + 2rR'f_{RR} \right] \right\}
\end{aligned} \tag{2.115}
$$

$$B' = \frac{B}{r(2f_R + rR'f_{RR})} \left[Ar^2(f - Rf_R + 2\kappa^2 T^r{}_r) + 2(A - 1)f_R - 4rR'f_{RR} \right] \tag{2.116}$$

$$B'' = \frac{2AB}{f_R}\left[\kappa^2 T^{\theta}{}_{\theta} - \frac{1}{6}\left(Rf_R + f + 2\kappa^2 T\right) + \frac{R'}{rA}f_{RR}\right]$$
$$+ \frac{B}{2r}\left[2\left(\frac{A'}{A} - \frac{B'}{B}\right) + \frac{rB'}{B}\left(\frac{A'}{A} + \frac{B'}{B}\right)\right] \tag{2.117}$$

Equations (2.116) and (2.117) are not independent and we can choose either one for our calculations. Also, using the conservation of the stress-energy tensor for a perfect fluid $T_{\mu\nu} = (\rho + p)u^{\mu}u^{\nu} + pg^{\mu\nu}$ we get

$$p' = -\frac{(\rho + p)B'}{2B} \tag{2.118}$$

The system of equations (2.114) - (2.117) and (2.118) is the set of structure equations for a static spherically symmetric relativistic star. In order for the set to be complete we also need to provide an EoS. The same polytropic EoS described in section 2.1.6 is used. The parameters chosen are shown in table 3.1.

The JPS field equations can be solved analytically in vacuum, far away from the star where one obtains the asymptotic solution

$$B(r) = A^{-1}(r) = 1 - \Lambda_{eff}\frac{r^2}{3} \tag{2.119}$$

$$R = R_1 = \text{const} \qquad , \ \Lambda_{eff} = \frac{R_1}{4} \tag{2.120}$$

This is a de Sitter solution, where the asymptotic value of the Ricci scalar plays the role of the cosmological constant. This corresponds to the point where the first derivative of the potential, as defined in (2.111), becomes zero. This means that the local minima of the potential play the role of the asymptotic value of the Ricci scalar. The behavior of the potential for a certain $f(R)$ model strongly depends on the parameters of the model. As an example, the number of minima of the Starobinsky model depends on the value of the parameter λ for $n = 1$. As we can see in Fig. 2.1, there is a critical value $\lambda = 8/\sqrt{27}$, below which the potential has only one minimum. We discuss the behavior of the potentials of

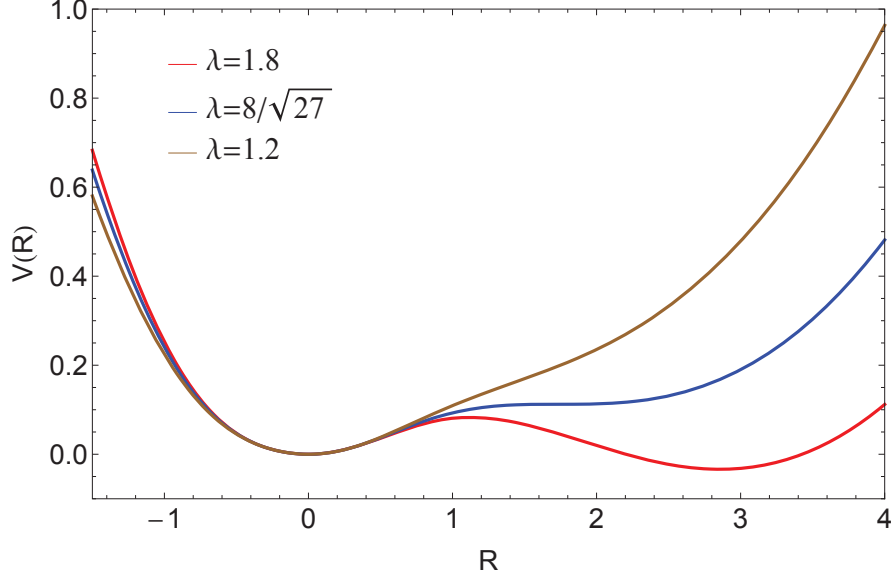various $f(R)$ models, more extensively in chapter 3.

Figure 2.1: The potential of the Starobinsky model vs the Ricci scalar for different values of the parameter λ

Finally, to be able to integrate the equation numerically, we need to provide a set of initial conditions at the center of the star. The integration starts at some $r = \Delta r$, very close to the origin. We expand the quantities $A(r)$, $p(r)$, $R(r)$ in Taylor series around the origin

$$A(\Delta r) = A(0) + A_1 \frac{\Delta r^2}{2} + \mathcal{O}(r^4) \tag{2.121}$$

$$p(\Delta r) = p(0) + p_1 \frac{\Delta r^2}{2} + \mathcal{O}(r^4) \tag{2.122}$$

$$R(\Delta r) = R(0) + R_1 \frac{\Delta r^2}{2} + \mathcal{O}(r^4) \tag{2.123}$$

$$R'(\Delta r) = R_1 \Delta r + \mathcal{O}(r^3) \tag{2.124}$$

with the choice, $A(0) = B(0) = 1$. We plug in the expansion in the structure equations and solve for A_1, p_1, R_1. The full expressions for the initial conditions for all the models used can be found in appendix A.

Chapter 3

Numerical method and results

3.1 Scalar tensor theories

3.1.1 Numerical integration

The numerical method used to solve the structure equations presented in chapter 2 is called the shooting method. This is a widely used method for systems of differential equations with the boundary conditions defined at two different points. For a more extensive discussion of the shooting method please refer to [56]. Here we give the basic principles of the method and we discuss further a few details specific to our code.

The first step is to write the set of the structure equation as a system of first order ODEs in the form $y_i'(x) = f_i(x, y_i, y_i')$, where y_i are the dependent variables and x is the independent variable. The systems (2.12) - (2.18) and (2.43) - (2.49) are already in this form with r being the independent variable, while $M, \nu, \varphi, \psi, p, \bar{M}, \omega, \varpi$ are the dependent variables. In numerical work it is desirable to use dimensionless variables, and therefore all variables will need to be re-scaled as we discuss in the next section. Furthermore, we need to provide boundary conditions at the two boundary points. In our case all the boundary conditions are defined at the first boundary $r = 0$, except for the scalar field, which is defined

at infinity $\varphi(\infty) = \varphi_0$. Choosing the EoS and central density at the center of the star, ρ_c defines a specific model.

Next, we integrate the equations, starting from the center of the star, where we have provided the initial conditions (2.74) - (2.81). The value for the scalar field at the center of the star is initally a guess. The real value will be obtained after the boundary conditions at the second point are met. The numerical integration is done by using a Runge-Kutta method. In each step of the code, the integration progresses by one step size Δr. The values of the dependent variables are calculated using the values of the previous step. The process is repeated until the second boundary is reached, where the stopping condition is met. In this case this is the surface of the star where the pressure becomes zero, $p = 0$.

When the boundary has been reached, several quantities are calculated using equations (2.60) - (2.73). One of the quantities is the scalar field φ at the surface. The required value of the scalar field at infinity – the required boundary condition – can be linked to the value at the surface using equation (2.68). The difference of the value of the field at the surface obtained by the numerical integration and the value obtained from the asymptotic boundary condition is calculated. If the difference is greater than some tolerance of the code, the process starts over. The difference is used to obtain a better guess for the central value of the scalar field. This process is repeated iteratively, until the difference between the two surface values of the scalar field is below the tolerance, where we can declare that the final boundary conditions has been met.

At this point all the relevant quantities of the star are calculated and recorded, and this constitutes one star model that corresponds to some initial central density. This process also yields the value of the first sensitivity in the Einstein frame α_A. This is because there is a straightforward relation to calculate α_A from the quantities at the surface of the star (2.67). Unfortunately, no such relation exists for the second sensitivity β_A. In order to calculate the second sensitivity, we calculate models around the initial star model that differ by $\Delta \rho_c$ and

numerically calculate the derivative $\left(\frac{\partial \alpha_A}{\partial \varphi}\right)_0$, by using a five-point formula

$$f'(x) = \frac{-f(x+2h) + 8f(x+h) - 8f(x-h) + f(x-2h)}{12h} + \mathcal{O}(h^4) \qquad (3.1)$$

In this case $f(x+h) \equiv \alpha(\rho_c + \Delta\rho_c, \varphi_0 + \Delta\varphi_0)$ and $h \equiv \Delta\varphi_0 = \varphi_{02} - \varphi_{01}$. The same formula is used for the moment of inertia sensitivity as well. This, though has to be done keeping the baryonic mass constant. This means that the value of the baryonic mass $\bar{M}$ of the first model becomes an additional boundary condition at the surface of the star for the next four models. Thus, for the next four models the process is repeated iteratively until both conditions are met.

Finally, when all the quantities, including the sensitivities, have been calculated a new central density is chosen. The process as described above is repeated, to obtain a second neutron star model. This is repeated until a range of central densities that includes both stable and unstable branches of the M vs R diagram is covered. The step size for the density between two models might be different, but the total number of models is ~ 200 for all EoSs.

In order to test the good behavior and the convergence of the code, several tests were done. One example is monitoring the total mass of the star for decreasing values of the step size Δr. The results are shown in figure 3.1.

3.1.2 Equations used for numerical analysis

In this section we analyze the equations used in the numerical code. Unit-less variables are preferred for numerical analysis. Also, dealing with number that differ by several orders of magnitude in the same calculation introduces more numerical error. Thus, starting with the
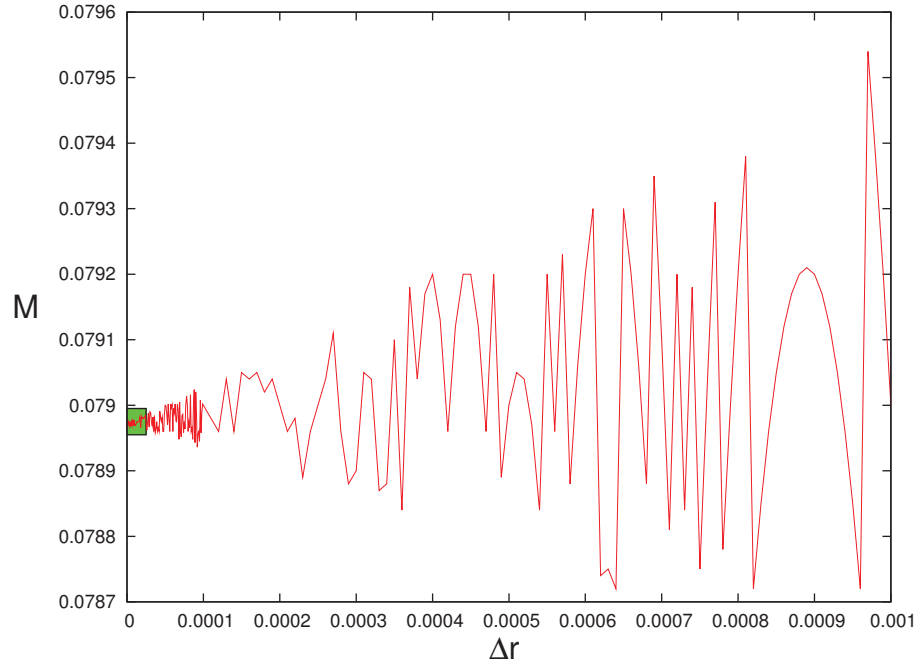
Figure 3.1: Total mass $\hat{M}$ dependance on step size $\Delta\hat{r}$. We start with a large value for the step size $\Delta\hat{r} = 10^{-3}$ and we decrease it in discrete steps. The green box denotes the range of values used in the code, $10^{-6} < \Delta\hat{r} < 2 \times 10^{-5}$. The mass value clearly converges for decreasing step size.

static spacetime case, we use the following re-scaling for our variables

$$r = r_0 \hat{r} \tag{3.2}$$

$$M = r_0 \hat{M} \tag{3.3}$$

$$\rho = \rho_0 \hat{\rho} \tag{3.4}$$

$$p = \rho_0 \hat{p} \tag{3.5}$$

while the rest of the variables remain the same. We choose $\rho_0 = \rho_c$ in almost every model, so $\hat{\rho}_c = 1$. Under this re-scaling the EoS becomes

$$\hat{\rho} = \frac{\hat{p}}{\Gamma - 1} + A \, \hat{p}^{1/\Gamma} \tag{3.6}$$

where $A = \frac{m_b n_0}{(K m_b n_0)^{1/\Gamma} \rho_c^{1-1/\Gamma}}$. We obtain the initial condition for $\hat{p}_c = \hat{p}(0)$ by solving numerically the algebraic equation

$$\frac{\hat{p}_c}{\Gamma - 1} + A \, \hat{p}_c^{1/\Gamma} = 1. \tag{3.7}$$

When using more realistic equations of state, as described in section 2.1.6, the values of density and pressure are just divided by the initial value of density, ρ_c. We re-write the structure equations using the re-scaled variables. We notice that the form of all the terms of the equations remains the same, while the original variables change to "hatted" ones, other than that some terms are multiplied by a $\rho_c r_0^2$ coefficient. By setting $\rho_c r_0^2 = 1$ the form of the equations remains exactly the same, but all the original variables have been replaced with the re-scaled ones.

The initial conditions are also re-scaled in the same manner. The initial guess for the value of the scaler field at the origin, φ_c, is set to be of the same order of magnitude as the value at infinity, since tests of the code reveal that the value of the scalar field does not change significantly. This reduces the number of steps required to reach the desired value at

infinity. The structure equations are then integrated outwards, until the value of the pressure is lower than some threshold value, usually set to be $\hat{p}(R) < 10^{-9}$. The re-scaled matching equations with the exterior metric are used to calculate the physical quantities of the star. The value for the scalar field at infinity is set either to zero or to some value which is lower than the allowed value from Solar System experiments. Specifically for the "spontaneous scalarization" case we set $\varphi_0 < 4.3 \times 10^{-3}$ to follow Damour and Esposito-Farese [18].

When the integration is over and the value of the scalar field at infinity has been reached within tolerance, the re-scaled variables are changed back to the original variables. In addition we change to SI units, from geometric units where $G = c = 1$.

3.1.3 Results

In this section we present the numerical results obtained with our code. We start with the FJBD case for a static metric. A polytropic EoS is used. The value of the parameter coupling constant is chosen to be $10^{-2} < \tilde{\alpha} < 10^{-4}$. The models shown here have $\alpha = 10^{-3}$ so they are very close to those obtained in General Relativity. The parameters of the equation of state that we use are shown in Table 3.1.

	Γ	K
EOS I	2.00	0.1
EOS II	2.34	0.0195
EOS III	2.46	0.00936

Table 3.1: EOS parameters

These are the same parameters used by Damour and Esposito-Farese [18]. More specifically, EOS II is fitted to the equation of state II of [21] and EOS III is fitted to the equation of state A of [4].

About 200 models were integrated as we increased the value of the central density. The lowest value for the central density was around $\rho_c = 10^{15} \text{kg/m}^3$ while the highest value was

chosen to be about $\rho_c = 10^{21}\text{kg/m}^3$. The step size for the central density varies, depending on the value of the central density itself, as well as the behavior of the models. For example, we choose a smaller step size around the maximum mass of the star. The density and pressure profile of certain models obtained using EoS II is shown in Figures 3.2 - 3.5. As we can see, the trace of the energy momentum tensor $T = 3p - \rho$ becomes negative when the central density is higher than a certain value. This value is about $\rho_c = 2.27 \times 10^{18}\text{kg/m}^3$ for EoS II. The derivative of the scalar field at the center of the star also changes sign when the trace T changes sign (see (2.78)).
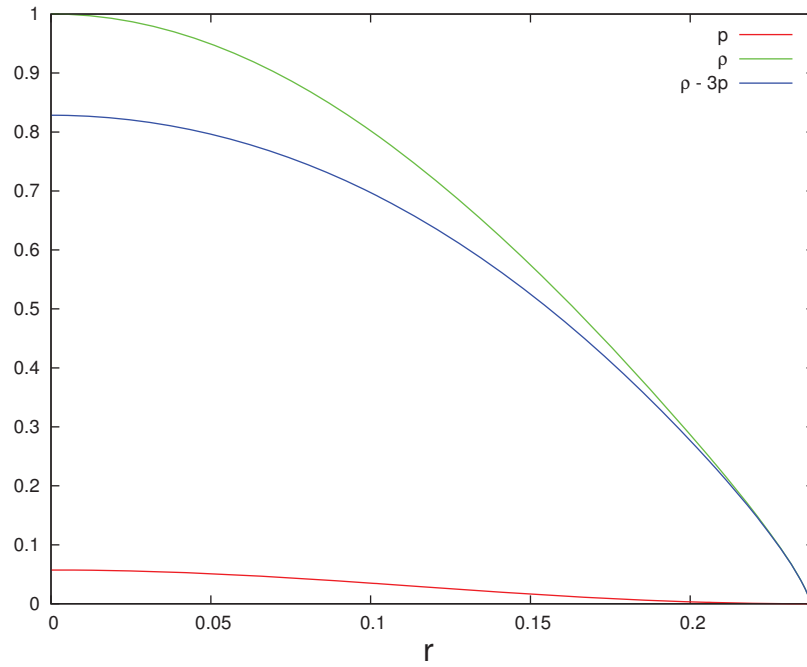
Figure 3.2: EOS II: Density profile for $\rho_c = 4 \times 10^{17} \text{ kg/m}^3$
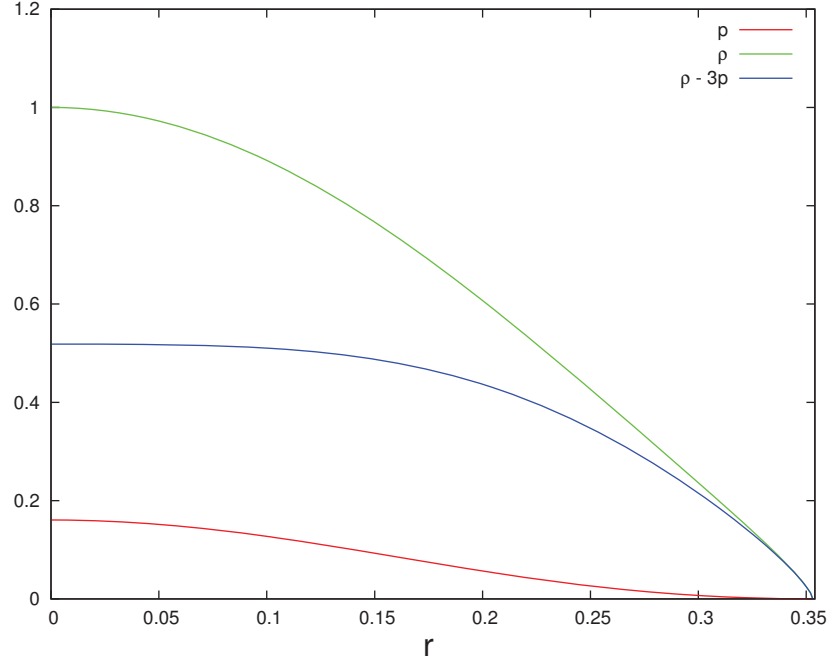
Figure 3.3: EOS II: Density profile for $\rho_c = 1 \times 10^{18}$ kg/m^3
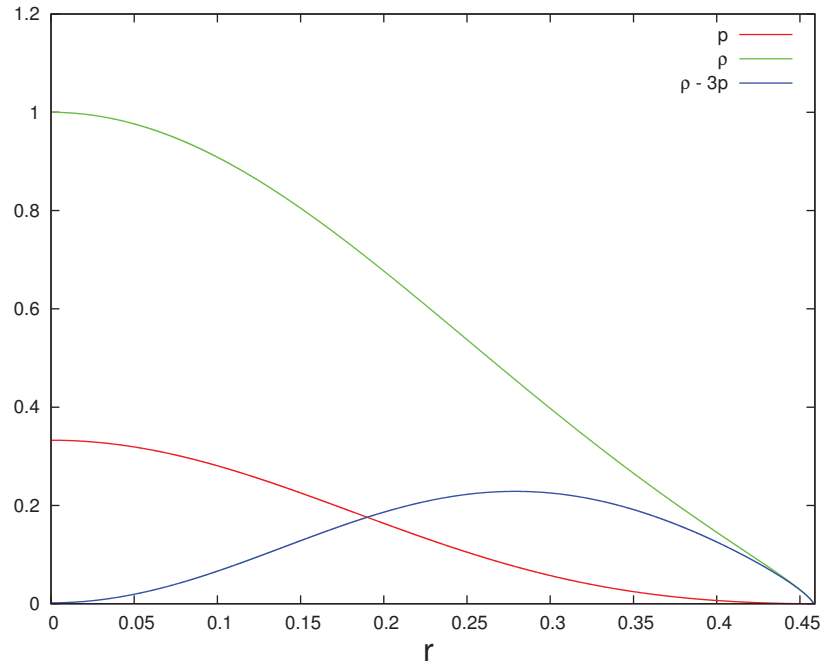
Figure 3.4: EOS II: Density profile for $\rho_c = 2.27 \times 10^{18}$ kg/m^3
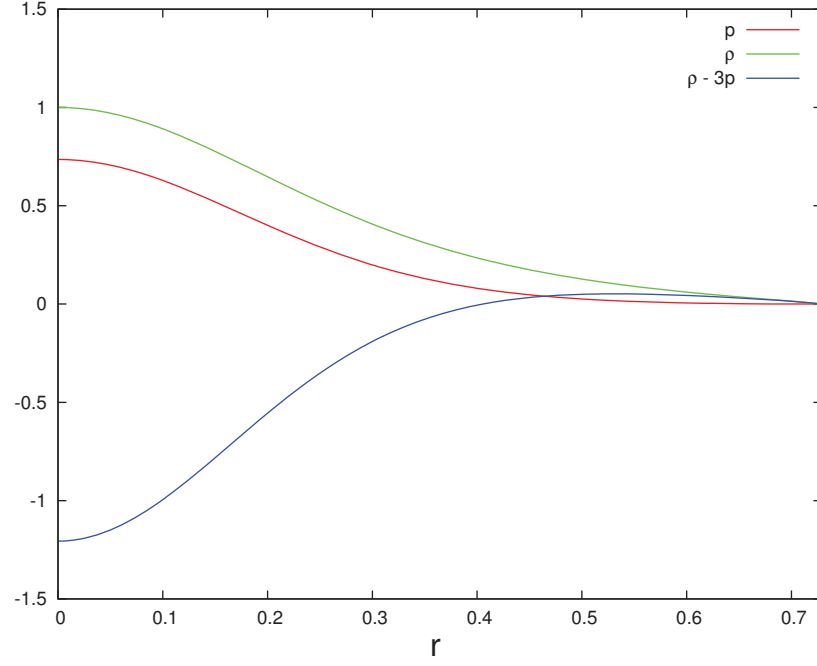
Figure 3.5: EOS II: Density profile for $\rho_c = 1 \times 10^{19}$ kg/m^3

All these models can be used to create a M vs R diagram for a specific choice for the EoS. These diagrams are shown in figures 3.6 - 3.9. As in General Relativity, all the models have a maximum total mass and the along that sequence with larger central density are expected to be unstable.
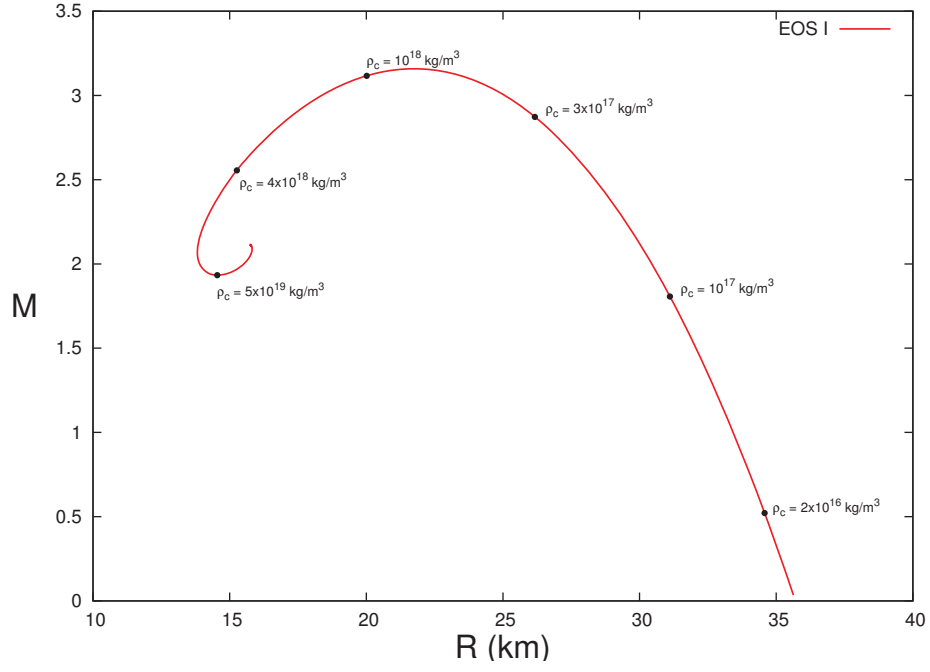
Figure 3.6: EOS I: Mass of the star $M/M_\odot$ vs star radius R in km
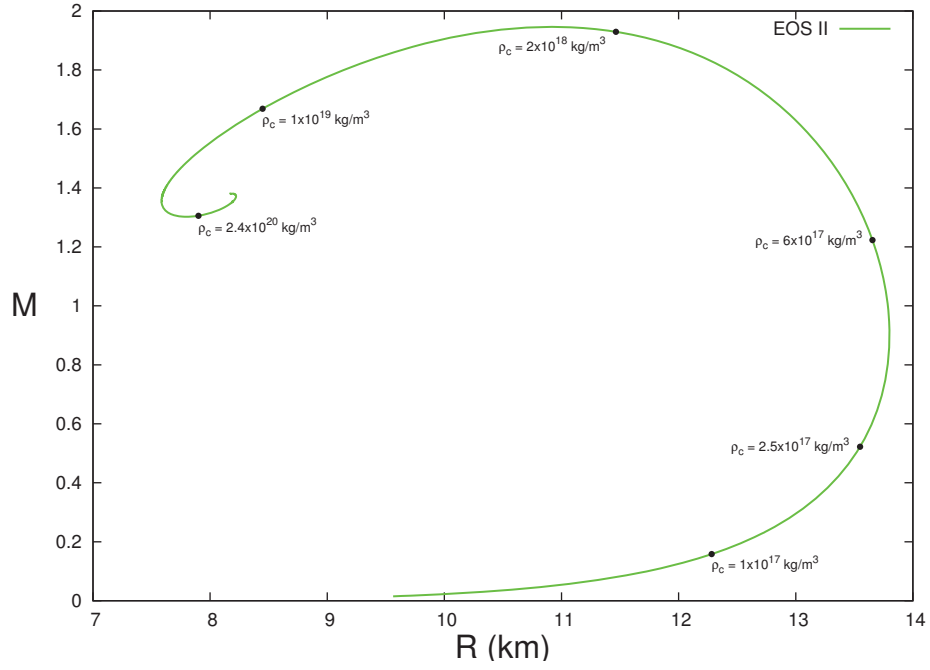
Figure 3.7: EOS II: Mass of the star $M/M_\odot$ vs star radius R in km
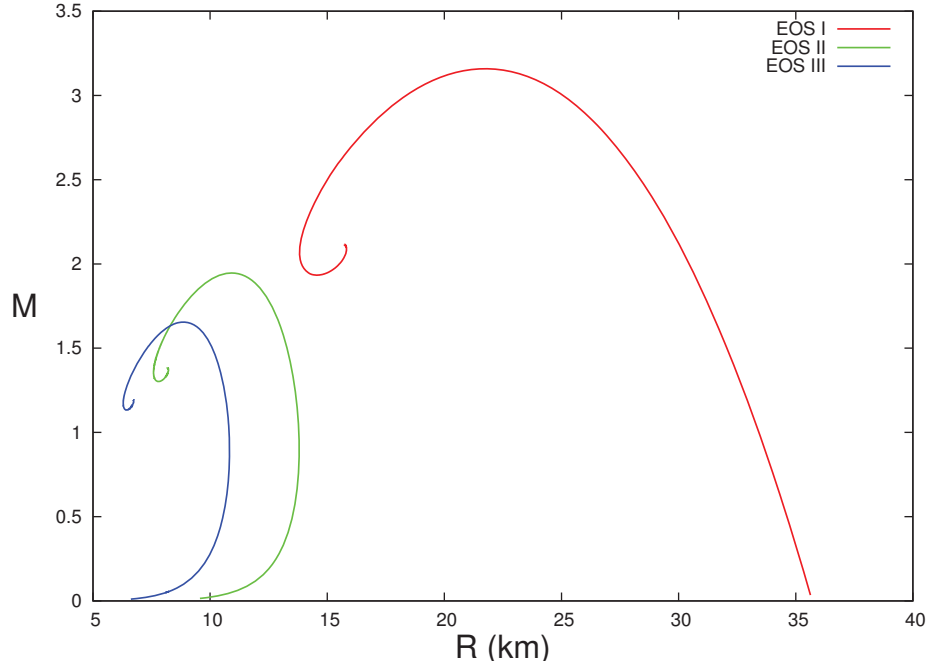
Figure 3.8: Mass of the star $M/M_\odot$ vs star radius R in km
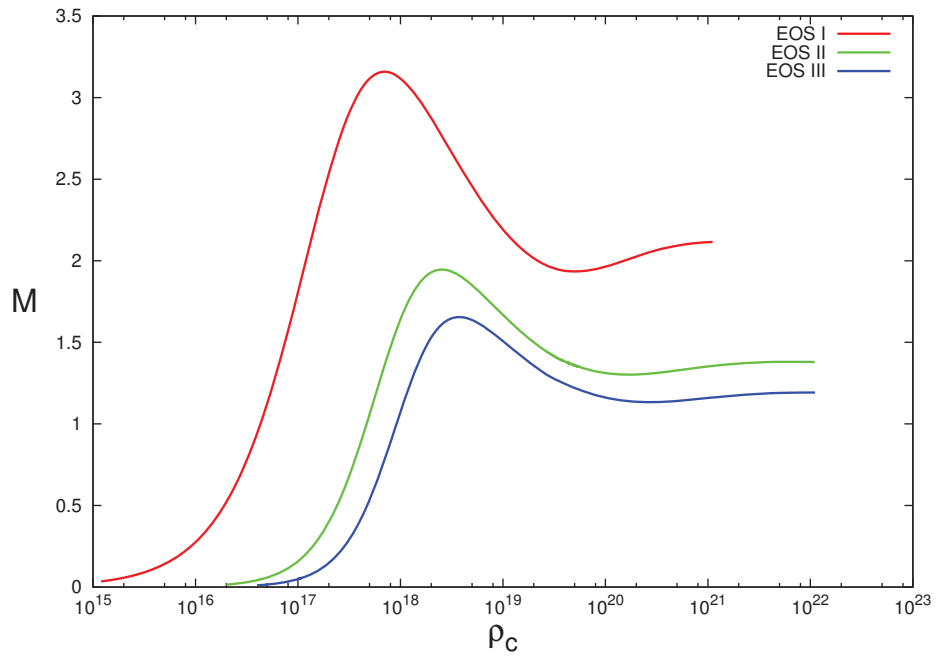
Figure 3.9: Mass of the star $M/M_\odot$ vs central density ρ_c in kg/m^3

Now we are moving on to "spontaneous scalarization" models [18], [19] were the coupling function takes the form

$$A(\varphi) = e^{\frac{1}{2}\tilde{\beta}\varphi^2} \tag{3.8}$$

Here the value of the derivative of the coupling constant is negative and is given different values while the value the scalar field at infinity is taken to be $\varphi_0 = 4.3 \times 10^{-3}$. This makes the PPN parameters $|\gamma - 1| \simeq 1.3 \times 10^{-3}$ and $|\beta - 1| \simeq 4 \times 10^{-3}$ for $\tilde{\beta} = -6$. These values are chosen to follow Damour and Esposito-Farese [18], even though the bounds on these parameters are stricter today (see (1.23), (1.26)). We show here the "sensitivity" in the Einstein frame α_A as well as in the Jordan frame s_A. We also show the M vs R diagram where the effects of "spontaneous scalarization" become obvious. These results completely agree with Damour and Esposito-Farese.
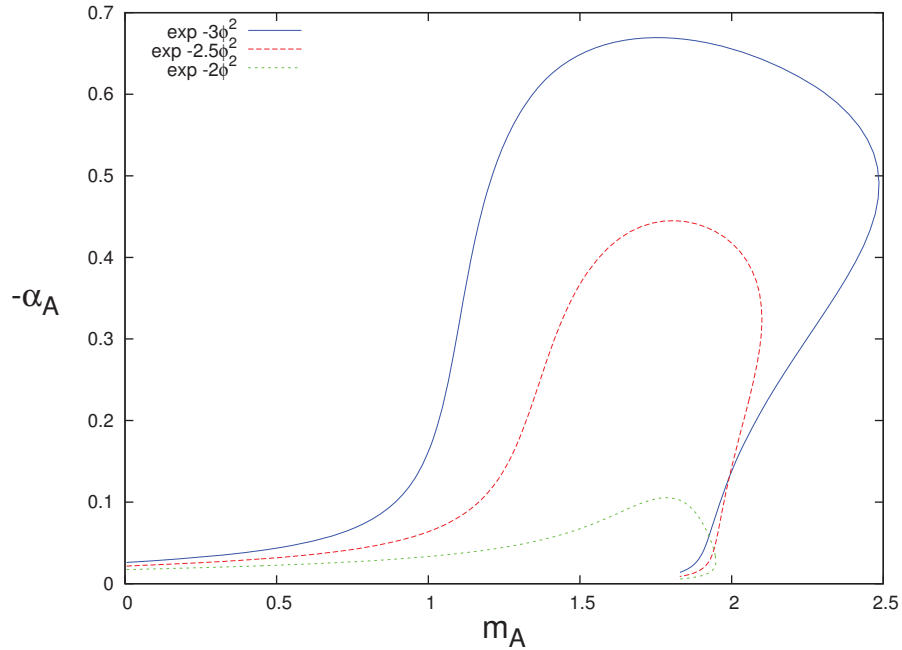
Figure 3.10: Sensitivity α_A vs total mass $m_A/M_\odot$ for different values of the parameter β
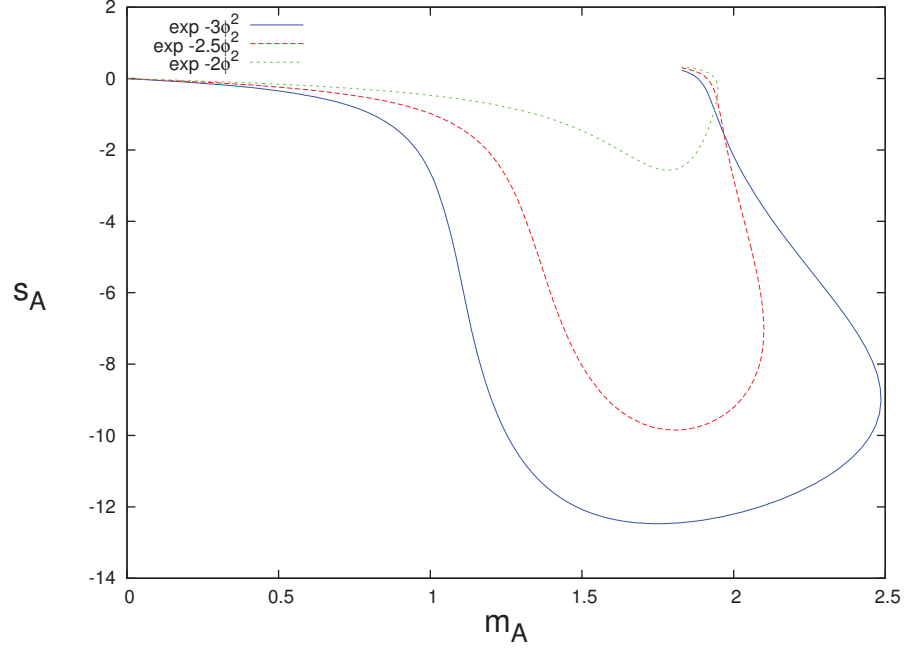
Figure 3.11: Sensitivity s_A vs total mass $m_A/M_\odot$ for different values of the parameter β. In the high density limit the sensitivities become positive, and approach the 0.5 limit which corresponds to the sensitivity of a black hole.
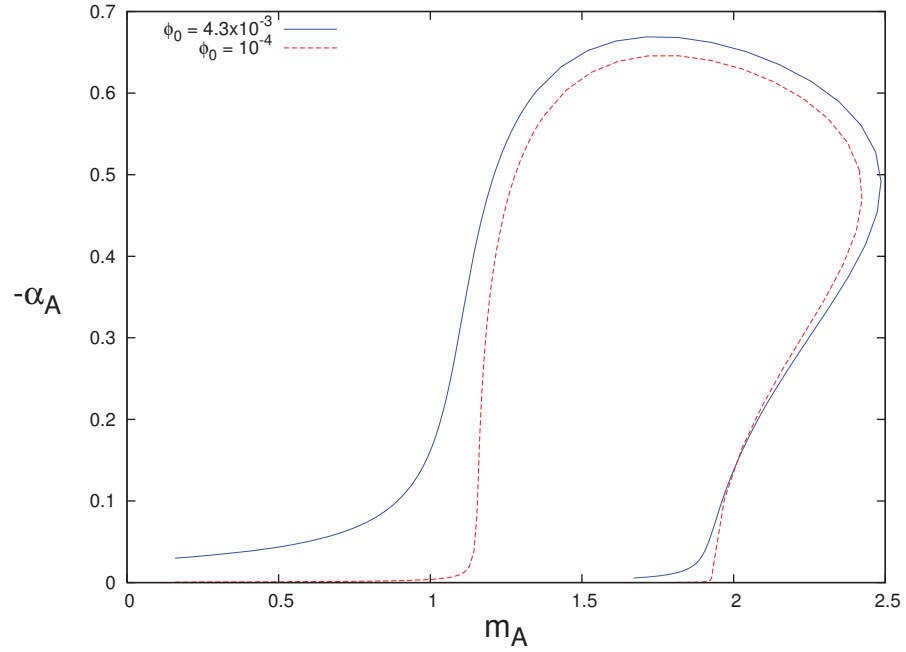
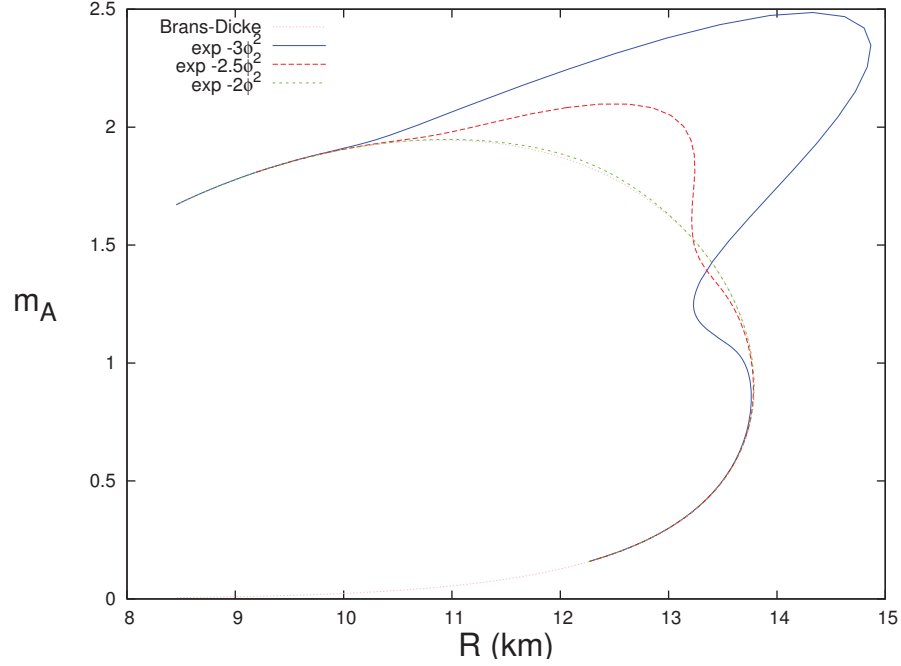Figure 3.12: Coupling constant α_A vs total mass $m_A/M_\odot$ with $A(\varphi) = \exp(-3\varphi^2)$

Figure 3.13: EOS II: Total mass $m_A/M_\odot$ vs star radius R in km for different values of the parameter β

Finally, we present here models for the slow rotation case (Fig. 3.14 - 3.22). This is the most realistic case. In addition to rotation, realistic equations of state are used, as described in section 2.1.6. The Einstein frame first "sensitivity" α_A, second "sensitivity" β_A, as well as the moment of inertia sensitivity are shown here, for various values of the coupling constant α_0. Also the moment of inertia itself is shown in figure 3.20 .
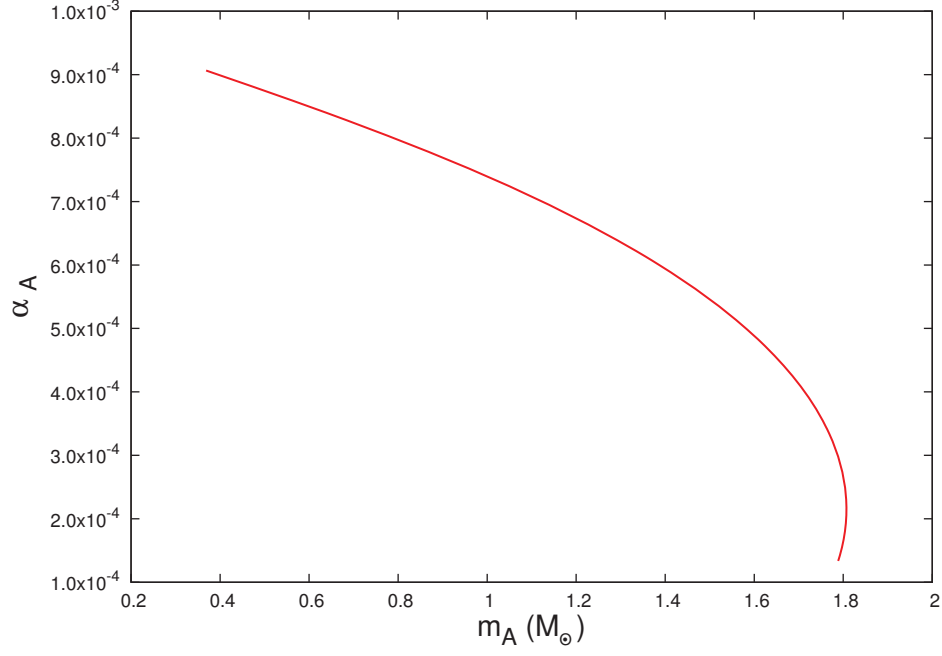
Figure 3.14: EOS AP4: First coupling constant α_A vs the total mass of the star m_A in solar masses for $\alpha_0 = 10^{-3}$
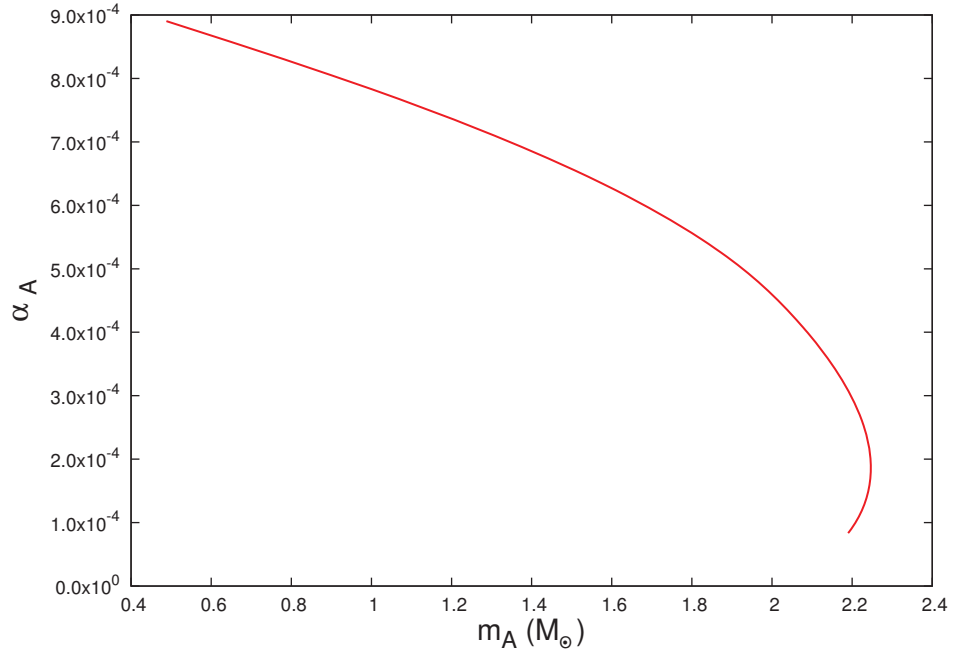
Figure 3.15: EOS ENG: First coupling constant α_A vs the total mass of the star m_A in solar masses for $\alpha_0 = 10^{-3}$
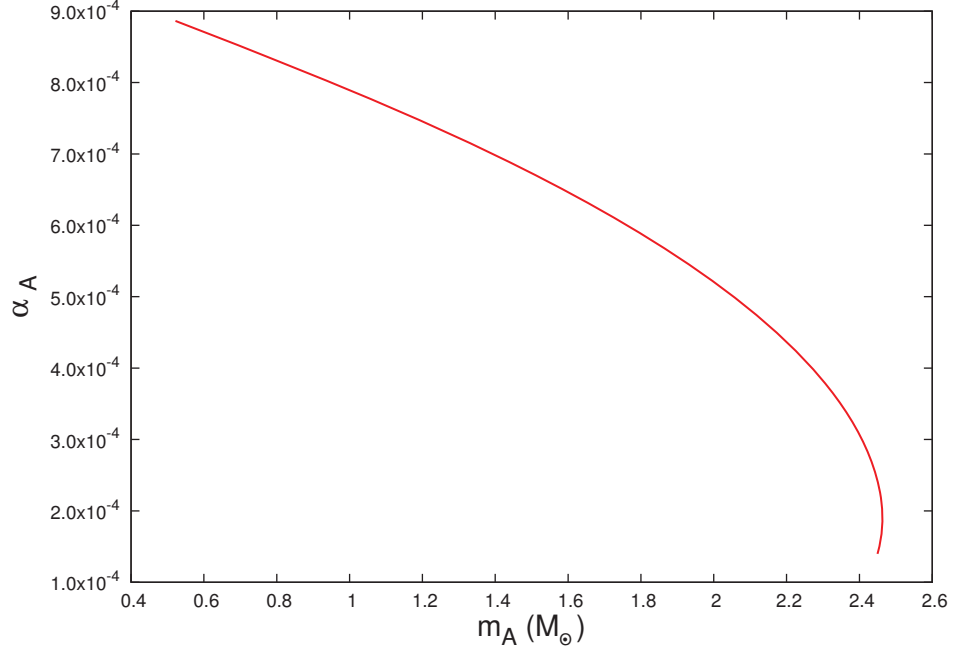
Figure 3.16: EOS MPA1: First coupling constant α_A vs the total mass of the star m_A in solar masses for $\alpha_0 = 10^{-3}$
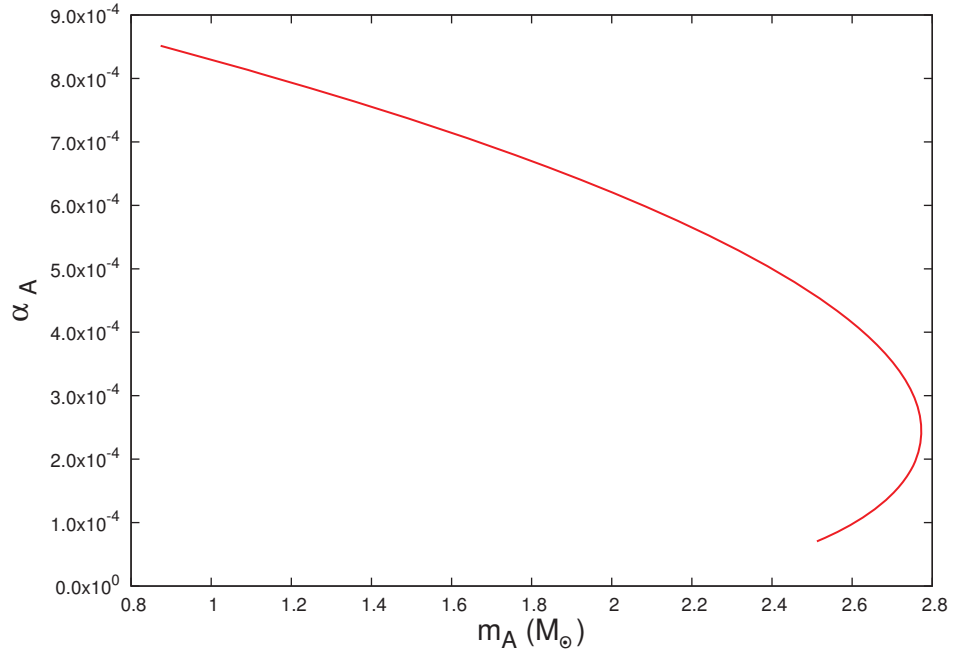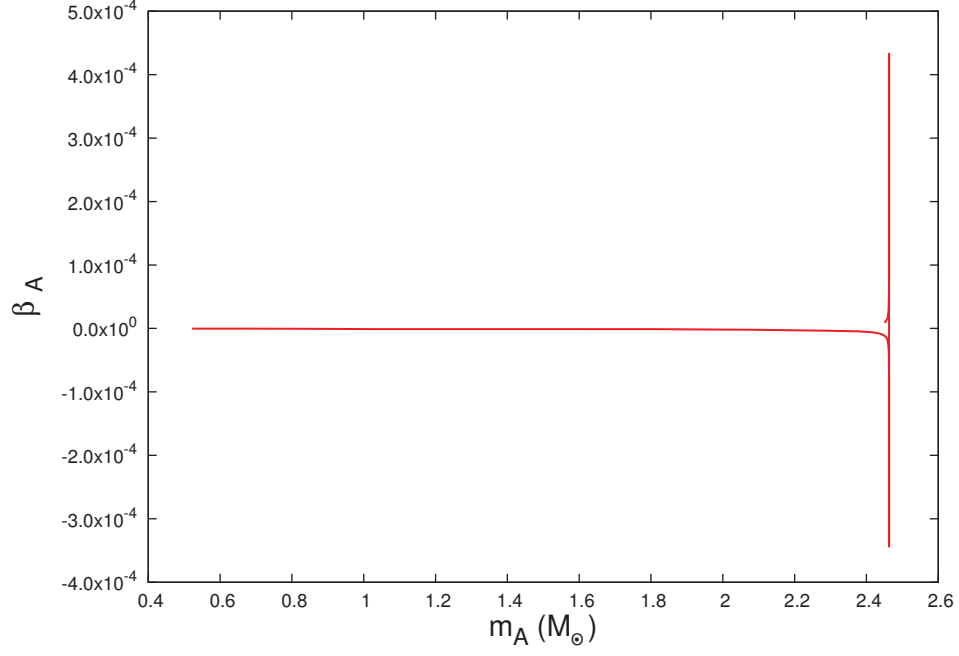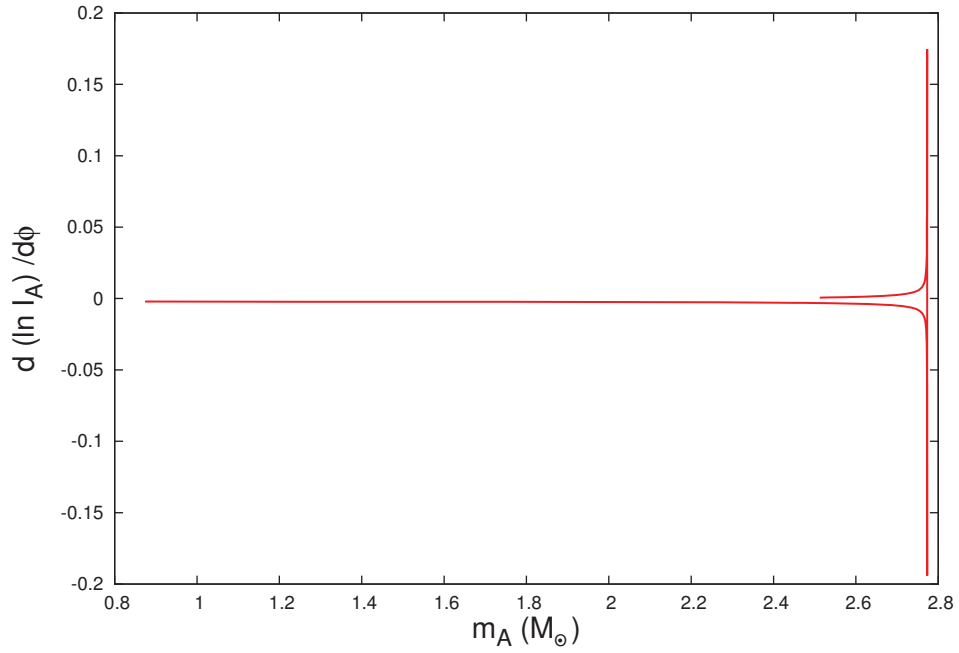

Figure 3.17: EOS MS1: First coupling constant α_A vs the total mass of the star m_A in solar masses for $\alpha_0 = 10^{-3}$

65

Figure 3.18: EOS MPA1: Second coupling constant β_A vs the total mass of the star m_A in solar masses for $\alpha_0 = 10^{-3}$

Figure 3.19: EOS MS1: Moment of inertia sensitivity $\frac{\partial \ln I_A}{\partial \varphi_0}$ vs the total mass of the star m_A in solar masses for $\alpha_0 = 10^{-3}$
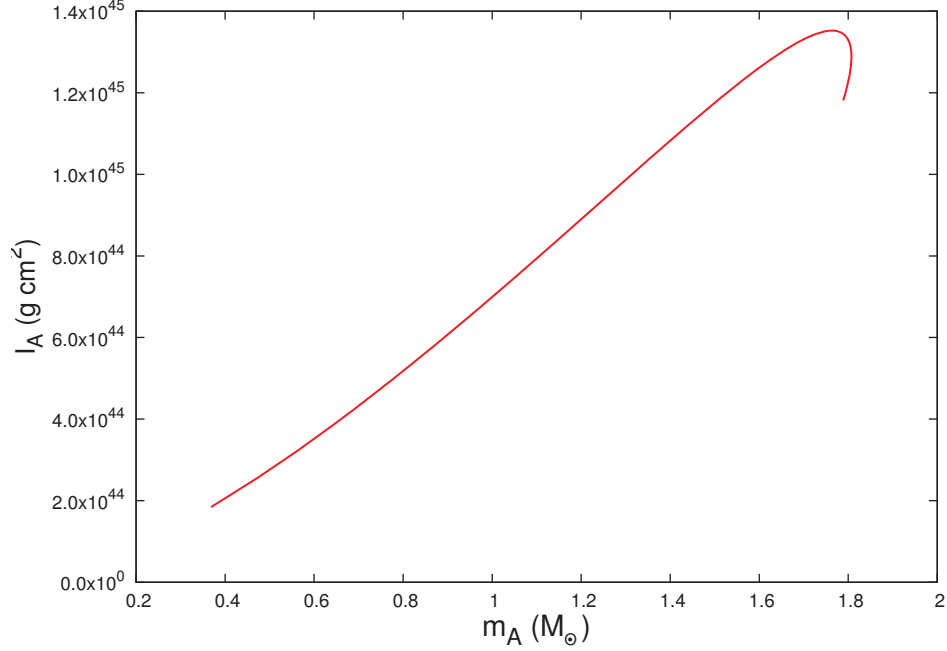
Figure 3.20: EOS AP4: Moment of inertia vs the total mass of the star m_A in solar masses for $\alpha_0 = 10^{-3}$

3.1.4   Discussion

We have calculated models of neutron star in Scalar Tensor theories of gravity. A wide range of parameters of these models was studied. The main goal of our study was to calculate the sensitivities of realistic neutron star models. Initially we calculated static models in the FJBD theory. A low value for the parameter $\tilde{\alpha}_0 \sim 10^{-4}$, or a high value for the parameter $\omega \sim 500,000$ in the Jordan frame respectively, was used for these models. These are used as test models to confirm the we can reproduce results of prior works. The M vs R diagrams show no significant changes from General Relativity for very high values of ω. Then, we calculated static models for the "spontaneous scalarization" case. These models have already been studied by Damour and Esposito-Farese [18] and we were able to completely reproduce their results. In addition, we calculated the Jordan frame sensitivities for these models, which Damour and Esposito-Farese had not done. We notice that the Jordan frame sensitivities
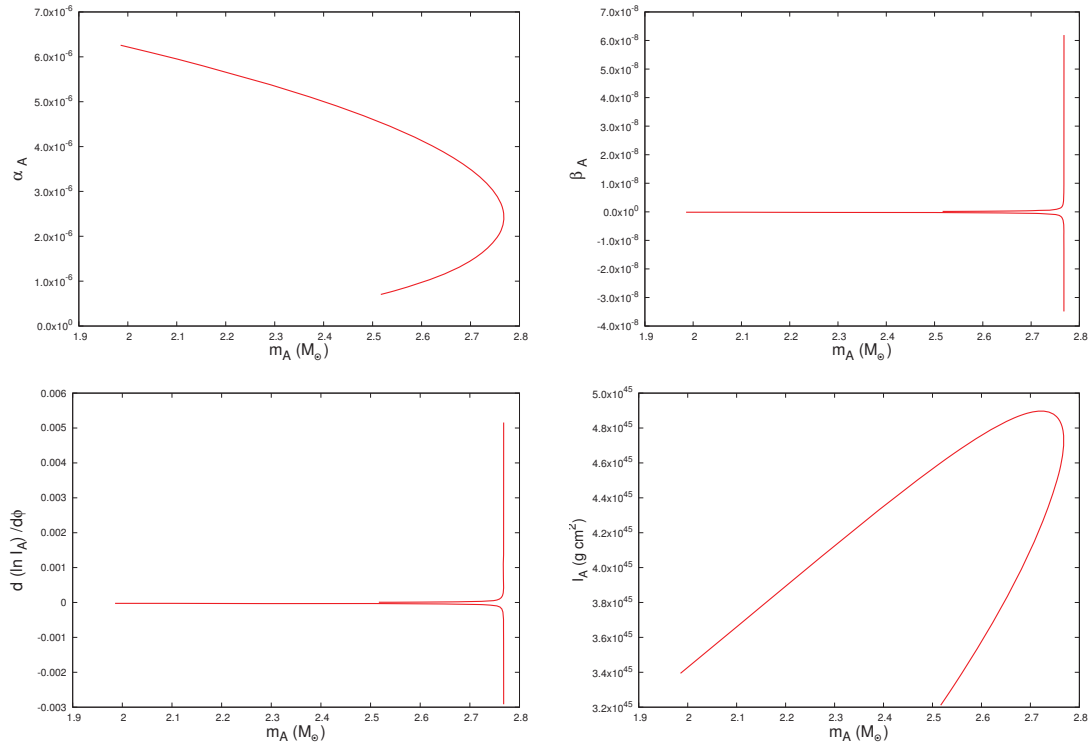
Figure 3.21: EOS MS1: Sensitivities and moment of inertia vs the total mass of the star m_A in solar masses for $\alpha_0 = 10^{-5}$
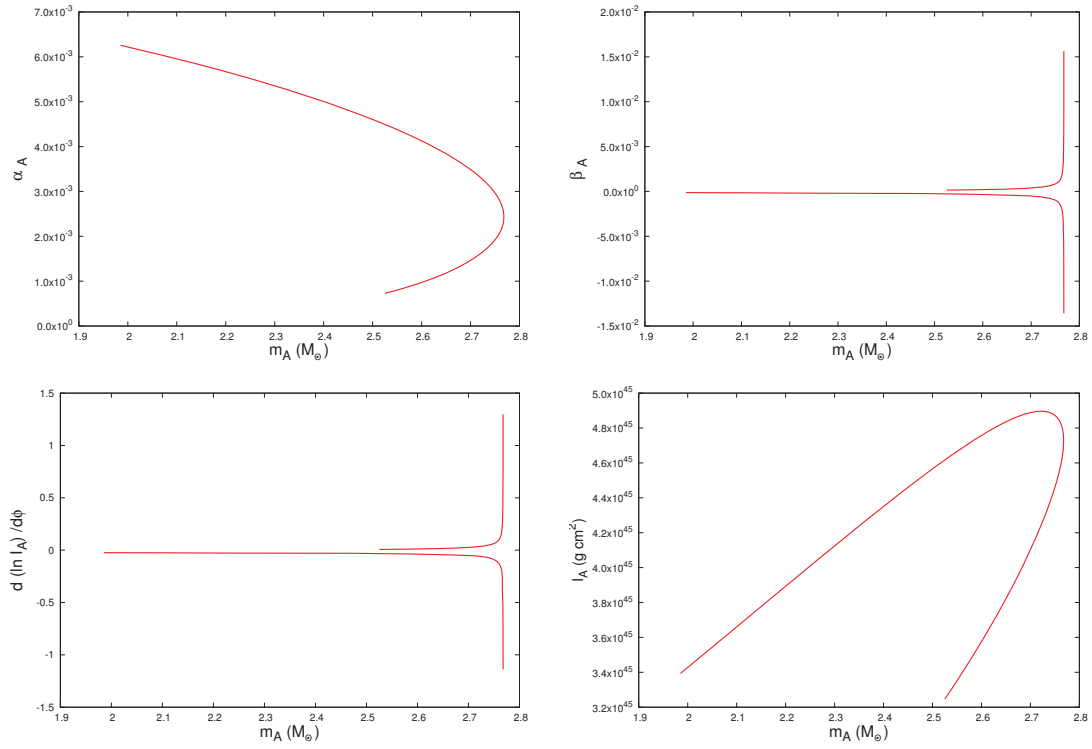
Figure 3.22: EOS MS1: Sensitivities and moment of inertia vs the total mass of the star m_A in solar masses for $\alpha_0 = 10^{-2}$

become negative in the "spontaneous scalarization" case, which never happens in FJBD theory. Finally, slow ration models with a realistic equation of state were produced. Here, a wide range for the values of the coupling constant $\tilde{\alpha}_0$ was used and both the first, second and moment of inertia sensitivities are calculated. The form of the sensitivities as a function of the mass of the star in the Einstein frame remains the same, while the magnitude depends on the value of $\tilde{\alpha}_0$. The sensitivity α_A approaches the value of $\tilde{\alpha}_0$ in the low central density limit. On the other hand, the value of the Jordan frame sensitivities asymptotically approaches 0 in the low central density limit and it asymptotically approaches 0.5 in the high density limit, for all models. The value 0.5 corresponds to the sensitivity of a black hole.

This study is part of a greater project with Michael Horbatsch, Emanuele Berti and Justin Alsing. The final goal of the project is to calculate the energy fluxes of binary systems in Scalar Tensor theories. In order to do that, the calculation of sensitivities for the allowed range of both parameter $\tilde{\alpha}_0$ and $\tilde{\beta}_0$ is required. For the most stringiest bounds on these parameters see [28]. Finally, this data can be used by future studies of compact binaries in Scalar Tensor theories, since the sensitivities are present in the equations of motion of compact binaries.

3.2 $f(R)$ theories

The same numerical method is used for $f(R)$ theories of gravity as Scalar Tensor theories. The initial conditions are defined at the origin, except for the Ricci scalar which is defined infinitely far away from the star, or at the cosmological horizon for de Sitter models. The cosmological horizon corresponds to the the point where the g_{rr} component of the de Sitter metric (2.119) becomes infinite. The boundary value of the Ricci scalar R_1 is defined as the minimum of the JPS potential $V_{JPS}(R)$ (2.111). The system (2.114) - (2.117) is already in the form $y_i'(x) = f_i(x, y_i, y_i')$ where the dependent variables are A, B, R, p and the independent

variable is r. These equations are re-scaled as we will see in the following section. The integration proceeds until the pressure becomes vanishingly small, at which point we define the radius of the star. The integration continues, with the pressure set to zero until we reach a radius very close to the cosmological horizon $r = r_H$. Notice that since we know the asymptotic value for the Ricci scalar we can know the value for the cosmological horizon,

$$r_H = \sqrt{\frac{3}{\Lambda}} = \sqrt{\frac{12}{R_1}} \tag{3.9}$$

Then, we check the difference of the value for R_1 found with the code against the desired asymptotic value of the Ricci scalar. The difference is used to change the initial guess for the Ricci scalar and the process is repeated. After several iterations the desired value is reached and the computation stops after the physical quantities of the star have been calculated. As we will see, picking the initial condition for R can be problematic, since the code crashes if the value differs significantly from the real solution. Before that though, we need to discuss the re-scaled equations that are actually used in the code.

3.2.1 Equations used for numerical analysis

Following the same procedure as in section 3.1.2 we use re-scaled dimensionless variables. We use the following re-scaling

$$r = r_0 \hat{r} \tag{3.10}$$

$$R = R_0 \tilde{R} \tag{3.11}$$

$$\rho = \rho_0 \hat{\rho} \tag{3.12}$$

$$p = \rho_0 \hat{p} \tag{3.13}$$

71

where we set $\rho_0 = \rho_c$, corresponding to the central value. This re-scaling leaves the structure equations unchanged except for some coefficients of $R_0 r_0^2$ and $\rho_0 r_0^2$. We set

$$R_0 r_0^2 = 1 \tag{3.14}$$

$$\rho_0 r_0^2 = C \tag{3.15}$$

so the equations are unchanged except for a factor of C. The parameter C controls the ratio of the matter density inside the neutron star and the cosmological matter density ρ_Λ. We define

$$\upsilon = \frac{\rho_\Lambda}{\rho_c} \tag{3.16}$$

Assuming a typical value for the central density of a neutron star is $\rho_c = 10^{17}\,\mathrm{kg/m^3}$ and the density that corresponds to the cosmological constant is $\rho_\Lambda \sim 10^{-26}\,\mathrm{kg/m^3}$ makes $\upsilon \sim 10^{-43}$. Such a large difference in the two scales is extremely hard to handle numerically, so larger values must be used. In our code, the lowest value that is used is $\upsilon = 5 \times 10^{-11}$. Since $\rho_\Lambda = \frac{\Lambda}{8\pi G}$ from (2.120) it follows that

$$\upsilon = \frac{\tilde{R}_1}{32\pi G} C^{-1} \tag{3.17}$$

where $\tilde{R}_1 = \tilde{R}(\hat{r}_H)$ is the value of the Ricci scalar that we will seek as a boundary condition at the cosmological horizon.

3.2.2 Results

We firstly present results for constant density stars, like the ones used by JPS. Various choices of the model of the $f(R)$ theory and the parameters of the chosen model were used. Unlike JPS, we are able to produce models with $p > \rho/3$. We show here the re-scaled Ricci scalar R/R_c and the radial component of the metric g_{rr} for different choices of the central

pressure. We notice that for models where a non-zero value for the Ricci scalar has been selected as the boundary condition, there exists a cosmological horizon, as expected. This is obvious in our figures since the g_{rr} component of the metric becomes infinite when the cosmological horizon is reached (Fig. 3.23, 3.25). We also notice, that the value of the Ricci scalar at the origin increases with central pressure, until some value very close to $p_c = \rho_c/3$, and then it decreases again. The Ricci scalar becomes negative for Starobinsky models with no cosmological horizon, $R(\infty) = 0$, as we can see in figure 3.29. The values of the models presented here are chosen so we can show that our models are in complete agreement with JPS.
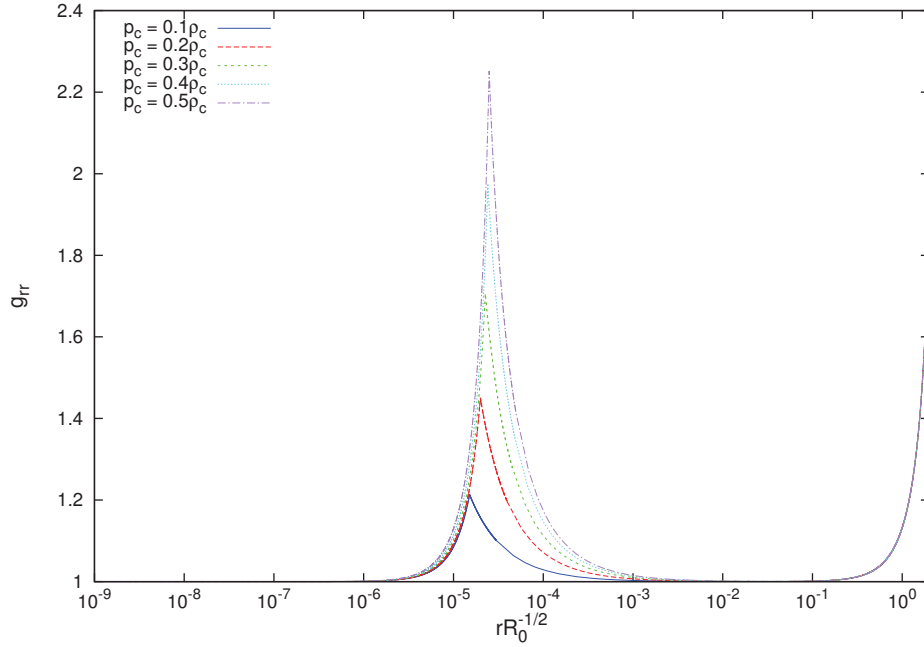
Figure 3.23: Radial component of the metric g_{rr} for the Miranda model with $\alpha = 1.2$, $\rho_0 = 5 \times 10^7 R_1/G$ and $R_1 \sim 1.405 R_0$. The first sharp peak corresponds to the radius of the star, while the second peak corresponds to the cosmological horizon.

Next we check the dependance of the the models on the value of the cosmological density. As we explained this value is inversely proportional to the parameter C used in our code. By changing the constant C we obtain the mass and the radius of the star for different
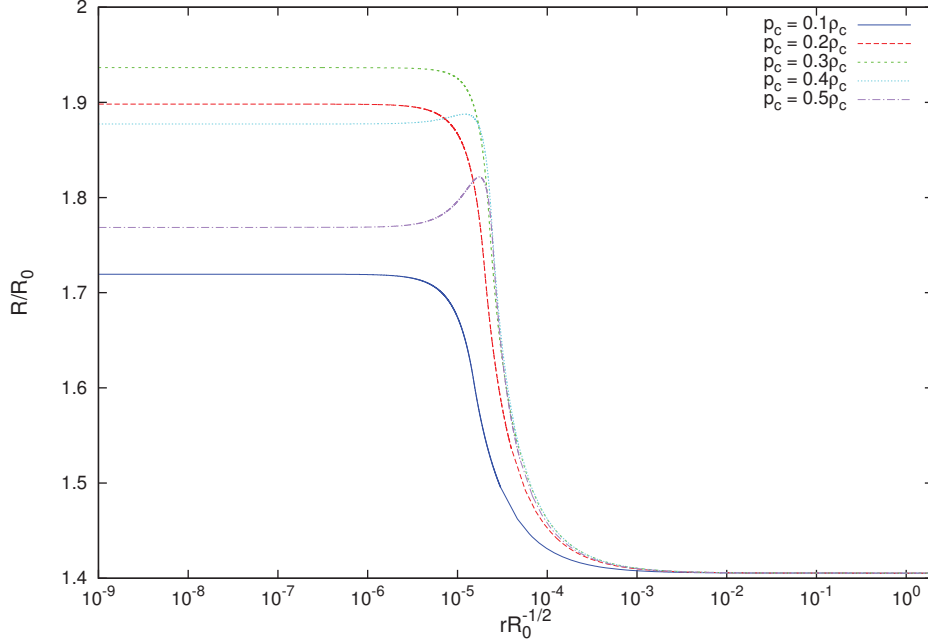
Figure 3.24: Scalar curvature R for the Miranda model with $\alpha = 1.2$, $\rho_0 = 5 \times 10^7 R_1/G$ and $R_1 \sim 1.405 R_0$

values of υ, keeping the central density constant. Firstly, we use the Starobinsky model with $\lambda = 1.56$. The potential has two minima for this value, $\tilde{R}_{11} \simeq 1.984$ and $\tilde{R}_{12} = 0$. The first corresponds to a de Sitter solution with a cosmological constant $\Lambda = \frac{R_{11}}{4}$, while the second one corresponds to an asymptotically flat solution.

The two cases give considerably different values for the mass and the radius of the star for any value of υ in the range $10^{-4} > \upsilon > 5 \times 10^{-11}$. The mass for the first case is $M \simeq 1.739 M_\odot$ and the radius is $r \simeq 9.578$ km, while for the second case the mass is $M \simeq 1.909 M_\odot$ and the radius is $r \simeq 11.09$ km for a central density $\rho_c = 2.98 \times 10^{18} \text{kg/m}^3$. The scalar curvature as a function of the radius is also completely different for the two cases. We plot the percentage difference for the first case, $\tilde{R}_1 \simeq 1.984$ (Fig. 3.32)

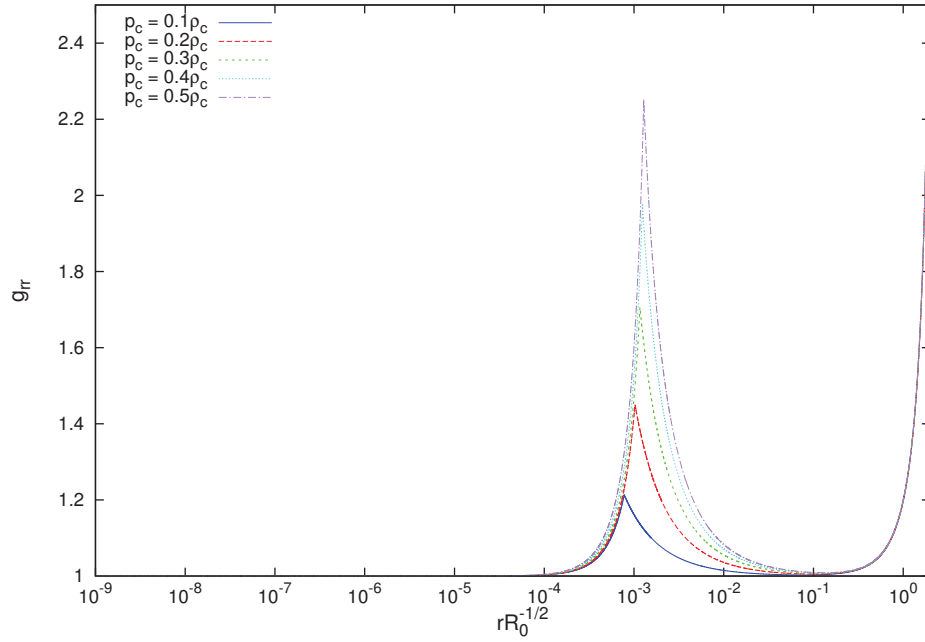$$\alpha = \frac{|x - x_{real}|}{x_{real}} \times 100\% \tag{3.18}$$

Figure 3.25: Radial component of the metric g_{rr} for the Starobinsky model with $\lambda = 1.56$, $\rho_0 = 10^6 R_1/(16\pi G)$ and $R_1 \sim 1.984 R_0$. The first sharp peak corresponds to the radius of the star, while the second peak corresponds to the cosmological horizon.
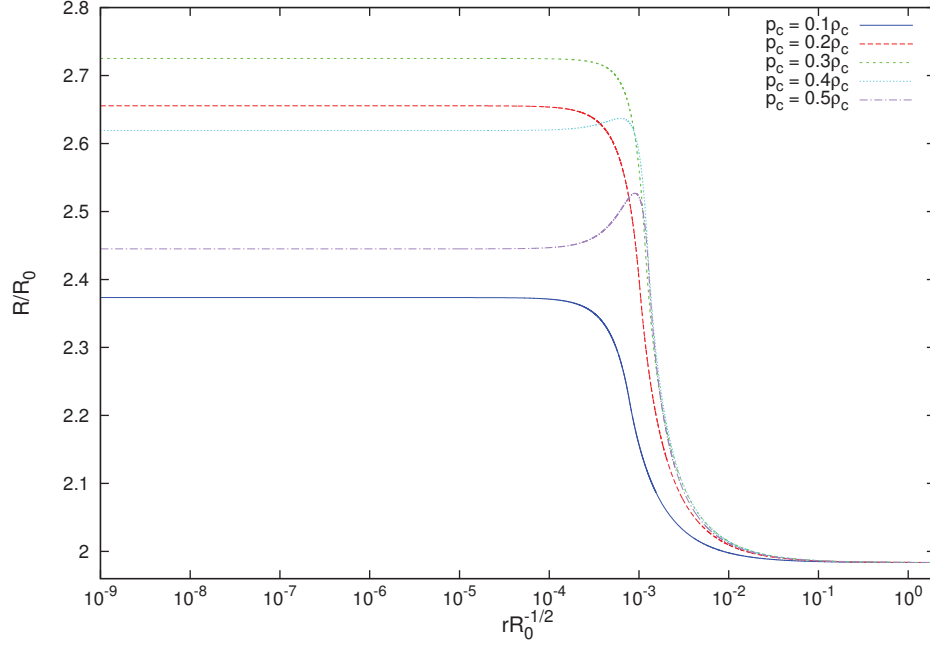
Figure 3.26: Scalar curvature R for the Starobinsky model with $\lambda = 1.56$, $\rho_0 = 10^6 R_1/(16\pi G)$ and $R_1 \sim 1.984 R_0$
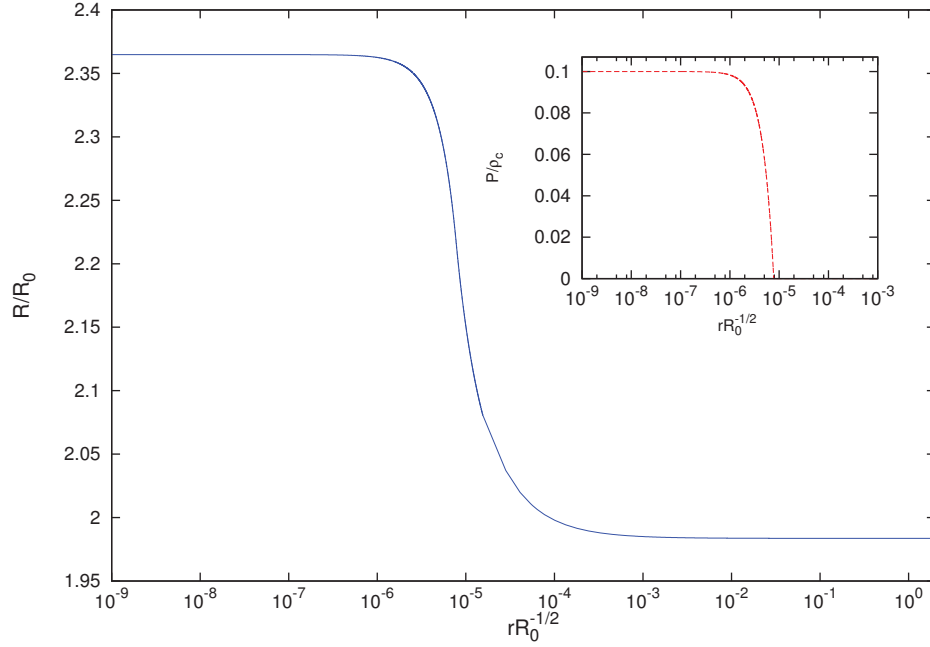

Figure 3.27: Scalar curvature R for the Starobinsky model with $\lambda = 1.56$, $\rho_0 = 10^{10} R_1/(16\pi G)$ and $R_1 \sim 1.984 R_0$
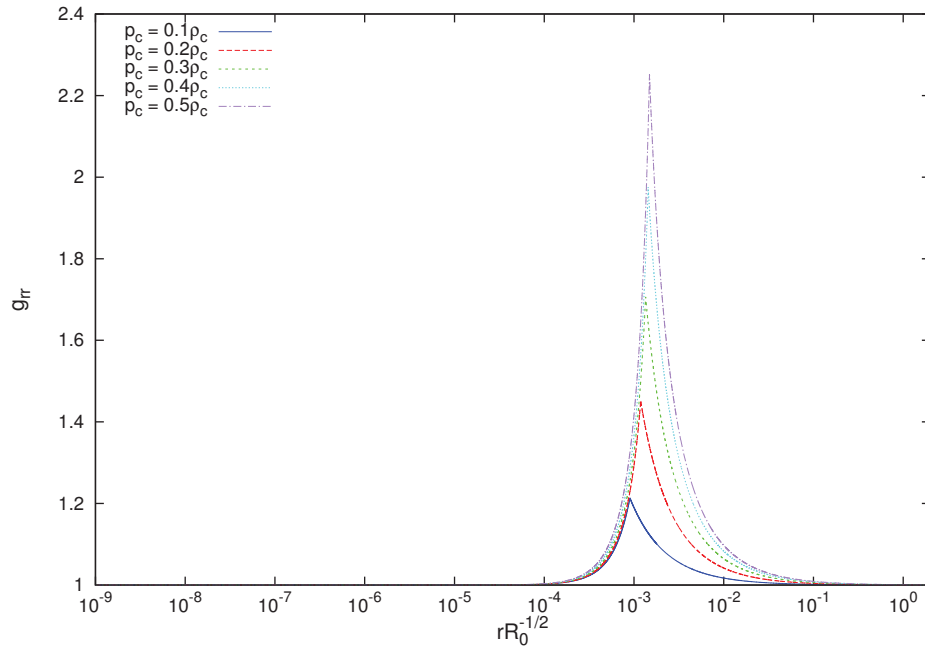
Figure 3.28: Radial component of the metric g_{rr} for the Starobinsky model with $\lambda = 1.2$, $\rho_0 = 10^6 R_1/(16\pi G)$ and $R_1 \sim 1.984 R_0$. The sharp peak corresponds to the radius of the star.
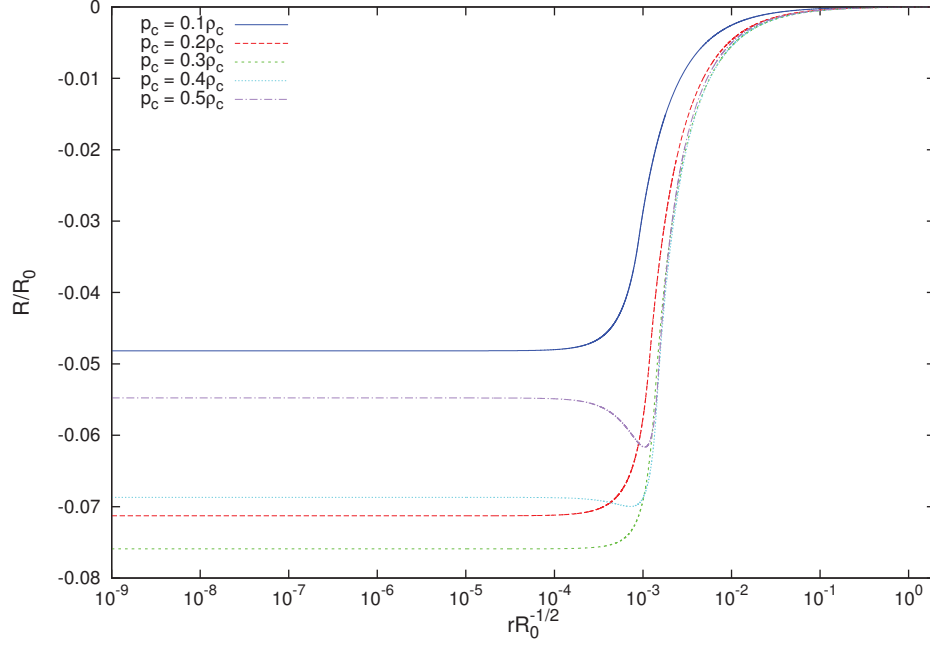
Figure 3.29: Scalar curvature R for the Starobinsky model with $\lambda = 1.2$, $\rho_0 = 10^6 R_1/(16\pi G)$ and $R_1 \sim 1.984R_0$
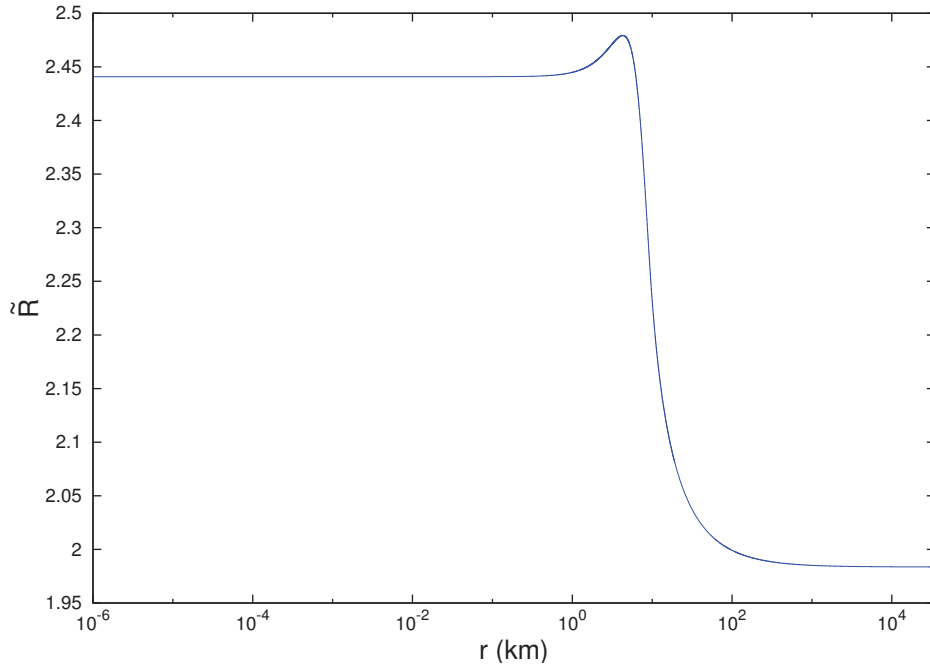

Figure 3.30: The scalar curvature $\tilde{R}$ vs the radius of the star for the Starobinsky model with $\lambda = 1.56$, $\tilde{R}_1 \simeq 1.984$ and $\rho_0 = 2.98 \times 10^{18}\text{kg/m}^3$
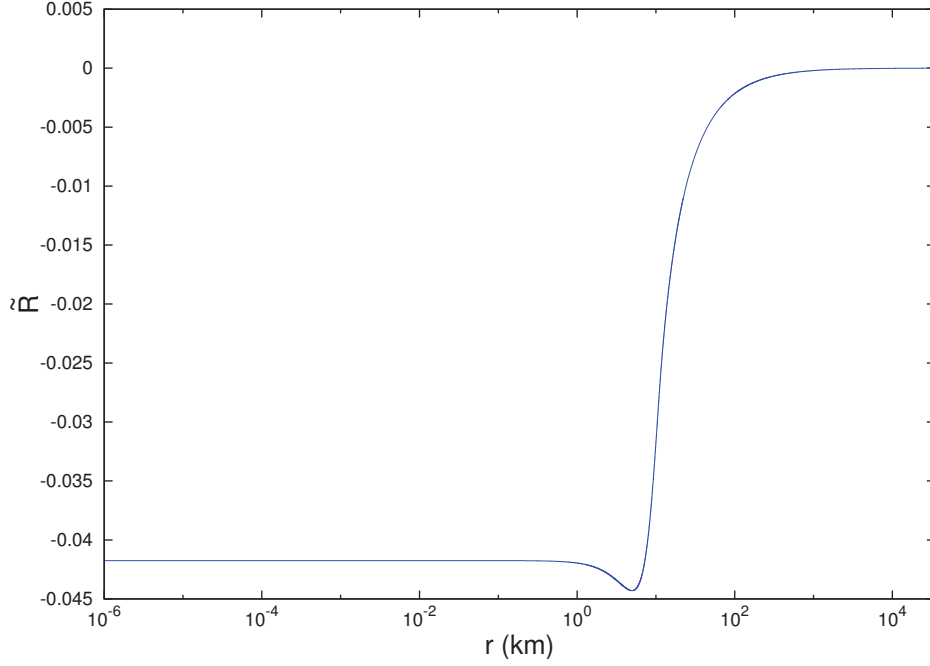
Figure 3.31: The scalar curvature $\tilde{R}$ vs the radius of the star for the Starobinsky model with $\lambda = 1.56$, $\tilde{R}_1 = 0$ and $\rho_0 = 2.98 \times 10^{18} \mathrm{kg/m^3}$

for values of mass and radius compared to the value x_{real} obtained with the smallest υ, which should be the most realistic one. For comparison, we plot the percentage difference of the mass and the radius for the asymptotically flat $R_1 = 0$ case (Fig. 3.34). In this case $\Lambda = 0$ so $\upsilon = 0$. The constant C is changed in the same manner as the previous case. In this case the constant C corresponds only to a re-scaling of the equations according to (3.15). The difference in the values is due to numerical errors. We can see that the percentage differences for the two cases (de Sitter and asymptotically flat case), especially for the radius, are comparable. Thus, we can conclude that the mass and radius remain more or less constant for different values of υ but only for the same value of $\tilde{R}$ at infinity. If we choose a different minimum for the potential, the mass and the radius change significantly.

Finally, we present results obtained by using a polytropic EoS. The parameters of the EoS are the same as in table 3.1. Using the same steps as in section 3.1.3 we are able to create M vs R diagrams for different values of the parameters of the $f(R)$ models. Unlike
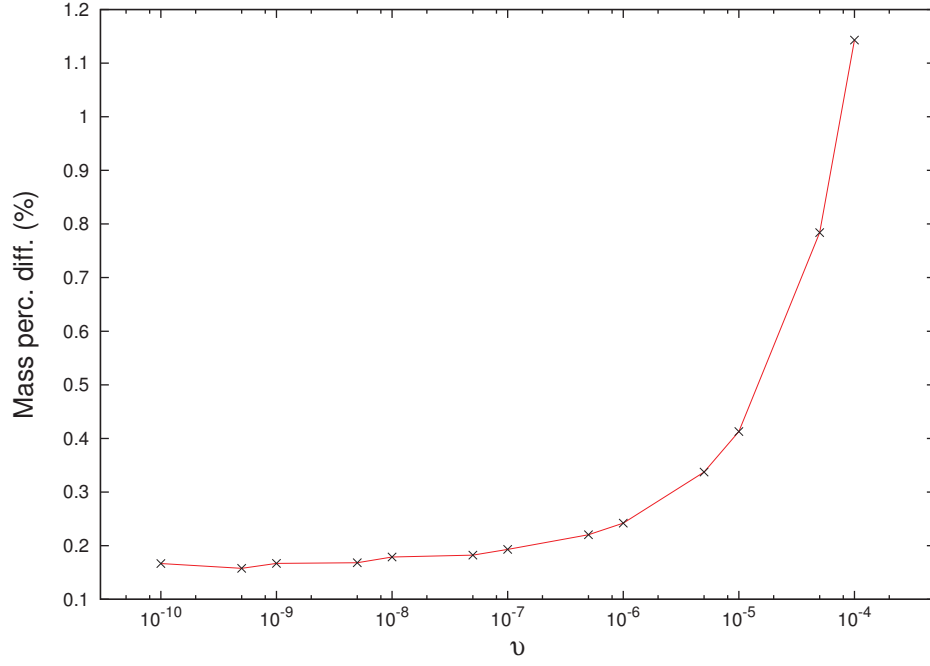
Figure 3.32: The percentage difference of the total mass of the star vs υ for the Starobinsky model with $\lambda = 1.56$ and $\tilde{R}_1 \simeq 1.984$

Figure 3.33: The percentage difference of the radius of the star vs υ for the Starobinsky model with $\lambda = 1.56$ and $\tilde{R}_1 \simeq 1.984$

Figure 3.34: The percentage difference of the total mass of the star vs υ for the Starobinsky model with $\lambda = 1.56$ and $\tilde{R}_1 = 0$
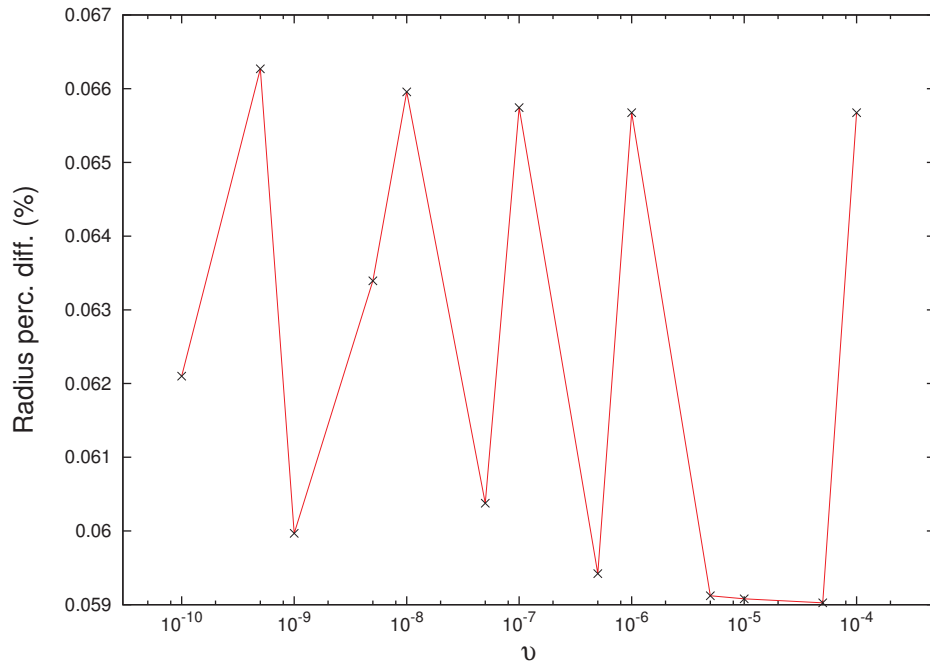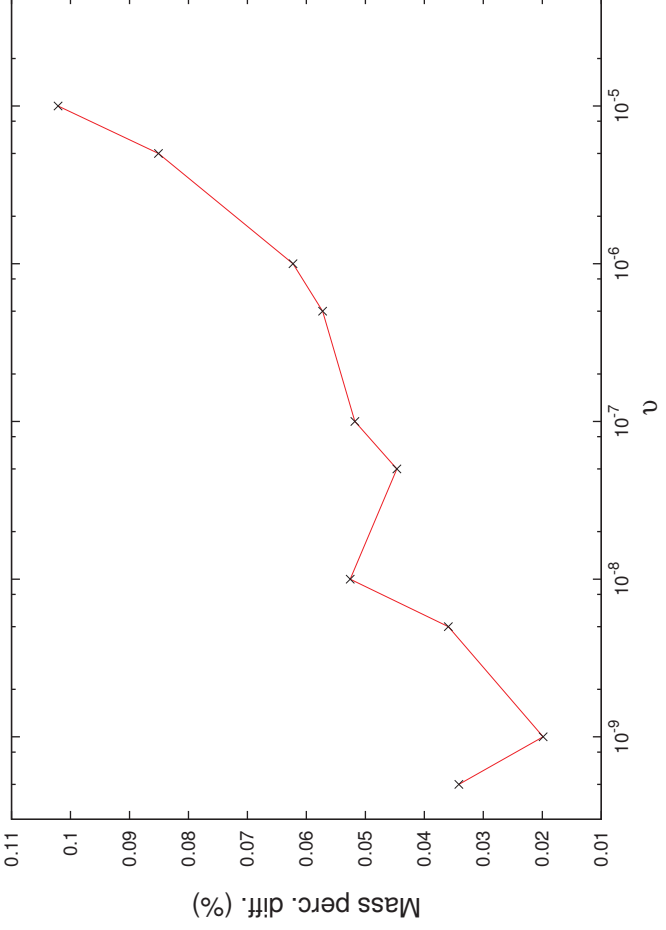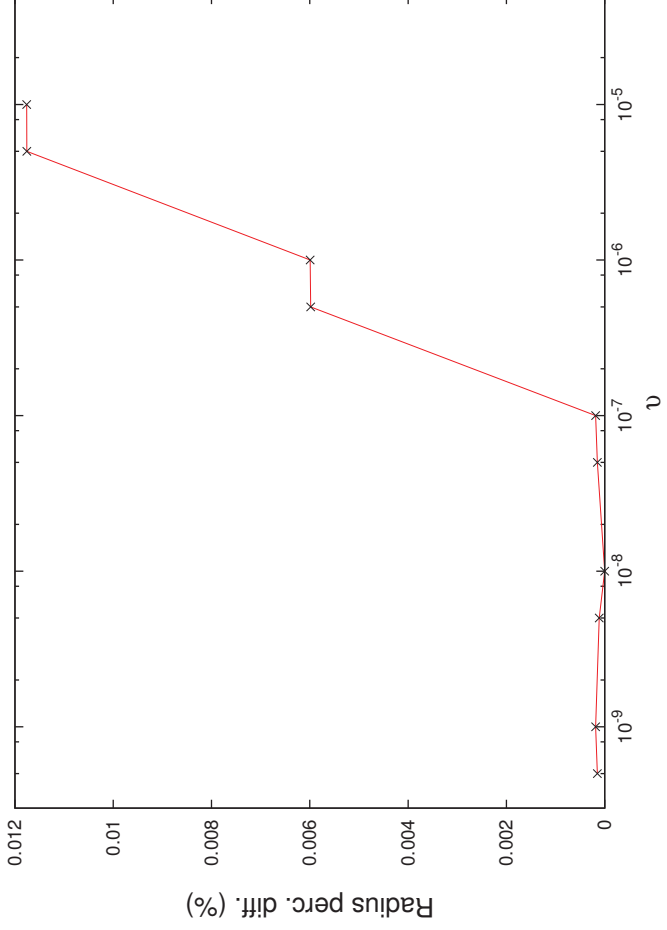

Figure 3.35: The percentage difference of the radius of the star vs υ for the Starobinsky model with $\lambda = 1.56$ and $\tilde{R}_1 = 0$

81

the Scalar Tensor theory case, where about 200 models were used for each diagram, this number is significantly lower here, due to the difficulty of integrating the models, especially in the case of a cosmological horizon. The code is very sensitive to the initial guess for the initial condition of the Ricci scalar. If the initial guess is not close enough to the real value, which is obtained after several iterations using the shooting method, the code will quickly crash. This means that the process cannot be easily automated, since the initial guess needs to be carefully chosen for each individual model.

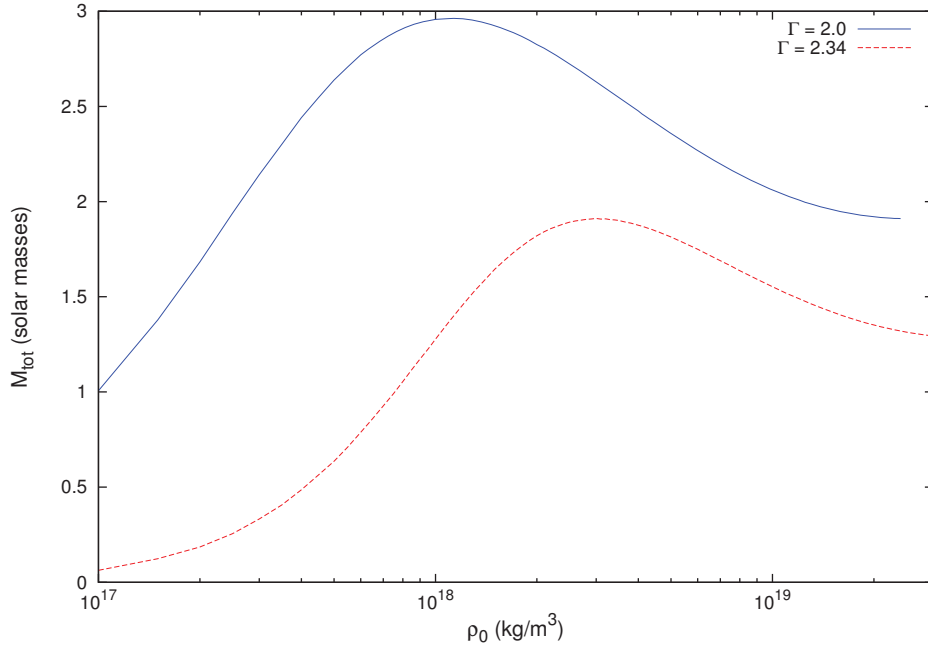Figure 3.36: The total mass of the star vs the central density for the Starobinsky model with $\lambda = 1.2$ and $R_1 = 0$.

3.2.3 Discussion

We have shown that numerical models of neutron stars can be constructed by using the JPS formalism and a polytropic EoS. Two main points can be made about our models compared with the already existing models by UH, KM, BL and JPS. First, we were able to construct
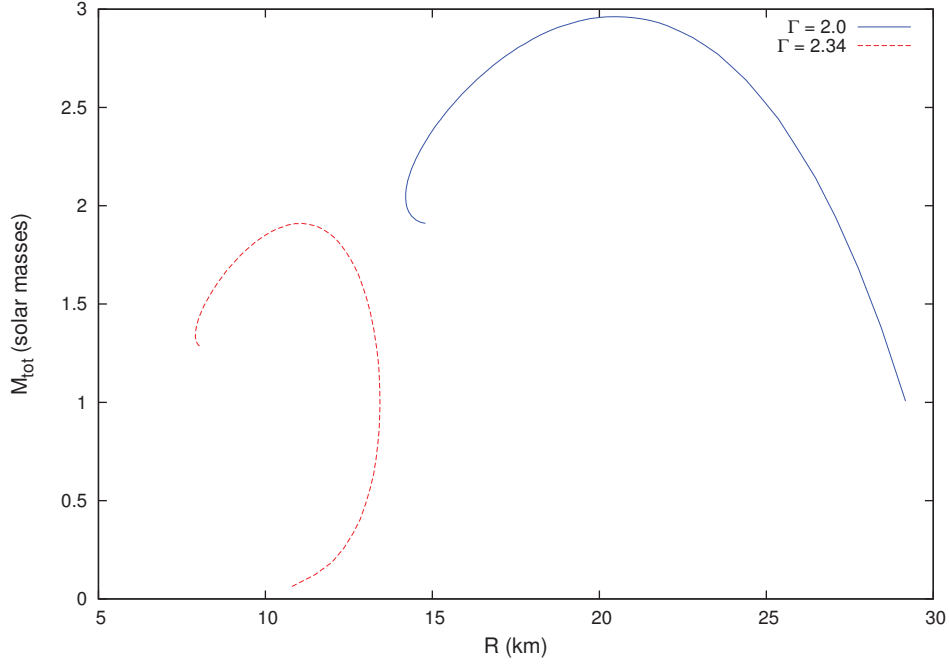
Figure 3.37: The total mass of the star vs the radius of the star for the Starobinsky model with $\lambda = 1.2$ and $R_1 = 0$.

models with high interior pressure, namely $p_c > \rho_c/3$, both for the constant density and the polytropic EoS case. BL had claimed that instabilities would make it impossible for models with $p_c > \rho_c/3$ to be constructed, while UH claimed they could construct them but it was numerically challenging. JPS also did not show any models where $p_c > \rho_c/3$ but we see no reason that they would not be able to construct them. In General Relativity as in Scalar Tensor theories of gravity, star models with arbitrarily high pressure exist, so we see no a priori reason why they wouldn't exist in $f(R)$ theory. With our results we show that constructing models with $p_c > \rho_c/3$ is no more challenging than models with $p_c > \rho_c/3$ if a better theoretical approach is used, namely the JPS method. Thus, we have shown that earlier objections to $f(R)$ theories on the basis of the inability to construct viable neutron star models are unfounded.

Another point is that our numerical models are more realistic of those of BL and JPS. JPS were trying to illustrate their new approach, so they only constructed unrealistic constant
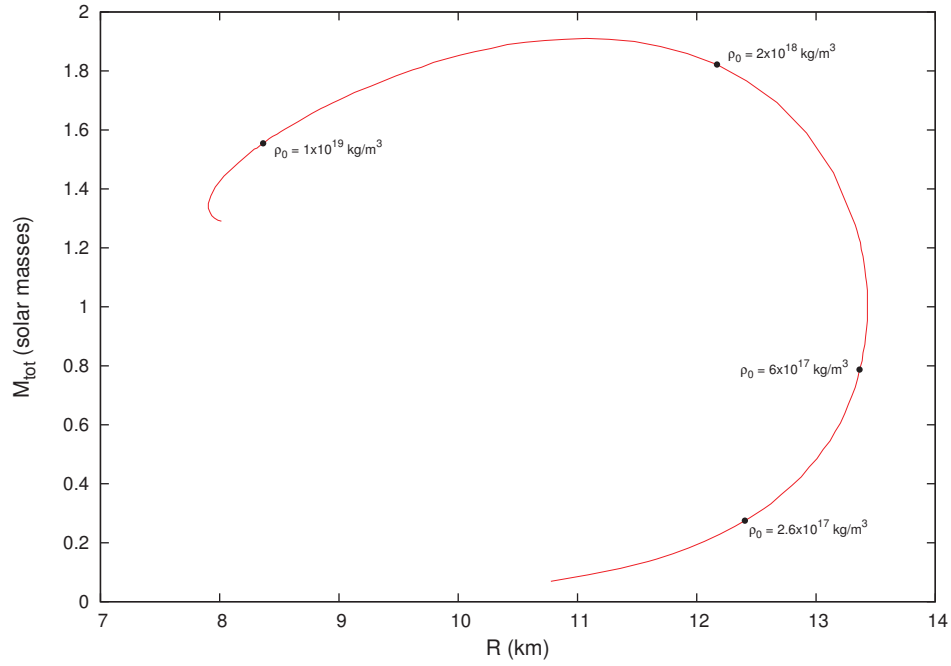
Figure 3.38: EOS II: The total mass of the star vs the radius of the star for the Starobinsky model with $\lambda = 1.2$ and $R_1 = 0$, with the corresponding densities shown. Models with $\rho_c \geq 2.2 \times 10^{18} \text{kg/m}^3$ have $p_c > \rho_c/3$.

density models. Even though BL used a polytropic EoS, as we discussed, they found it challenging to construct models with a realistic cosmological density. The values for v they used were in the range of $10^{-4} < v < 10^{-2}$. The realistic value for v is of order $\sim 10^{-43}$. Constructing models with such a huge difference between the two scales, the density inside the star and the cosmological density, is numerically challenging even in General Relativity. However, we should strive to construct models with a value as realistic as possible. This is because, in a de Sitter space the cosmological horizon, determined by the value of Λ, needs to be far away enough for us to be able to extract realistic quantities such as the mass of the star. We have demonstrated that we can construct models with a value of v as small as 5×10^{-11}, where the cosmological horizon is more than 1000 times larger than the radius of the star. Even though this is still very unrealistic, it is a significant improvement on previous results. In addition we also demonstrated that, just because the value of the cosmological density is so small, one can not naively set this to zero for practical reasons, since this corresponds to a different scalar curvature and yields very different results.

These results help strengthen the argument of the existence of neutron stars in $f(R)$ theories. We have demonstrated that using the JPS method we can produce polytropic EoS models of neutron stars for all the viable $f(R)$ models. Since there exists a method free of the difficulties previous researchers had encountered, we can employ this method to produce more realistic neutron star models, like the ones that already exist for General Relativity. The next immediate step would be to use more realistic EoSs like the ones used in the Scalar Tensor theory case we discussed earlier. Furthermore, another step is to construct models using a slow rotation metric, again like the one used in the Scalar Tensor case. Finally, when results for these cases have been obtained and the argument of the existence of neutron stars in $f(R)$ theories has been settled, numerical models of neutron star mergers can be studied along with gravitational radiation in $f(R)$ theories. Such studies are necessary to be able to determine the viability of $f(R)$ theories when results of the new generation of gravitational

wave detectors are available.

Bibliography

1. Akmal, A. and Pandharipande, V. R., Phys. Rev. C **56**, 2261 (1997).

2. Amendola, L., Gannouji, R., Polarski, D., and Tsujikawa, S., Phys. Rev. D **75**, 083504 (2007).

3. Antia, H. M., Chitre, S. M., and Gough, D. O., Astron. Astrophys. **477**, 657 (2008).

4. Arnett, D. W. and Bowers, R. L., Astrophys. J. **33**, 415 (1977).

5. Babichev, E. and Langlois, D., Phys. Rev. D **80**, 121501 (2009).

6. Babichev, E. and Langlois, D., Phys. Rev. D **81**, 124051 (2010).

7. Bergmann, P. G., Int. J. Theor. Phys. **1**, 25 (1968).

8. Bertotti, B., Iess, L., and Tortora, P., Nature **425**, 374 (2003).

9. Brans, C. and Dicke, R. H., Phys. Rev. D **124**, 925 (1961).

10. Capozziello, S., Int. J. Mod. Phys. D **11**, 483 (2002).

11. Capozziello, S., Cardone, V., Carloni, S., and Troisi, A., Int. J. Mod. Phys. D **12**, 1969 (2003).

12. Carroll, S., Duvvuri, V., Trodden, M., and Turner, M. S., Phys. Rev. D **70**, 043528 (2004).

13. Chamel, N. and Haensel, P., Living Reviews in Relativity **11**, 10 (2008).

14. Chatziioannou, K., Yunes, N., and Cornish, N., Phys. Rev. D **86**, 022004 (2012).

15. Coquereaux, R. and Esposito-Farese, G., Annales de l'institut Henri Poincar (A) Physique thorique **52**, 113 (1990).

16. Dabrowski, M., Garecki, J., and Blaschke, D., Annalen der Physik **18-1**, 13 (2009).

17. Damour, T. and Esposito-Farese, G., Classical and Quantum Gravity **9**, 2093 (1992).

18. Damour, T. and Esposito-Farese, G., Phys. Rev. Lett. **70**, 15 (1993).

19. Damour, T. and Esposito-Farese, G., Phys. Rev. D **54**, 1474 (1996).

20. De Felice, A. and Tsujikawa, S., Living Reviews in Relativity **13**, 3 (2010).

21. Diaz Alonso, J. and Ibanez Cabanell, J. M., Astrophys. J. **291**, 308 (1985).

22. Dolgov, A. and Kawasaki, M., Phys. Lett. B **573**, 1 (2003).

23. Engvik, L., Hjorth-Jensen, M., Osnes, E., Bao, G., and Ostgaard, E., Phys. Rev. Lett. **73**, 2650 (1994).

24. Faraoni, V., Gunzig, E., and Nardone, P., Fund. Cosmic Phys. **20**, 121 (1999).

25. Faraoni, V. and Nadeau, S., Phys. Rev. D **72**, 124005 (2005).

26. Fienga, A., Laskar, J., Kuchynka, P., Manche, H., Desvignes, G., Gastineau, M., Cognard, I., and Theureau, G., Celestial Mechanics and Dynamical Astronomy **111**, 363 (2011).

27. Fierz, M., Helv. Phys. Acta **29**, 128 (1956).

28. Freire, P. C. C., Wex, N., Esposito-Farse, G., Verbiest, J. P. W., Bailes, M., Jacoby, B. A., Kramer, M., Stairs, I. H., Antoniadis, J., and Janssen, G. H., Monthly Notices of the Royal Astronomical Society **423-4**, 3328 (2012).

29. Gold, T., Nature **218**, 731 (1968).

30. Hartle, J. B., , Astrophys. J. **150**, 1005 (1967).

31. Hartle, J. B., *Gravity* (2003).

32. Hewish, A., Bell, S. J., Pilkington, J. D. H., Scott, P. F., and Collins, R. A., Nature **217**, 709 (1968).

33. Hu, W. and Sawicki, I., Phys. Rev. D **76**, 064004 (2007).

34. Jaime, L. G., Patino, L., and Salgado, M., Phys. Rev. D **83**, 024039 (2011).

35. Jordan, P., Schwerkraft und Weltall (1955).

36. Khoury, J. and Weltman, A., Phys. Rev. D **69**, 044026 (2004).

37. Khoury, J. and Weltman, A., Phys. Rev. Lett. **93**, 171104 (2004).

38. Kobayashi, T. and Maeda, K.-i., Phys. Rev. D **78**, 064019 (2008).

39. Lambert, S. B. and Le Poncin-Latte, C., Astron. Astrophys. **499**, 331 (2009).

40. Landau, L. D. and Lifshitz, E. M., *The Classical Theory of Fields* (1975).

41. Lattimer, J. M. and Prakash, M., Astrophys. J. **550**, 426 (2001).

42. Lattimer, J. M., Prakash, M., and Yahil, A., Astrohys. J. **355**, 241 (1990).

43. Lorimer, D. R., Living Reviews in Relativity **11**, 8 (2008).

44. M., E. D., Astrohys. J. **196**, L59 (1975).

45. Mecheri, R., Abdelatif, T., Irbah, A., Provost, J., and Berthomieu, G., Solar Phys. **222**, 191 (2004).

46. Miranda, V., Jors, S. E., Waga, I., and Quartin, M., Phys. Rev. Lett. **102**, 221101 (2009).

47. Misner, C. W., Thorne, K., and Wheeler, J., *Gravitation* (1974).

48. Muller, H. and Serot, B. D., Nucl. Phys. A **606**, 508 (1996).

49. Muther, H., Prakash, M., and Ainsworth, T. L., Phys. Lett. B **199**, 469 (1987).

50. Navarro, I. and Van Acoleyen, K., J. Cosmol. Astropart. Phys. **2007(02)**, 022 (2007).

51. Nojiri, S. and Odintsov, S., Phys. Rev. D **68**, 123512 (2003).

52. Nordvedt, K. J., Astrophysical Journal **161**, 1059 (1970).

53. Olmo, G. J., Phys. Rev. D **72**, 083505 (2005).

54. Oppenheimer, J. R. and Volkoff, G. M., Physical Review **55**, 374 (1939).

55. Postnov, K. A. and Yungelson, L. R., Living Reviews in Relativity **9**, 6 (2006).

56. Press, W. H., Teukolsky, S. M., Vetterling, W. T., and Flannery, B. P., *Numerical Recipes* (2007).

57. Richards, D. and Comella, J., Nature **222**, 551 (1969).

58. Schutz, B. F., *A first course in general relativity* (1985).

59. Shapiro, S. L. and Teukolsky, S. M., *Black Holes, White Dwarfs and Neutron Stars* (1983).

60. Sotiriou, T. P. and Faraoni, V., Rev. Mod. Phys. **82**, 451 (2010).

61. Stairs, I. H., Living Reviews in Relativity **6**, 5 (2003).

62. Starobinsky, A. A., Phys. Lett. B **91**, 99 (1980).

63. Starobinsky, A. A., J. Exp. Theor. Phys. Lett. **86**, 157 (2007).

64. Stergioulas, N., Living Reviews in Relativity **6**, 3 (2003).

65. Tolman, R. C., Physical Review **55**, 364 (1939).

66. Tsujikawa, S., Phys. Rev. D **77**, 023507 (2008).

67. Upadhye, A. and Hu, W., Phys. Rev. D **80**, 064002 (2009).

68. Verma, A. K., Fienga, A., Laskar, J., Manche, H., and Gastineau, M., Astron. Astrophys. **561**, A115 (2014).

69. Wagoner, R. V., Phys. Rev. D **1**, 3209 (1970).

70. Will, C. M., *Theory and experiment in gravitational physics* (1993).

71. Will, C. M., Living Reviews in Relativity **9**, 3 (2006).

72. Yunes, N. and Siemens, X., Living Reviews in Relativity **16**, 9 (2013).

Appendices

Appendix A

$f(R)$ Potentials

We provide here useful expressions for the various models used in our $f(R)$ theory models. The function $f(x)$ is shown, where $x = R/R_c$. This is related to $f(R)$ as

$$f(R) = R_c f(x) \tag{A.1}$$

$$\frac{d^n}{dR^n} f(R) = R_c^{1-n} \frac{d^n}{dx^n} f(x) \tag{A.2}$$

Then, the potential $V(x)$ is shown, as defined by JPS, along with its derivative. Finally, the coefficients of Taylor expansion of the quantities A, p, R are shown, as defined in equations (2.121) - (2.123).

A.1 Miranda et al

The function is given by

$$f(x) = x - \alpha \ln(1 + x) \tag{A.3}$$

The potential is given by

$$V(x) = \frac{1}{6}(x(6\alpha + x) - 2\alpha(2x + 3)\log(x + 1)) \tag{A.4}$$

$$\frac{dV}{dR} = \frac{1}{3}\left(\frac{\alpha x}{x+1} - 2\alpha \log(x+1) + x\right) \tag{A.5}$$

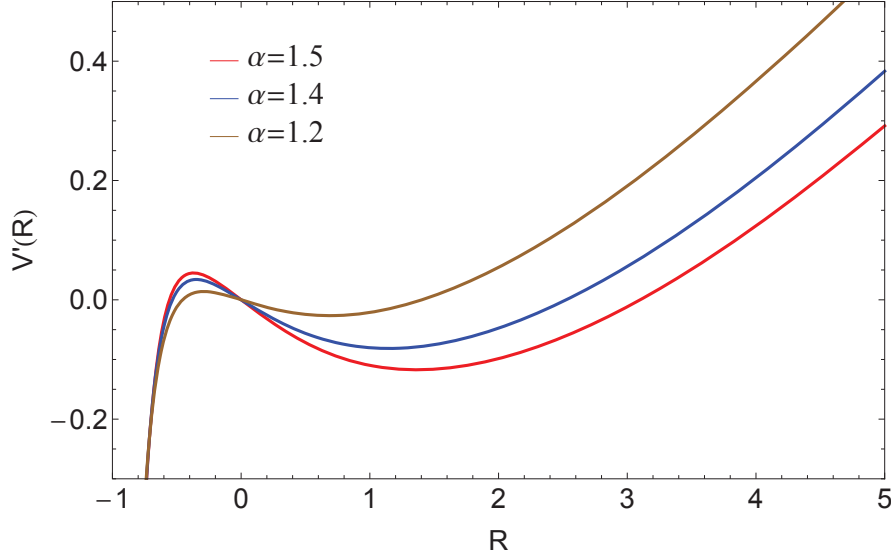Figure A.1: The potential of the Miranda et al model vs the Ricci scalar for different values of the parameter λ

The Taylor expansion coefficients are

$$A_1 = \frac{48\pi p_0(x+1) + R_c x(-\alpha + 2x + 2) - \alpha R_c(x+1)\ln(x+1) + 32\pi \rho_0(x+1)}{12(-\alpha + x + 1)} \tag{A.6}$$

$$p_1 = \frac{(p_0 + \rho_0)[-16\pi(x+1)(7p_0 + 6\rho_0) + R_c x(-3\alpha + 2x + 2) + \alpha R_c(x+1)\ln(x+1)]}{40(-\alpha + x + 1)} \tag{A.7}$$

$$R_1 = \frac{R_c(x+1)[24\pi p_0(x+1) + R_c x(\alpha + x + 1) - 2\alpha R_c(x+1)\log(x+1) - 8\pi \rho_0(x+1)]}{15\alpha} \tag{A.8}$$

A.2 Starobinsky

The function is given by

$$f(x) = x - \lambda[1 - (1 + x^2)^{-1}] \tag{A.9}$$

The potential is given by

$$V(x) = \frac{6\lambda\left(x^2+1\right)\tan^{-1}(x) + x\left(-6\lambda + x^3 - 4\lambda x^2 + x\right)}{6\left(x^2+1\right)} \tag{A.10}$$

$$\frac{dV}{dR} = \frac{1}{3}x\left[1 - \frac{2\lambda x^3}{\left(x^2+1\right)^2}\right] \tag{A.11}$$
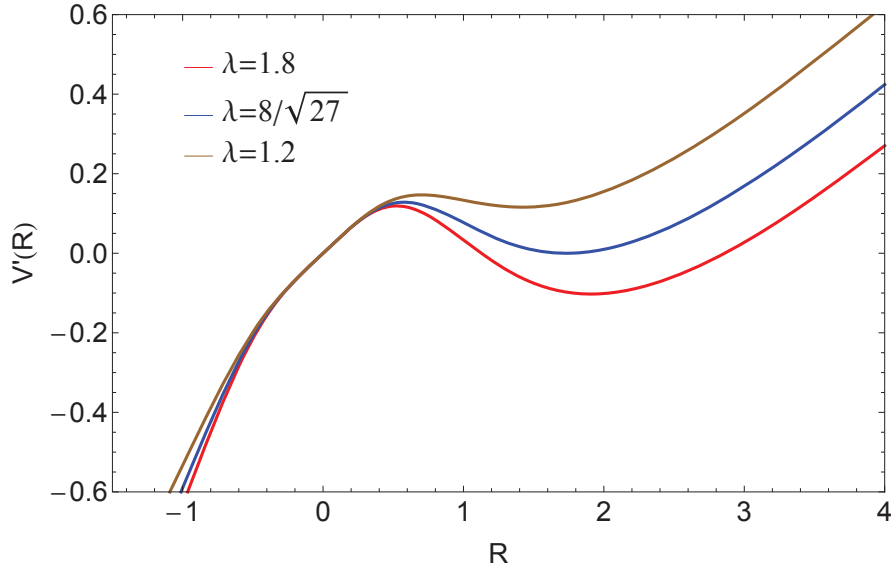

Figure A.2: The potential of the Starobinsky model vs the Ricci scalar for different values of the parameter λ

The Taylor expansion coefficients are

$$A_1 = \frac{48\pi p_0\left(x^2+1\right)^2 + R_c x\left[2\left(x^2+1\right)^2 - \lambda x\left(x^2+3\right)\right] + 32\pi\rho_0\left(x^2+1\right)^2}{12\left[\left(x^2+1\right)^2 - 2\lambda x\right]} \tag{A.12}$$

$$p_1 = -\frac{\left(p_0+\rho_0\right)\left\{112\pi p_0\left(x^2+1\right)^2 - R_c x\left[\lambda x\left(x^2-5\right) + 2\left(x^2+1\right)^2\right] + 96\pi\rho_0\left(x^2+1\right)^2\right\}}{40\left[\left(x^2+1\right)^2 - 2\lambda x\right]} \tag{A.13}$$

$$R_1 = \frac{R_c\left(x^2+1\right)\left\{24\pi p_0\left(x^2+1\right)^2 + R_c x\left[\left(x^2+1\right)^2 - 2\lambda x^3\right] - 8\pi\rho_0\left(x^2+1\right)^2\right\}}{30\lambda\left(3x^2-1\right)} \tag{A.14}$$

A.3 Tsujikawa

The function is given by

$$f(x) = x - \mu \tanh x \tag{A.15}$$

The potential is given by

$$V(x) = \frac{1}{6} \left(x^2 + 2\mu x \tanh x - 6\mu \ln(\cosh x) \right) \tag{A.16}$$

$$\frac{dV}{dR} = \frac{1}{3} \left(-2\mu \tanh x + \mu x \operatorname{sech}^2 x + x \right) \tag{A.17}$$
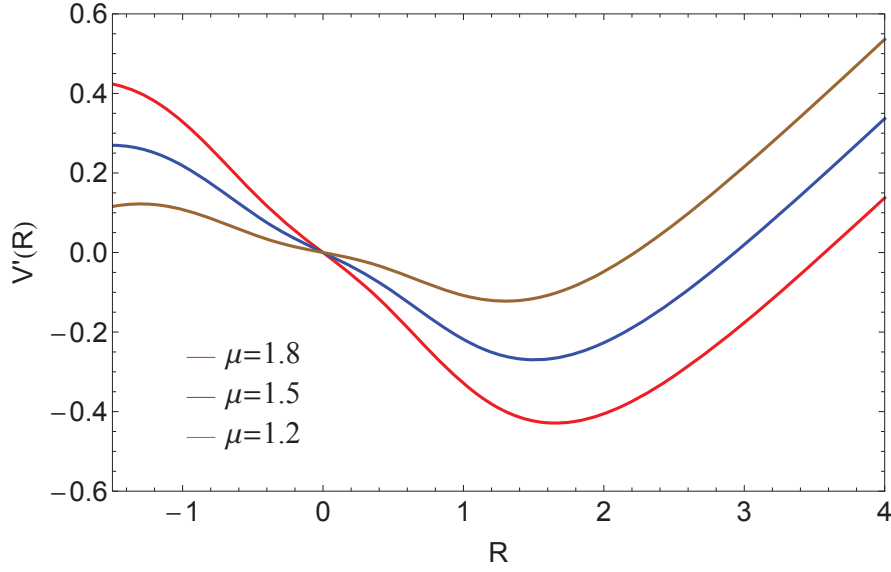

Figure A.3: The potential of the Tsujikawa model vs the Ricci scalar for different values of the parameter λ

The Taylor expansion coefficients are

$$A_1 = \frac{\mu R_c \left(\tanh x + x \operatorname{sech}^2 x \right) - 2(24\pi p_0 + 16\pi \rho_0 + R_c x)}{12 \left(\mu \operatorname{sech}^2 x - 1 \right)} \tag{A.18}$$

$$p_1 = \frac{(p_0 + \rho_0) \left(112\pi p_0 + 96\pi \rho_0 - \mu R_c \tanh x + 3\mu R_c x \operatorname{sech}^2 x - 2R_c x \right)}{40 \left(\mu \operatorname{sech}^2 x - 1 \right)} \tag{A.19}$$

96

$$R_1 = \frac{R_c \coth x [\cosh(2x)(24\pi p_0 - 8\pi\rho_0 + R_c x) + 24\pi p_0 - 8\pi\rho_0 + 2\mu R_c x - 2\mu R_c \sinh(2x) + R_c x]}{60\mu}$$

$$(A.20)$$